Effects of chemical properties of healing agents on self-healing ability of oxidation induced self-healing ceramics

酸化誘起型自己治癒セラミックスの自己治癒性に及ぼす治癒発現物質の化学的特性の影響

A dissertation submitted to
Department of Materials Science and Engineering
of YOKOHAMA National University
for the degree of Doctor of Engineering

By

Shunsuke Yoshioka

Department of Materials Science and Engineering
Graduate School of Engineering
YOKOHAMA National University
Kanagawa, JAPAN

2017.03

Dear curious readers,

From dismal office with whole lotta love.

Contents

Chapter 1

Introduction

Abstract

Oxidation-induced self-healing ceramics are the potential candidate for advanced high temperature structural materials in transportation. The oxidation-induced self-healing is an autonomous function that enables composites to fully restore mechanical properties in situ, and is induced by the high temperature oxidation of non-oxide particles, called 'healing agents', which are embedded in oxidic ceramics. Owing to this remarkable property, the ceramic matrix composites are able to avoid catastrophic failure and actively maintain their structural integrity during operation. Furthermore, since the composites have lightweight properties and heat resistance equivalent to conventional ceramic materials, the implementation of self-healing ceramics results in both weight reduction and improvement of heat resistance of high temperature components within transportation technology.

Despite being composed of high temperature structural materials that have various operating temperature ranges, self-healing ceramics must fall within an extremely limited temperature range in order to facilitate the observation of the desired healing reaction. This temperature range, called the healable temperature range T_H, is significantly affected by the chemical properties of the healing agent. This study was designed to provide a methodology for quantitatively evaluating the effects of the chemical properties of healing agents on the healing temperature range of oxidation-induced self-healing ceramics. Based on the results, a fundamental design strategy for oxidation-induced self-healing ceramics has been proposed.

The chapter begins with an introduction to the engineering background of the study. Current development status and practical issues of high temperature structural materials for transportation is investigated, and the favourability of implementing self-healing ceramics as opposed to their classical counterparts is suggested. In order to bring the study to a wider context, the scientific background of self-healing ceramics in the self-healing material field is discussed as well. Subsequently, the current issues in the self-healing ceramics field are extracted from those discussions, and the key aspects of the studies are shown.

1.1 Engineering Background

1.1.1 Current Status and Practical Issues of High Temperature Structural Materials for Transportation

While on the one hand the accessibility of our world has been drastically improved owing to the development and spread of transportation, environmental and energy problems due to our transportation activity have become one of the biggest issue for our society. In fact, 17.2 % of CO_2 emissions in Japan during 2014 were from transportation sectors, as shown in Figure 1.1[1, 2]. When we evaluate the breakdown of the sectors, the highest proportion of this CO_2 is from the automobile sector, accounting for 86 % of the total. Shipping and aviation are the second and third highest proportions respectively, with shipping accounting for 5.0 % and aviation accounting for 4.7 %. In this study, we focused on high temperature structural materials used in the automotive and aviation industries, where the advantages of self-healing ceramics, which are both lightweight and heat resistant, can be maximized. The current development status of new materials and issues of the traditional materials used in the specified applications are discussed below.

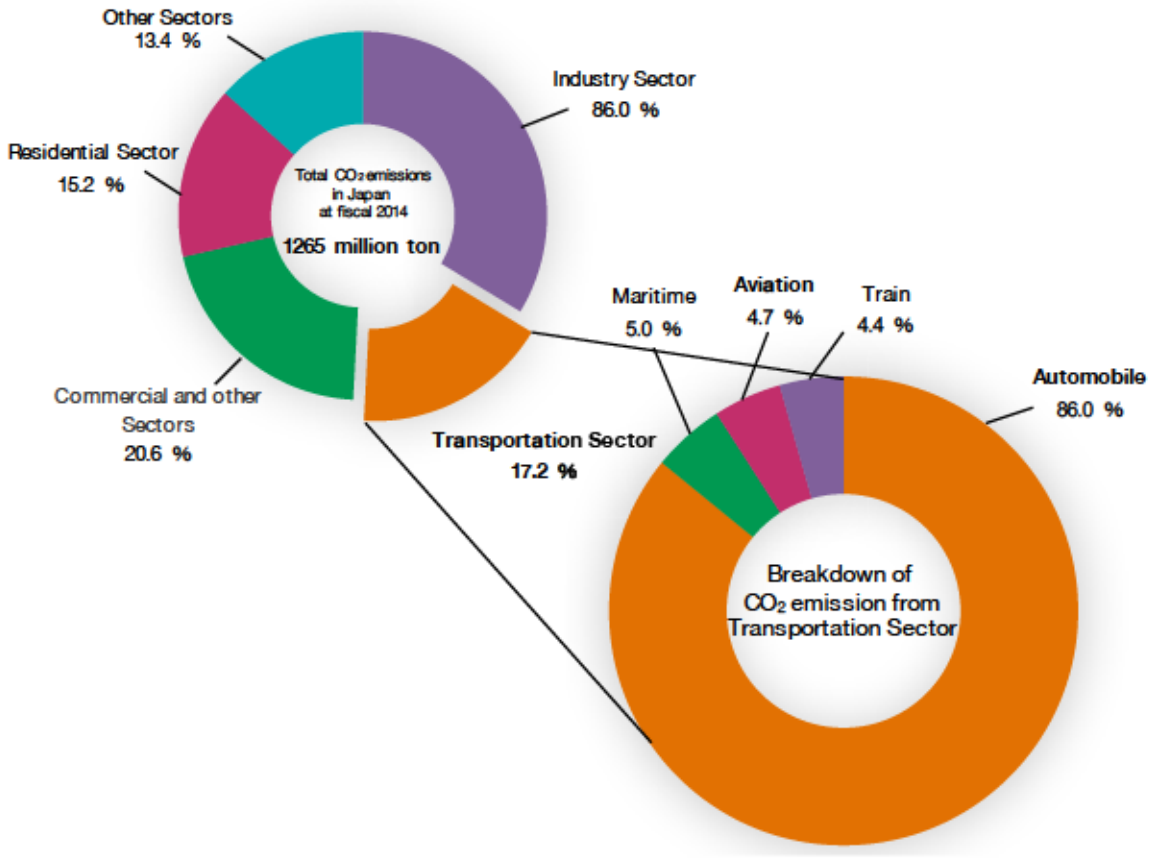

Figure 1.1 Percentage of Total CO_2 Emissions for Each Sector in Japan in 2014

The CO_2 emissions from fuel combustion account for 88% of Japan's total greenhouse gas emissions.

1.1.1.1 High Temperature Structural Materials in the Automotive Industry

Since the unit sales of automobiles and total number of registered automobiles are still growing in the world[3, 4] (Figure 1.2), each government and automotive company is busily working on the improvement of automobile fuel consumption. According to reports[5], the world's total travel distance by automobile will increase by 1.9 times by the year 2030. While smoothing traffic is one solution to improve fuel consumption, and some governments including Japan are promoting it, the most important countermeasure is an enhancement of performance of the automobiles themselves. Environmental measures have been advanced owing to the appearance of some innovative automobiles, including HV, PHV, EV and FCV. On the other hand, the research company suggested that the reduction in weight of conventional engine cars is the most viable solution, because the conventional automobiles will remain the dominant market force until at least 2030[6].

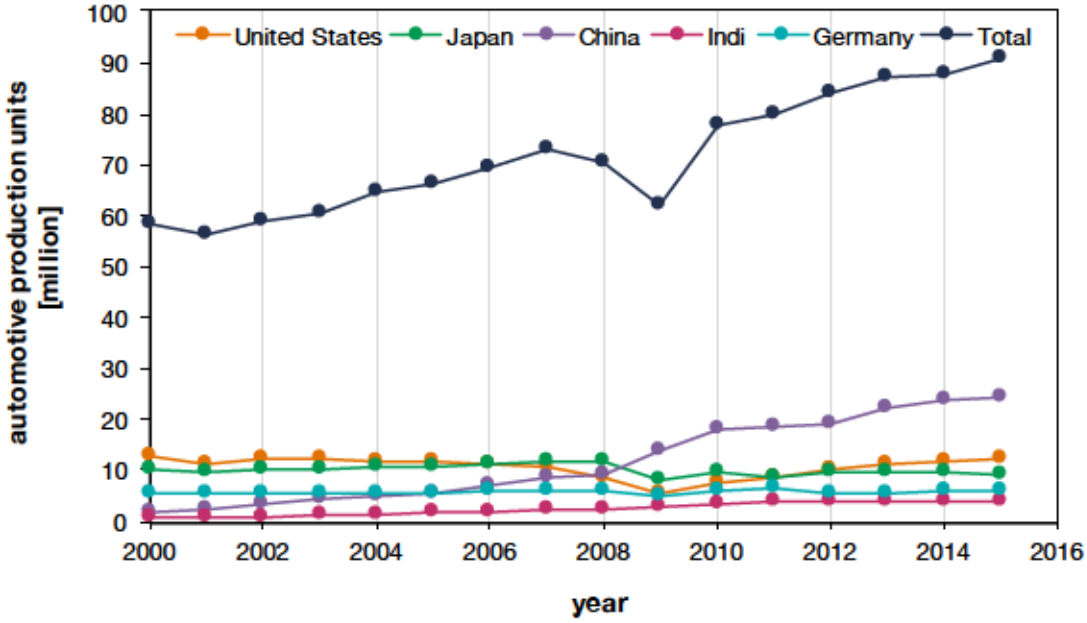

Figure 1.2 Changes in Automotive Production Volume of Major Countries and Overall Total
The sudden drop in global production in 2009 is due to the Lehman shock.

High Temperature structural materials in automobiles are mainly used in powertrain components and exhaust systems, such as intake and exhaust manifolds, turbochargers and engine components illustrated in Figure 1.3. Since those components comprise a relatively high percentage of the automobile's total weight (~15 %[7]), weight reduction in the high temperature materials can lead to a significant improvement in overall fuel consumption. Table 1.1[8] shows the typical operation temperature ranges, required properties and conventional materials used in those applications.

In the field of engine valve system components, heat resistance properties are especially necessary in the intake and exhaust valves. In general, martensitic heat resisting steel such as SUH11(0.5C -1.5Si-8.5Cr) is used in intake valves, where the operation temperature is around 400 °C. Austenitic heat resisting steel such as SUH35(21Cr -4Ni-9Mn) is used in exhaust valves where the operation temperature is ~800 °C. In the advanced engines using diameter-thinning valves and in

diesel engines, Inconel 751 (Ni-15Cr-1.2Ar-2.4Ti-1Nb-7Fe) and Nimonic 80A (Ni-19Cr-1.4Al-2.4Ti) representing Ni-based super alloys are adopted, respectively[9,10]. Recently, several Ti based alloys such as Ti6242S[11] (Ti-6Al-2Sn-4Zr-2Mo-Si) and TiAl based alloys have been implemented in those valve systems[12, 13]. The developments of the lightweight high temperature structural materials lead to between 56% and 57 % weight reduction of valve system components. However, improvements in high temperature strength, wear resistance and cost reduction are still anticipated. Recent exhaust manifolds also require higher temperature resistance to make use of new materials as temperatures of exhaust gas increase[14]. Ferrite based stainless steels such as SUH409L (11Cr-Ti-low C) and SUS430J1L (19Cr-0.4-Cu-0.4Nb) have replaced conventional ductile cast irons traditionally used in the manifold. Types 429Nb (15Cr-Si-Nb) or SUS444 (18Cr-2Mo-Nb) are sometimes employed when the high temperature strength exceeding that of SYH409L is required. Recent turbine inlet temperatures (T.I.T.) of turbochargers for high-powered gasoline engines already reaches 1000 ˚C, and it is expected that the T.I.T. will reach 1050 ˚C soon[15]. In contrast to ductile cast iron with high Si content or Ni-resist cast iron which are frequently used as housing material in general diesel engines, ferritic or austenitic heat resisting steel is adopted in gasoline engines where the temperature of exhaust gas is higher than that of diesel engines. In the wheel of a turbine rotor, Inconel 713C (Ni-12.5Cr-4.2Mo-2Nb-6.1Al-0.8Ti) or GMR235 (Ni-15.5Cr-5.3Mo-3Al-2Ti-10Fe) are employed because of their great creep resistance properties. Mar-M247 (Ni-8.3Cr-10Co-0.7Mo-10W-3Ta-5.5 Al-1Ti-1.5Hf) is used in some higher temperature turbochargers[15].

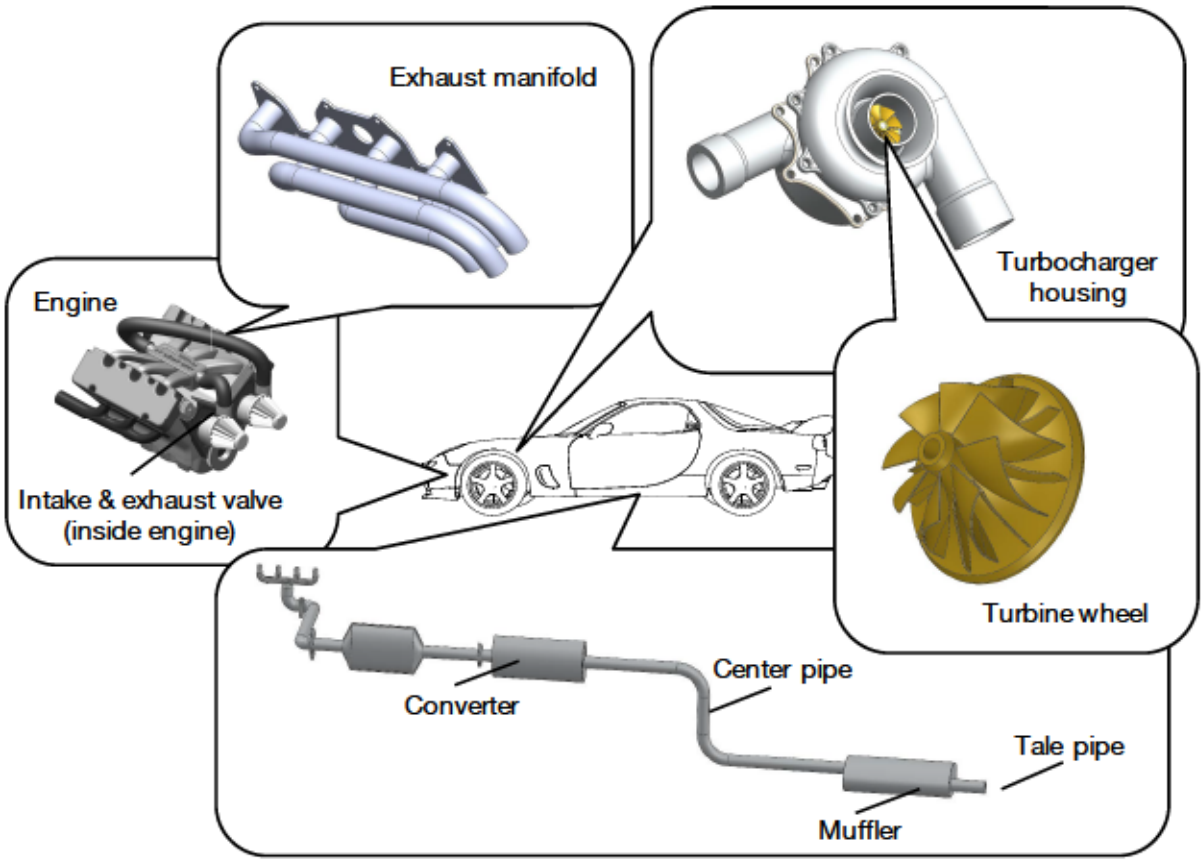

Figure 1.3 Main High Temperature Structural Components Used in Automobiles

As summarized in Table 1.1, high-density materials are still used in most high temperature structural applications in automobile engines. In some components, a great weight reduction has been achieved as a result of the development of lightweight alloys such as Ti6242S. However, it is expected that the temperature of exhaust gas will keep increasing due to improvements in the efficiency of engines and turbochargers, and as such will keep activating purification catalysts for exhaust gasses. Due to this projection, it is urgently necessary to develop advanced high temperature structural materials for automobiles which are both lightweight and heat resistant.

Table 1.1 Operation Temperature Ranges of High Temperature Components in Automobiles[8] and Densities of Currently Used Conventional Materials

Component	Part name		Operation temperature region [°C]	Typical material used	Density [g/cm^3]
Valve system component	Intake valve		300-500	SUH11	7.7
				SUH35	7.8
	Exhaust valve		700-850	Inconel 751	8.2
				Ti6242S	4.5
Exhaust system component	Exhaust manifold		750-1000	SUH409L	7.8
				SUS430J1L	7.7
				Type429Nb	7.7
				SUS444	7.8
	Turbocharger	Turbine wheel	750-1000	Inconel 713C	7.9
				GMR235	8.0
		Turbine housing	750-1000	Ductile iron	6.8-7.4
	Front pipe		600-800	SUH409L	7.8
				SUS410L	7.8
	Flexible pipe		600-800	SUS304	7.9
				SUSXM 15J1	7.8
	Converter	Shell	600-800	SUH409L	7.8
				SUS436J1L	7.7
		Catalyst support	1000-1200	SUH21	7.8
				20Cr-5Al	7.7
	Center pipe		400-600	SUH409L	7.8
	Muffler		100-400	SUH430type	7.7
	Tale pipe		100-400		

1.1.1.2 High Temperature Structural Materials in Aviation

A significant increase in CO_2 emissions from the aviation industry is also one of the biggest problems we face. As shown in Figure 1.4, a large increase in CO_2 emissions from the international aviation sector is expected. According to Airbus and Boeing, Revenue Passenger-Kilometres (RPK) will double the current rate within the next 15 years, increasing at an annual rate of 4.5 % to 6%[16-19]. Consequently, the International Civil Aviation Organization (ICAO) estimates that 4.5 billion tons of CO_2 will be emitted by the sector by the year 2050 in the worst case scenario[20-22]. As a countermeasure to this situation, the new goal of CO_2 reduction was identified during the High-Level Meeting on International Aviation and Climate Change in October 2009. The meeting agreed on a set of comprehensive measures known as the ICAO Programme of Action on International Aviation and

Climate Change[23]. It includes the agreement on a global goal of 2% annual improvement in fuel efficiency and 50% reduction of CO_2 emissions until the year 2050. It is expected that the global goal can be achieved mainly by the development of aircraft technology, such as improvement of fuel efficiency in jet engines or decreasing the overall weight of airframes.

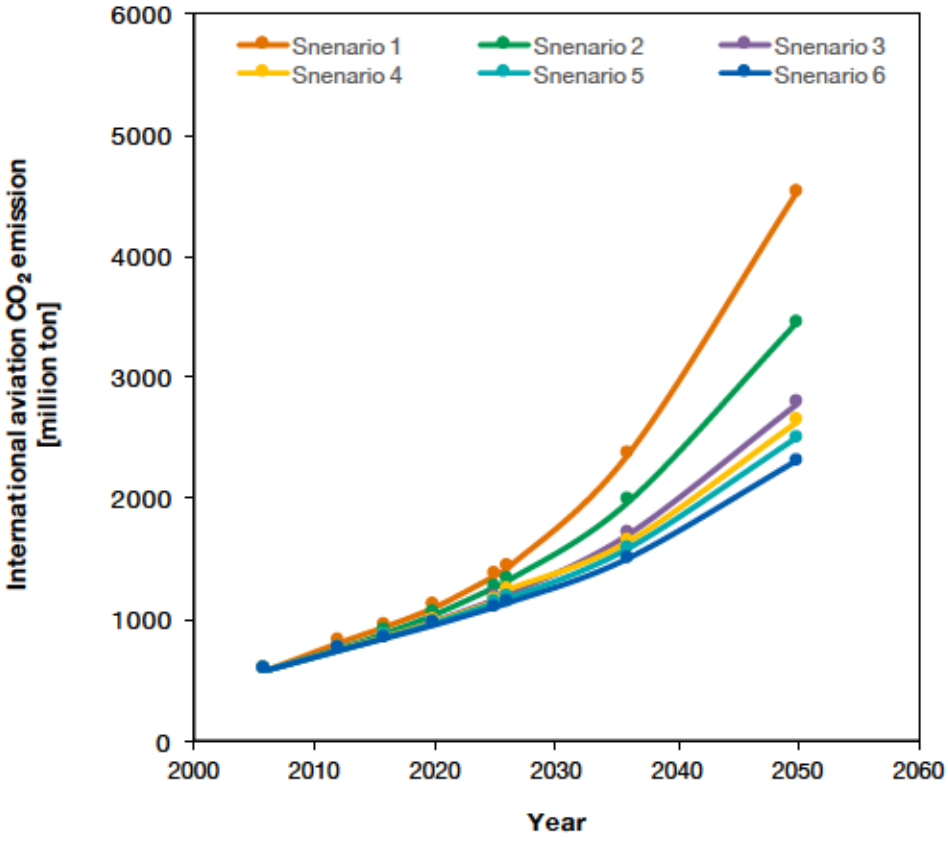

Figure 1.4 CO_2 Emissions Trends from International Aviation (2005 – 2050)

The trends are computed from MODTF models consistent with the FESG CAEP/8 central demand forecast for 2006, 2016, 2026 and 2036. Fuel burn has been computed for the following modelling scenarios: Scenario 1 - Do Nothing, Scenario 2 - CAEP/7 Baseline, Scenario 3 - Low Aircraft Technology Improvement and Moderate Operational Improvement, Scenario 4 - Moderate Aircraft Technology and Operational Improvements, Scenario 5 - Advanced Aircraft Technology and Operational Improvements, Scenario 6 - Optimistic Aircraft Technology and Operational Improvements.

High temperature structural materials in jet engines are mainly used in the turbine section as shown in Figure 1.5. Some of the air drawn in by the turbine is bypassed by fan and directly used to generate driving force. The remaining air is compressed and mixed with fuel in combustion chambers. The mixed fuel is combusted in the chambers and the turbines are driven by the resulting high speed, high temperature gas. Since jet engines operate under the Carnot cycle, increasing the turbine inlet temperature (T.I.T.) is an effective way to improve their efficiency. This indicates that the heat resistance properties of the high temperature materials in turbine components directly affect the fuel efficiency of jet engines. Further, turbines can be divided into three categories by their operation temperature range: 1600-1200°C (high-pressure), 1200-1000°C (middle-pressure) and 1000-600°C

(low-pressure).

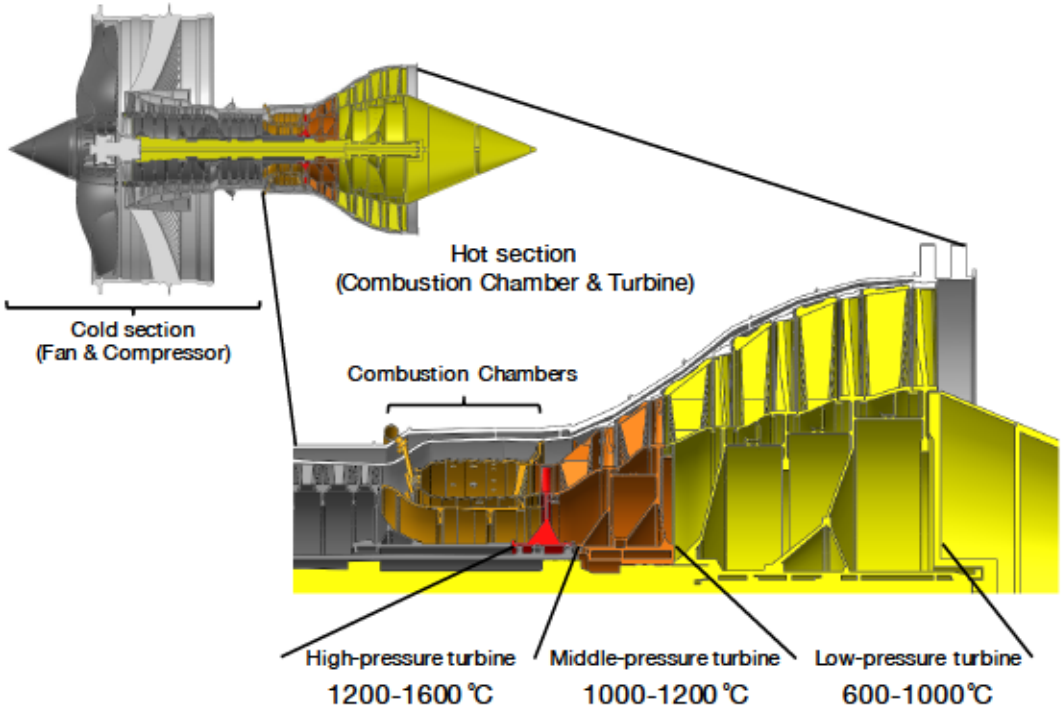

Figure 1.5 Schematic Illustration of Jet Engine and Service Temperature Ranges of Turbine Blades

The jet engine model is based on the Trent 1000.

Currently, single crystal Ni-based superalloys are used in the hot section. Generations of these superalloys are divided by their Re content and are listed in Table 1.2[24, 25]. In the 1970s, first-generation single crystal Ni-based superalloys were developed. These alloys had durability temperatures of 50°C higher than those of the conventional directional solidification Ni-based superalloys. As soon as the positive effects of Re on high temperature strength and corrosion resistance were reported, the second generation of Ni-based superalloys, such as PWA1484, Rene N5 and CMSX-4, were developed. This generation of alloys contained about 3% of Re. The durability temperature of second-generation alloys is about 25°C higher than first-generation alloys. These second-generation Ni-based superalloys are widely used in current aircraft. In third-generation alloys, the Re content has reached 6 wt.%. In fourth-generation alloys, 2-3 wt.% of Ru in addition to Re has been added to improve the high temperature stability of the alloy's micro structure. The newest Ni-based superalloys, TMS-162 and TMS-196, were developed by National Institute of Material Science in Japan (NIMS) and have durability temperatures around 1100°C[26].

As shown in Table 1.2, as the percentage of rare metals such as Re and Ru are increased, the density of Ni-based superalloys also increases. This weight increase in turbine blades not only leads the increase of centrifugal stress on the blades but also requires thicker turbine disks to hold turbine blades. Moreover, the durability temperatures of TMS-162 and TMS-196 are still lower than the

surrounding temperature of high-pressure turbine blades, so the blades require complex cooling systems to protect the materials[27, 28], leading to an increase in overall engine weight. Since improvements in both weight and heat resistance of Ni-based superalloys seems to be reaching physical limits, the development of advanced high temperature materials for turbine blades of jet engines to replace conventional Ni-based alloys is urgently required.

Table 1.2 Chemical Compositions and Densities[28] of Single Crystal Ni-based Superalloys[24] [wt.%]

Gen.	Alloy	Cr	Co	Mo	W	Ta	Re	Ru	Nb	Al	Ti	Hf	Ir	Ni	Density [g/cm³]
1st	PWA1480	10	6	-	4	12	-	-	-	5	1.5	-	-	Bal.	8.7
	Rene N4	12.8	9	1.9	3.8	4	-	-	0.5	3.7	4.2	-	-		8.55
	SRR99	8	5	-	10	3	-	-	-	5.5	2.2	-	-		8.56
	AM1	8	6	2	6	9	-	-	-	5.2	1.2	-	-		8.59
	AM3	8	6	2	5	4	-	-	-	6	2	-	-		8.25
	CMSX-2	8	5	0.6	8	6	-	-	-	5.6	1	-	-		8.56
	MC2	8	5	2	8	6	-	-	-	5	1.5	-	-		8.63
2nd	CMSX-4	6.5	9	0.6	6	6.5	3	-	-	5.6	1	0.1	-	Bal.	8.7
	PWA1484	6	10	2	6	9	3	-	-	5.6	-	0.1	-		8.95
	SC180	5	10	2	5	8.5	3	-	-	5.2	1	0.1	-		8.94
	Rene N5	7	7.5	1.5	5	6.5	3	-	-	6.2	-	0.15	-		8.63
3rd	CMSX-10	2	2	0.4	5	8	6	-	0.1	5.7	0.2	0.03	-	Bal.	9.05
	Rene N6	4.2	12.5	1.4	6	7.2	5.4	-	-	5.75	-	0.15	-		8.98
	RR2100	2.5	12	-	9	5.5	6.4	-	-	6	-	-	-		-
	TMS-75	3	12	2	6	6	5	-	-	6	-	0.1	-		8.89
4th	EPM102	2	16.5	2	6	8.25	5.95	3	-	5.55	-	0.15	-	Bal.	9.2
	RR2101	2.5	12	-	9	5.5	6.4	2	-	6	-	-	-		-
	TMS-173	2.8	5.6	2.8	5.6	5.6	6.9	5	-	5.6	-	0.1	-		9.11
	TMS-138	2.9	5.8	2.9	5.8	5.5	4.9	-	-	5.8	-	0.1	3		8.95
5th	TMS-162	2.9	5.8	3.9	5.8	5.6	4.9	6	-	5.8	-	0.1	-	Bal.	9.04
	TMS-196	4.6	5.6	2.4	5	5.6	6.4	5	-	5.8	-	0.1	-		9.01

1.1.2 Ceramics for High Temperature Structural Material

One of the attractive candidates for advanced high temperature structural material is ceramics. While ceramics are a brittle material and have high defect sensitivity due to their low fracture toughness, ceramics also have greater heat resistance, corrosion resistance and specific strength than the usual metals and alloys.

Several projects developing high temperature structural ceramics for industrial gas turbines or automobiles have been implemented in Europe and America, and the short history on the development of these products is summarized below[30]. Ceramic first gained attention as a high temperature structural material in Germany at the end of World War II[31].Germany focused on ceramics as a replacement for Ni-based alloys used in jet engine components of fighter planes. After

World War II, the United States began research on ceramics as structural material based on Germany's work in the field, developing cermets such as the combination of TiC and Ni. Reaction sintered SiC was studied in the United Kingdom, but it was unusable because of low strength due to excess porosity[32]. The hot-pressing technique of Si_3N_4 containing MgO as a sintering additive was developed in the United Kingdom in 1961[3]. The development of ceramic gas turbines started in the United States in 1971 using the hot-pressed Si_3N_4 as the main structural material[33]. Throughout the project, significant improvements were made in manufacturing techniques for ceramic components having complex shape, sintering techniques for non-oxides ceramics and understanding of the fracture mechanics of ceramics.

In Japan, there are also several projects that were implemented during the 1980s in economically significant areas of industry through the collaboration of industry, university and government resources. These projects include the development of gas turbines for power generation[34-40], aircraft components[41-44] and engines and exhaust systems for automobiles[30, 45]. The project, named the 'New Sunshine' project, was implemented from 1988 to 1999 in Japan. This project aimed to develop two classes of ceramic gas turbine, 100 kW and 300kW[5]. The small size gas turbines, called micro gas turbines, were designed to be used in a hybrid engine for automobiles and distributed power supply systems. In this application, ceramics are used in turbine blades in order to increase turbine inlet temperature and achieve a non-cooling system. Another project deals with the development of ultra-high temperature gas turbines for power plants[46]. In power plants, the operation temperature of gas turbine blades is believed to reach between 1700°C and 1800°C, which current metal based materials cannot withstand. Ceramic matrix composites can be the only choice for structural material in such a high temperature application.

Within the field of aerospace engineering, the lightweight properties of ceramics are very attractive. For example, significant research progress has been made in the field of ceramic matrix composites. This progress has been reported through the project named 'HYPER', carried out from 1991 to 1998[41], and the project named 'ESPR', carried out from 1999 to 2003[42] under a collaboration between Japan's Ministry of Economy, Trade and Industry and the New Energy and Industrial Technology Development Organization.

In the Japanese automotive industry, there have been several attempts to use ceramics in automotive components, such as diesel engines[30] and turbochargers[45]. The adiabatic ceramic diesel engine was first developed by Cummins Inc. in the United States during the 1970s, and was subsequently developed in Japan under the collaboration of Isuzu Motors Ltd. and KYOCERA Co. In both projects, Si_3N_4 was used in main components such as cylinders, pistons and head plates because of the great thermal resistance and thermal shock resistance.

While there have been numerous projects that aimed to implement ceramic into high temperature structural materials due to their excellent thermal resistance and specific strength properties, the implementation of high temperature structural ceramics did not advanced significantly until 2016. Aside from cost and manufacturing difficulties, the biggest practical problem with the implementation of ceramic in structural components is the inherent brittleness of ceramics. Ceramics will be catastrophically fractured from micro defects in the matrix or on the surface when excessive

stress is applied because they do not have an effective plastic deformation mechanism as is present in metal materials.

In the 'New Sunshine' project mentioned above[35], ceramics turbine blades were never realized because they could not withstand the foreign object damage (FOD). FOD is the phenomena that rotating turbine materials are chipped or, in worst case scenarios, broken due to the collision of debris or foreign material with high speed combustion gases, as shown in Figure 1.6. Ceramic materials cannot withstand such impacts because they do not have an effective plastic deformation mechanism. For the same reason, ceramics can be cracked due to thermal shock. Thermal shock occurs when a thermal gradient causes different parts of materials to expand by different amounts. Since the thermal conductivity of ceramics is very low, a thermal gradient can be easily observed within the material. Ceramic materials cannot mitigate the expansion mismatch in the material itself, resulting in crack formation. Especially in materials subject to severe thermal cycling, such as those in a jet engine or an automobile engine, thermal shock resistance is the critical issue standing in the way of implementation. In order to integrate ceramics into high temperature structural materials, advanced ceramic materials with high damage tolerances must be developed.

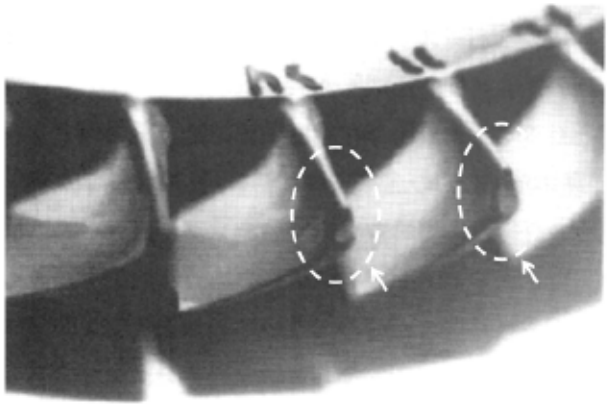

Figure 1.6 Photograph of Turbine Blade Tipped Due to Foreign Object Damage (FOD)[35]

1.1.3 Effectiveness of Integration of Self-healing Ceramics Into High Temperature Structural Materials in Transportation

As described above, significant amounts of research and development regarding the increased efficiency of high temperature components is being conducted in order to reduce our environmental footprint. Despite the fact that the potential of ceramic materials has drawn considerable attention, the implementation of ceramics into high temperature structural materials has not advanced significantly because conventional ceramics cannot withstand accidental damage, such as FOD, during operation.

Many approaches to dealing with the brittleness of structural ceramics have been proposed. Those approaches can be classified as outlined in Figure 1.7. First, approaches can be divided under two concepts: the Damage Prevention concept and the Damage Management concept[47]. It can be said that conventional ceramics, such as monolithic fine ceramics and ceramic matrix composites, are

developed under the concept of Damage Prevention. In contrast, the self-healing ceramics included within this study are a novel material which is being developed under the innovative Damage Management concept. In the following text, ceramics developed under each concept will be reviewed, and the advantages of self-healing functionality will be clearly articulated.

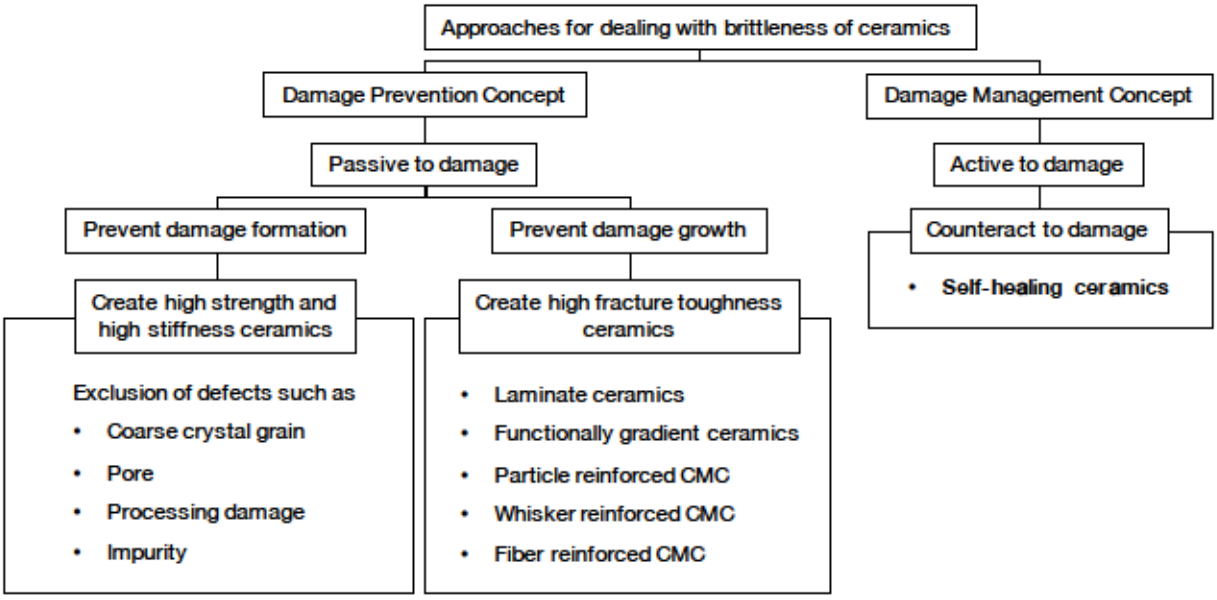

Figure 1.7 Classification of the Approaches to Dealing with Brittleness of Ceramic Materials

1.1.3.1 Conventional Ceramics Developed Under the Damage Prevention Concept

The main objective of the Damage Prevention concept is to create microstructures which can prevent damage formation or growth. The term 'strong material' in this context means that the material has high stiffness, high strength, or high fracture toughness. In the field of ceramic materials, the simplest way to achieve this concept is through the approach that aims to prevent damage formation by excluding or minimizing defects such as coarse crystal grain, pores, processing damage and impurities. Since ceramic materials do not have an effective plastic deformation mechanism due to their strong cohesion or ionic bonds, stresses can be concentrated to the largest defect in the material, leading to fractures in the material in accordance with the weakest link model. The Damage Prevention concept is strongly related to manufacturing technology because defects are mostly introduced in the bulk ceramic manufacturing process[48-51].

The other approach utilized under the Damage Prevention concept is intended to improve the fracture toughness of bulk ceramics. Recently, a lot of ceramic matrix composites (CMC) have been developed under this concept. These CMCs include laminar ceramics[52-55], functionally gradient ceramics[56-57], particle reinforced CMC[58-60], whisker reinforced CMC[61-62] and fibre reinforced CMC[63-65].

The current development of structural ceramics is progressing under the guidelines of the Damage Prevention concept. Thanks to the concept, some fine structural ceramics are being implemented in certain industrial fields. However, the damage formation during operation can never

be avoided in practice and once damaged, the ceramic components will deteriorate rapidly because of their low fracture toughness. This also indicates that the detection of damage formation and monitoring of damage development are essential technologies required for the implementation of ceramics that are considered 'passive' to damage formation or growth.

1.1.3.2 Oxidation Induced Self-healing Ceramics Developed Under the Damage Management Concept

Recently 'oxidation-induced self-healing ceramics' have drawn considerable attention as the advanced ceramic matrix composite developed using the paradigm of the Damage Management concept. The concept is based on the argument that the formation of damage is unavoidable but is not a problem as long as it can be offset by 'active' reactions such as oxidation-induced self-healing within the material itself. This concept is presented schematically in Figure 1.8 alongside the Damage Prevention concept. The materials developed with the goal of preventing damage formation, including conventional monolithic ceramics, have higher initial strength than other materials because defects in the material are excluded as frequently as possible. These materials can withstand small impacts to or loads on the material, such as the first impact in Figure 1.8, and damage will not be introduced at the time of impact. However, once impact forces exceed the materials' damage threshold, the materials suddenly fracture.

The initial strength of the ceramic created with the goal of preventing damage growth is sometimes lower than that of the ceramic developed with the goal of preventing damage formation. This is because the dispersed particles or fibres that act as reinforcement can act like defects. The material may survive several impacts due to the reinforcement, but damage accumulates as a function of overall service time, ultimately resulting in the fracture of the material.

As discussed above, the structural integrity of both conventional monolithic ceramics and ceramic matrix composites is passively determined by the probability of damage from sources including FOD that are present during operation. In contrast, oxidation-induced self-healing ceramics show totally different reactions to this type of damage.

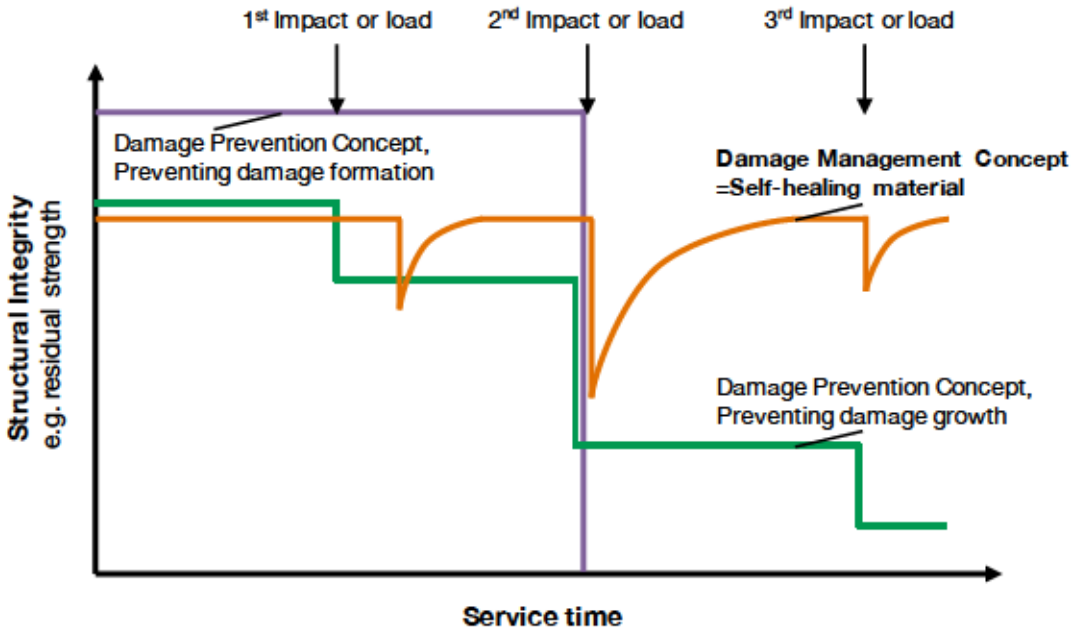

Figure 1.8 Schematic Illustration of Damage Recovery in Self-healing Material (Damage Management Concept) as Compared to Conventional Materials (Damage Prevention Concept)

Oxidation induced self-healing is an autonomous function that enables composites to fully restore their mechanical properties in situ, allowing the composites to avoid catastrophic failure and actively maintain their structural integrity during operation. Furthermore, since self-healing ceramics have the same light weight and heat resistance as conventional ceramics, the composites are attractive candidates in the search for advanced high temperature structural ceramics with high structural integrity. Nakao et al. suggest that the implementation of self-healing ceramic in turbine blades of jet engines would lead to a 22% reduction in the weight of jet engines, and would improve the fuel efficiency of these engines by between 10.2% and 14.8 %. This improvement in fuel efficiency results in a CO_2 reduction of 54 million tons by 2022 and 619 million tons by 2050[44]. The value of 619 million tons of CO_2 corresponds to the half of the current total CO_2 emissions in Japan. It should be noted that the calculation is based on a model in which the growth rate of RPK is a constant value of 5.1%. In addition, the high temperature components in automobiles, currently comprised of conventional steels, could see a weight reduction of between 48% and 51% when self-healing ceramics are used to replace conventional materials. These calculations prove the potential effectiveness of implementing self-healing ceramics in high temperature structural applications within transportation.

Self-healing functions do by nature have some limitations and conditions. Figure 1.9 shows a typical self-healing ceramics mechanism called particle dispersion self-healing ceramics. Self-healing is induced by the high temperature oxidation of non-oxide particles, called healing agents, which are embedded in oxide ceramics. As soon as the composite cracks, healing agents on the crack's surface are exposed to the high temperature atmosphere. They then start oxidizing intensely, filling and bonding the surface crack.

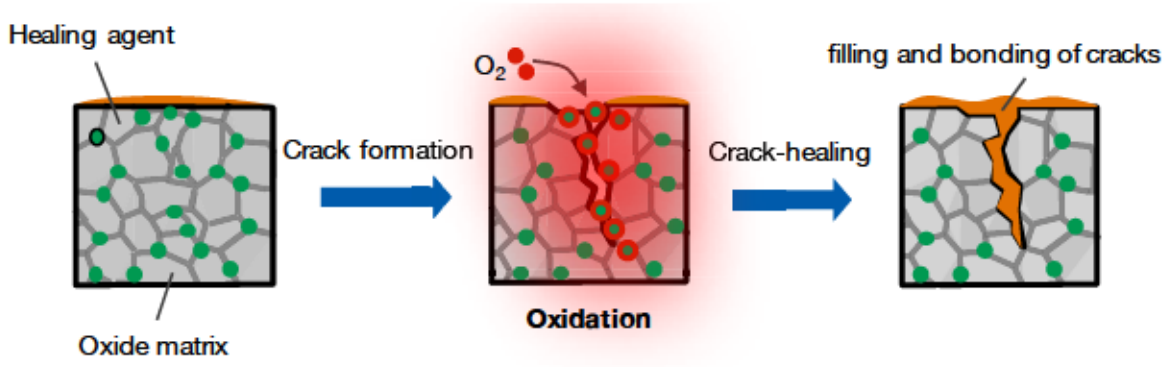

Figure 1.9 Schematic of Self-healing Mechanism of Oxidation Induced Self-healing Ceramics

Since self-healing function is induced by chemical reaction, the function is affected by surrounding conditions, i.e. operating temperature. The temperature range within which desirable self-healing can be attained is called the healing temperature range (T_H) in this study. The T_H is dramatically affected by the chemical properties of healing agents. High temperature structural materials, which are attractive applications for self-healing ceramics, have various operating temperature ranges. As a result, a variety of self-healing ceramics which have a T_H corresponding to respective operation temperature ranges should be developed in order to implement self-healing ceramics in a wider variety of situations.

Several self-healing ceramics have already been proposed and each has its own T_H. However, as we will see in the following section, the research and development of self-healing ceramics has progressed through trial and error, causing delays in the implementation of the materials. In order to break through the status quo, this study aims to establish the framework or design strategy for self-healing ceramics, especially the methodology for evaluating T_H.

The following sections review the previous studies on self-healing material and focus specifically on self-healing ceramics in order to deeply understand the principles of self-healing reactions which are essential in establishing a design methodology for these materials. Based on the reviews, self-healing reactions in structural ceramics have been classified into three states and the required properties determined for each component of self-healing ceramics i.e., healing agent and matrix.

1.2 Overview of Self-healing Materials and Previous Studies on Ceramics

1.2.1 Classification of Self-healing Materials Based on Self-healing Properties

In recent years, there has been a lot of research into the autonomous healing of physical damage not only in ceramic materials but also in other materials fields, including polymers[66-68], metals[69,70] and cementitious materials[71-73]. These materials possess different properties by nature, but the self-healing function in those materials is based on the same general principles and concepts. The general principles and concepts, which can be also regarded as the definition of self-healing materials, have been discussed by several researchers[74-78]. The classification of self-healing materials based on

previous research is summarized in Figure 1.10.

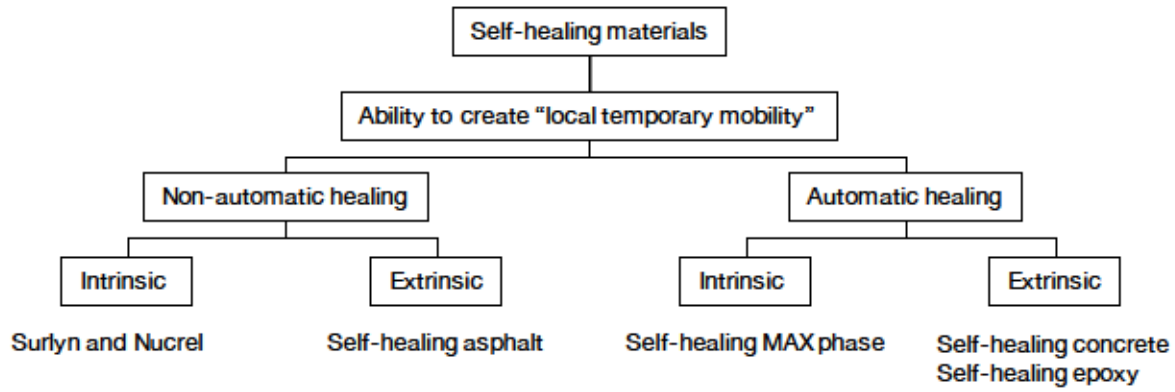

Figure 1.10 Classification of Self-healing Materials in Accordance with Previously Proposed Concepts

The most basic property that defines self-healing material is the creation of 'local temporary mobility'[78]. Conversely, the self-healing process within all self-healing materials should be divided into three factors as shown in Table 1.3: the local factor, the temporary factor and the mobility factor. The concept is well described in the self-healing epoxy matrix composite proposed by White et al.[79]. In the composite, the mobility factor is realized using a liquid healing agent called dicyclopentadiene (DCPD). The local factor is attained by encapsulating and dispersing the liquid healing agent in the epoxy matrix. The temporary factor is realized because the liquid DCPD can flow only in the period between the time the crack opens the capsule and the onset of cross-linking reactions upon contact with the Grabbs' catalysts also dispersed in the epoxy matrix. The concept can also be applied in the self-healing concrete field. In the self-healing concrete proposed by Jonkers et al.[80], the mobility factor is met by producing limestone resulting from the metabolism of either Bacillus pseudofirmus or Sporosarcina pasteurii bacteria. The local factor is attained by hibernating and dispersing the bacteria. The temporary factor is met as the bacteria are only activated when they contact with rain-water occurs through the opened crack. Of course, the concept can be applied in a variety of other materials, such as creep steel[81] and coatings[82], as shown in Table 1.3.

Table 1.3 Local, Temporary and Mobility Factors in Several Self-healing Materials

Material	Mobility	Local	Temporary
Self-healing epoxy	Flow of liquid healing agent, dicyclopentadiene (DCPD)	Encapsulation and dispersion of DCPD in epoxy matrix	DCPD can flow only in the period between the crack opening the capsule and the onset of cross-linking reaction upon contact with the Grabbs' catalysts.
Self-healing concrete	Formation of limestone owing to the metabolism of bacteria	Dispersion of bacteria in concrete	The bacteria are only activated when they come into contact with rain-water through the opened crack.
Self-healing creep steel	Diffusion of Cu or Au along dislocations and (sub)grain boundaries of creep steels	Dispersion of Au and Cu nanoparticle in creep steel	Diffusion of elements lost their driving force when the open-volume cavities are completely filled up.
Self-healing ceramic	Formation of oxides due to the oxidation reaction of non-oxides	Dispersion of non-oxide healing agent in oxidic ceramics	Oxidation reaction ends when non-oxides at crack-surface are completely consumed or protective oxide layer is formed and shields oxygen.

Self-healing materials, which are all able to create local temporary mobility, can be further divided into non-automatic and automatic[76, 77] classes by the required activation trigger for the self-healing reaction. Non-automatic self-healing materials require an adequate external energy source, such as heat and light, to activate the self-healing reaction. For instance, the self-healing asphalt proposed by Schlangen et al.[83] requires induction heating to create mobility. As a second example, the conductive fibres in bitumen generate heat through the energy lost when eddy currents meet with the resistance of the material, resulting in the melting of the bitumen. In some self-healing polymers, heating is required to diffuse the polymer chains and to allow the formation of new entanglements[84]. In contrast, automatic self-healing materials do not require any additional triggers in order to induce the self-healing reaction. The concept is suitable for any structural material because it is unnecessary to detect damage prior to the activation of the healing process.

An additional property of self-healing processes further divides self-healing materials into two subclasses: extrinsic and intrinsic self-healing materials. Intrinsic self-healing means that the material alone can undergo the self-healing reaction that results in partial or complete recovery of the material's mechanical properties. Intrinsic self-healing is mainly realized in self-healing polymer. For instance, polycarbonates possess reactive end groups which enable the reconnection of chemical bonds between crack surfaces[85]. As explored in Surlyn and Nucrel and developed by DuPont, ballistic damage can be healed by the formation of secondary chemical bonds [86-87]. Functional side groups of polymers can be used for reversible thermal crosslinking within Diels-Alder reactions[88, 89] and Michael additions[90]. In addition, multiple self-healing is realized at room temperature in supramolecular polymers [91, 92]. On the other hand, extrinsic self-healing materials do not have the capability to induce a self-healing reaction without additional components. These extra microcapsule or non-oxide particles components, called healing agents, should be added into systems to induce the desired reaction. Extrinsic self-healing can be observed in any self-healing materials field. For example, the self-healing epoxy[79] and asphalt[83] explained previously are classified within this group. Self-healing in creep steel[81] and concrete[80] have been only realized by this route, because existing counter materials are so widely used

that it is difficult to replace them with a totally new material.

As discussed above, intrinsic self-healing could be preferable because the material can induce self-healing from anywhere in material, which means that cracks can be healed without regard for the propagation route and multiple healing events can be attained. However, most intrinsic self-healing materials require extra energy, i.e. non-automatic self-healing. In contrast, most extrinsic self-healing materials have automatic self-healing abilities, and healing reactions can be optimized relatively easily by modifying the healing agent. However, an addition of healing components for the purpose of inducing extrinsic self-healing sometimes leads to the degradation of the material's mechanical properties as compared to existing materials, and in most cases multiple healing events cannot be attained in the same location because the healing agent is intended for one-time use.

1.2.2 Classification of Self-healing Ceramics Reported Previously

There are several self-healing ceramics that have been reported on previously[]),and they can be classified based on their self-healing properties as discussed above. Moreover, as mentioned in Chapter 1.1.3, the most important and specific index for evaluating the self-healing properties of self-healing ceramics is the available healing temperature range, T_H. In this study, characteristics of self-healing in ceramics and T_H of self-healing ceramics reported previously are reviewed in order of the properties discussed in Chapter 1.2.1. The classification of self-healing ceramics is shown in Figure 1.11, and their T_H are listed in Figure 1.12.

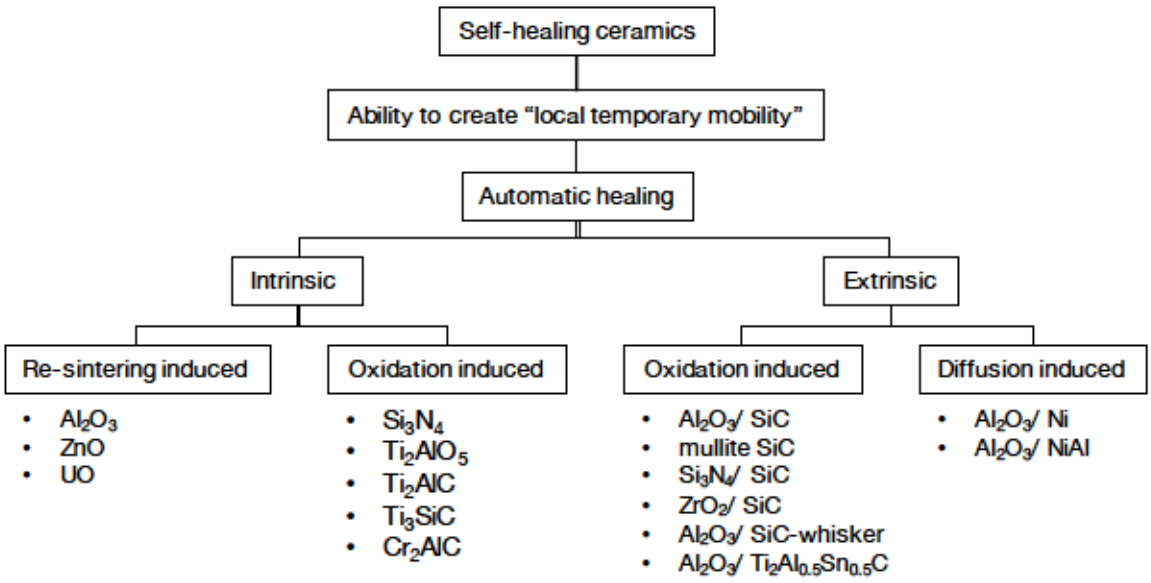

Figure 1.11 Classification of Previously Reported Self-healing Ceramics

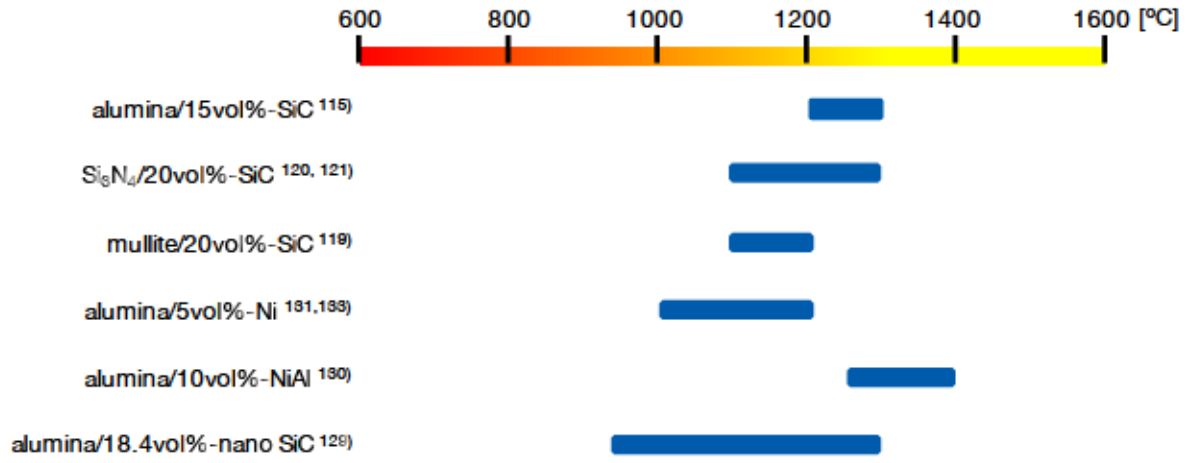

Figure 1.12 Healable Temperature Range *T*_ of Several Previously Reported Self-healing Ceramics

All previously reported self-healing ceramics are able to create local temporary mobility and to induce automatic self-healing. The local condition is met by selective oxidation of crack surfaces created in bulk non-oxide matrices or by healing agents dispersed in the oxide matrix. Mobility is attained by formation and growth of oxides. In most cases, the mobility phase is solid, but the phase does sometimes show high viscosity. The temporary condition is also met because the oxidation reaction completes when the healing agents on the crack surfaces have been consumed. Reactions can also become slower due to the creation of a sufficient protective oxidized layer on the surface. Some researchers suggest that the temporary condition is attained in the period between the melting of formed oxides due to local temperature increases and the solidification of the oxides due to the completion of oxidation reaction). In all cases, the temporary condition corresponds to the state of the oxidation reaction. In addition, all self-healing ceramics induce automatic self-healing because the oxidation reaction begins as soon as non-oxides are exposed to high temperature air.

Self-healing in ceramic materials can also divided into intrinsic and extrinsic categories. Intrinsic self-healing in ceramics such as Al_2O_3[93-98], ZnO[99], UO_2[100, 101] and MgO[98] has been reported since the pioneering research on self-healing materials in the late 1960s. Matsuo et al. reported that the strength of Al_2O_3 containing micro-cracks on its surface due to machining was recovered by annealing. In this research period, the term 'crack-healing' was used to explain the phenomenon during which the crack was closed. In those oxide ceramics, the crack closure was not induced by oxidation but by the re-sintering of the ceramics. Hence, we identify those materials as re-sintering induced self-healing ceramics. Re-sintering induced self-healing ceramics meet all the requirements for self-healing materials as discussed above, but their self-healing ability is quite limited because the diffusion of atoms for sintering requires temperatures mostly above 1400°C, and the diffusion rate is low.

Intrinsic oxidation-induced self-healing in ceramics was subsequently reported[102-112]. The self-healing mechanism schematic is shown in Figure 1.13. In contrast to the extrinsic

oxidation-induced self-healing ceramics represented in Figure 1.9, the composites in Figure 1.13 induce self-healing by the automatic oxidation of non-oxides. In early stages of research into the ceramics, the self-healing abilities of Ti_2AlO_5[102] and Si_3N_4[103] have been discussed. The crack closure in Si_3N_4 is achieved by the SiO_2,which is formed by the oxidation of Si_3N_4 itself. In Ti_2AlO_5, the mechanical strength is recovered due to the filling of cracks by the formation of Al_2O_3 and TiO_2. In recent years, there has been a lot of research into the intrinsic self-healing in metallo-ceramics (MAX phase materials)[104-112]. The general formula of MAX phase materials is written as $M_{n+1}AX_n$, where n=1, 2 or 3, M is an early transition metal, A is an A group element (mostly Al or Si), and X is C or N. The MAX phase compounds have an atomic layered and a hexagonal crystal structure. The crystal unit cell contains two sub units, i.e., the $M_{n+1}X_n$ layer and the pure A layer, forming an ABABAB structure. Due to the structure, MAX phase compounds show a unique oxidation behaviour. Within high temperature oxygen containing gases, the pure A layer is oxidized as priority, resulting in oxidative decomposition. As a result of this reaction, MAX phase material demonstrates intrinsic self-healing of surface cracks.

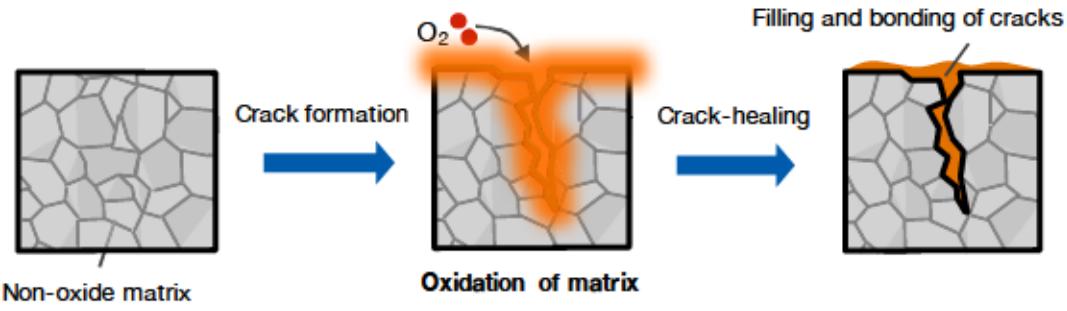

Figure 1.13 Schematic Illustration of Self-healing Mechanism of Intrinsic Oxidation Induced Self-healing Ceramics

The reaction is induced by oxidation of non-oxides matrix itself.

In contrast, earlier works on extrinsic self-healing ceramic systems focused on the oxidation of granular SiC particles embedded in several oxidic ceramic matrices[113-37]. The self-healing mechanism of the composite is already explained in Section 1.1.3.2, Figure 1.9. In the early stage, Harmer et al. observed that indentation-induced cracks in alumina/
5 vol.% SiC could be healed partially by means of annealing at 1300°C for 2h[113-114]. It was also noted that the formed SiO_2 could not seal the pre-cracks fully due to the low SiC particle content. Ando et al. were the first to report in detail on the self-healing behaviour of SiC particles containing alumina matrix composites as a function of temperature and annealing time[115-117]. It was shown that alumina/ 15 vol.%-SiC composites can attain a complete strength recovery by annealing in air at 1300°C for 1h or at 1200°C for 10h[23]. Ando et al. demonstrated that other structural ceramic matrix composites containing SiC particles as self-healing agents, such as mullite/SiC[118,119], Si_3N_4/SiC[120,121] and ZrO_2/SiC[122, 123], also show self-healing behaviour. It was demonstrated that mullite-based composites containing 20 vol.% of SiC particles could achieve complete strength recovery by various heat treatments at relatively high temperatures, such as annealing for 5h at 1200°C or for 1h at

1300°C[119]. In contrast, Si_3N_4/20 vol.%-SiC and ZrO_2/20vol.%-SiC composites recovered their room-temperature strength by annealing at relatively low temperatures, with the Si_3N_4/ SiC composite annealing at 1000°C for 1h[121] and the ZrO_2/SiC composite annealing at 800°C for 30h[122]. However, it was also observed that Si_3N_4/SiC specimens annealed above 1400°C and ZrO_2/SiC specimens annealed above 1000°C lose their mechanical properties due to excessive corrosion. In general, relatively high annealing temperatures (above 1200°C) are generally required for adequate oxidation of SiC particles in order to seal the crack gap and to recover the mechanical integrity of the ceramic matrix composites.

Several methodologies have been proposed with the goal of enhancing the crack healing ability of SiC containing composites. The first attempt involved the inclusion of SiC whiskers to simultaneously improve the fracture toughness (K_{Ic}) and self-healing ability of the composite[124-127]. Nakao et al.[126] observed that the K_{IC} value of 20 vol.% SiC whisker containing alumina based composites (K_{IC}=5.6 - 5.7 ± 0.2 MPa · $m^{1/2}$) is considerably higher than that of monolithic alumina (K_{IC}=3 - 4 MPa · $m^{1/2}$). Furthermore, it was found that, for alumina with a 20 vol.% of SiC whiskers, the minimum healing temperature at which the strength of the composite can recover within 1h is 100°C lower than that of alumina/granular SiC composites. The effect was attributed to the larger surface area of the SiC whiskers per unit of volume. An alternative method to enhance the healing ability is the downsizing of the healing agent[128, 129]. Nakao et al. reported that alumina composites containing 18 vol.% of nano-SiC particles having a diameter of 10-30 nm can attain full strength recovery within 10h when annealing at 950°C[129]. Depending on the morphology and size of the SiC fraction, the minimum required temperature for the complete strength recovery falls within a range of 950 °C to 1300°C.

Recently, new self-healing composites classified as diffusion-induced self-healing ceramics have been proposed. In those self-healing ceramics, crack healing is induced by both the oxidation of the healing agents and by the diffusion of Ni cations, as shown in Figure 1.14. Abe et al. developed alumina/10 vol.% NiAl composites which can heal cracks within 10h in 1250°C[130]. Nanko et al. proposed the use of nano-Ni powder as a healing agent[131-133], and Maruoka et al. observed that alumina/5 vol.% nano-Ni composites can attain full strength recovery by annealing for 1h at 1200°C[133].

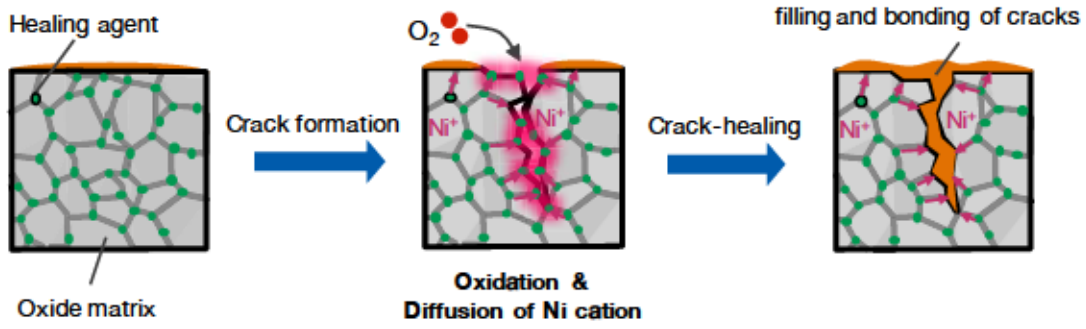

Figure 1.14 Schematic Illustration of Self-healing Mechanism of Intrinsic Oxidation-Induced Self-healing Ceramics

Crack healing is induced by the oxidation of healing agents and primarily by the diffusion of cation.

1.2.3 Required Properties for Healing Agents in Extrinsic Oxidation-Induced Self-healing Ceramics

As reviewed above, several self-healing ceramics have already been proposed, each with its own self-healing mechanism and characteristic properties such as T_H. However, the research and development of self-healing ceramics has been primarily advanced by the process of trial and error, and this has caused delays in the implementation of self-healing ceramics. In order to disrupt the current status quo, it is critical to establish a material design strategy.

In this study, the effects of the chemical properties of healing agents will be discussed, as will their reaction behaviour on self-healing behaviour, ultimately aiming toward the establishment of the material design strategy for extrinsic oxidation-induced self-healing ceramics. This is because extrinsic self-healing can only be induced using the chemical reactions of the healing agents.

Based on the discussions above, it is proposed that self-healing phenomena in composites can be divided into dormant, active and transition states as shown in Figure 1.15. The stage are defined as follows:

1. **Dormant State**
   This state is defined as the state in which damage formation has not yet resulted in the exposure of healing agents to high temperature air.

2. **Active State**
   This state, also known as the mobile phase, is defined as the period between the onset and completion of the oxidation reactions of healing agents on the crack surfaces resulting from exposure to high temperature air and triggered by damage formation.

3. **Transition State**
   This state is defined as the period between completion of the mobile phase oxidation reactions and the completion of chemical bond re-establishment between the newly formed oxide and the matrix.

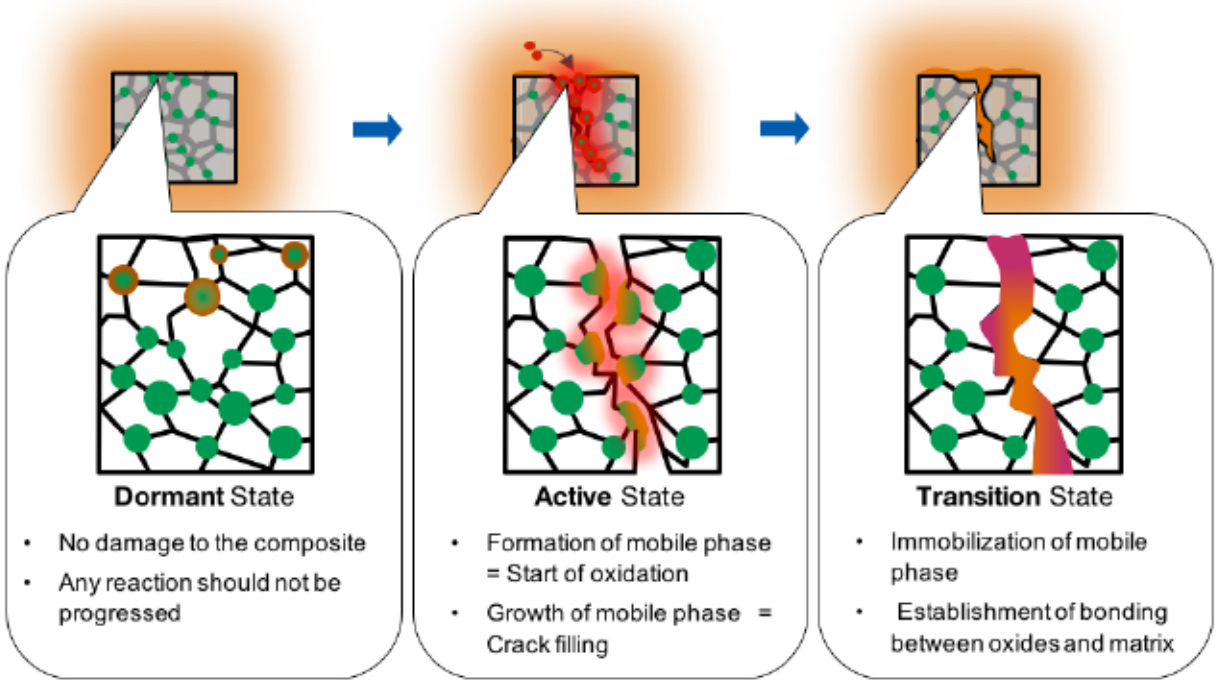

Figure 1.15 Schematic Illustration of Self-healing Phenomena Divided Into Three States

The dormant state is the default state of self-healing ceramics in high temperature operating conditions. There is no damage to the composite, but the composite is constantly exposed to a severely corrosive atmosphere. In this state, undesirable reactions should be avoided and healing agents should be intact. Undesirable reactions can include phase transformations of healing agents such as melting or evaporation, reactions (solution, oxidation, or reduction types) between healing agents and oxide matrices, and internal oxidation of self-healing agents. Undesirable reactions within the dormant state will deteriorate the material's self-healing ability and ultimately determine the lifetime of the material. To prevent this type of damage, the upper limit of the healing temperature range ($T_{\text{H-high}}$) should be related to this state.

The active state is the most important state within the self-healing process. Once damage to the self-healing ceramic occurs, the state of the composite shifts from the dormant state to the active state automatically. Behaviour of the composite in the active state is dominated by the oxidation behaviour of the healing agents, including such attributes as oxidation starting temperature, reaction heat and volume expansion upon oxidation. The initial strength recovery should correspond to the oxidation starting temperature of the healing agent, and by extension the lower limit of healing temperature range ($T_{\text{H-low}}$) should be related to this state. The strength recovery behaviour of the composite is dominated by the growth behaviour of formed oxides until complete strength recovery has occurred.

The transition state determines whether the composite can recover its mechanical strength completely. Although the introduced crack is filled with formed oxide, the strength of the composite can never be recovered if there is no interaction between the formed oxide and the matrix in the filled region. In this state, the properties of the healing agents, the formed oxide and the matrix should all be

considered.

As shown above, many chemical properties of the healing agents can affect each state of self-healing in oxidation-induced self-healing ceramics, and each self-healing state corresponds to the healing temperature range (T_H). The upper and lower limit of T_H, $T_{H\text{-high}}$ and $T_{H\text{-low}}$, can be quantitatively evaluated by clarifying the effect of these chemical properties on each self-healing state.

1.3. Purpose of the Study and Structure of the Thesis

This study aims to clarify the effects of the chemical properties of healing agents on self-healing ability. Based on the results, the material design strategy for oxidation-induced self-healing ceramics can be established. The objectives of the study are as follows:

1) **Clarification of the relationship between the oxidation behaviour of healing agents and the strength recovery behaviour of self-healing ceramics**
    a. Based on the results, the methodology for evaluating the lower limit temperature of the healing temperature range ($T_{H\text{-low}}$) is proposed.
2) **Clarification of the effect of cation in healing agents on self-healing behaviour**
3) **Clarification of the deterioration factor of self-healing ability.**
    a. Based on the result, the methodology for evaluating the upper limit temperature of the healing temperature range ($T_{H\text{-high}}$) is proposed.
4) **Clarification of the effects of interface conditions between matrices and crack-filling oxides on strength recovery behaviour in self-healing ceramics**

The present thesis contains six chapters and abstracts of each chapters are described below.

Chapter 1 Introduction

This chapter described the impacts of the study on both the scientific and industrial fields. Current development status and practical issues of high temperature structural materials used in transportation were investigated, and social requirements in the materials development were discussed. The promise of implementing self-healing ceramics in place of their classical counterparts was also described. To bring the study to a wider scientific context, the self-healing ceramics proposed earlier were organized by following the research and development of self-healing materials. The current issue in the field of self-healing ceramics was extracted from those discussions, and the purpose of the study was described.

Chapter 2 Methodology for Evaluating Healing Agents for Oxidation-induced Self-healing Ceramics

The chapter deals with the methodology for evaluating lower limit temperatures of the

healing temperature range ($T_{H\text{-}low}$). The methodology is proposed from the quantitatively evaluated relationship between oxidation behaviour of the healing agents and the strength recovery behaviour of self-healing ceramics. The estimated value of the lower limit ($T_{H\text{-}low}^{est}$) is determined from thermogravimetric analysis, and the experimental value ($T_{H\text{-}low}^{exp}$) is derived from strength recovery testing of self-healing ceramics. The estimated value ($T_{H\text{-}low}^{est}$) compares well with the experimental value ($T_{H\text{-}low}^{exp}$) in the case of the mullite/$TiSi_2$ composite and the alumina/SiC composite. It is shown that the proposed methodology is sufficient for evaluating the viability of healing agents.

Chapter 3 Effects of Cation in Healing Agents on Self-healing Behaviour

In this chapter, the presence of Ti cation in healing agents on and its effect on self-healing behaviour is studied. The effect is clarified through strength recovery tests and direct observation of the crack-healing area in the alumina/TiC composite. The selection of TiC is based on the proposed method described in Chapter 2. The introduced crack is sufficiently filled with TiO_2 and the strength of the composite returns to its original strength within 1h by annealing at 800°C. This result clearly shows the viability of healing agent containing Ti cation for lower temperature applications. The outward diffusion of Ti cation is observed at the higher temperature of 1000°C. The outward diffusion induces crack-healing for wider cracks, but also leads to strength deterioration.

Chapter 4 Methodology for Evaluating the Lifetime of Self-healing Ability

This chapter deals with the methodology for evaluating upper limit temperatures of the healing temperature range ($T_{H\text{-}high}$). Self-healing ceramics should maintain their self-healing ability even when constantly exposed to a high temperature atmosphere. However, in such severe conditions, healing agents embedded within the matrix can deteriorate due to inward diffusion of oxygen. In this chapter, it is shown that the self-healing ability has disappeared in the formed internal oxidation layer through the strength recovery test on alumina/SiC composite aged at 1200°C for 1000h. This indicates that the life span of self-healing ability can be evaluated as a function of the growth rate of the internal oxidation layer. Based on the results, the methodology for evaluating the upper limit temperature of the healing temperature range ($T_{H\text{-}high}$) is proposed.

Chapter 5 Interface Design between Matrices and Crack Filling Oxides

This chapter deals with the effects of interface conditions between matrices and crack-filling oxides on the strength recovery behaviour of self-healing ceramics. The effect is discussed based on the results of strength recovery testing of the alumina/TiC composite as a function of annealing time. The strength recovery of the composite at 600°C shows an almost constant value of 50% regardless of annealing time, even though the pre-crack is totally filled with the formed oxide TiO_2. The intermediate compound, Al_2TiO_5, is not detected below 600°C where the value of strength recovery is saturated. The results imply that the formation of intermediate compounds at crack-healed area plays an important role in achieving a desirable bond at the point of interface between matrices and formed

oxides, resulting in the complete strength recovery of self-healing ceramics. Based on those discussions, the methodology is proposed to allow for the evaluation of oxide matrices in which desirable interface bonding can be attained.

Chapter 6 Conclusion

This chapter concludes this study and offers suggestions for further research. In Chapters 2 and 4, methodologies for evaluating the upper and lower limit of the healing temperature range (T_H) are proposed. Additional practical methodologies for customizing healing agents utilizing cation and interface design are described in Chapters 3 and 5. By integrating those proposed methods, an advanced self-healing ceramics which shows desirable self-healing under the specific operation conditions of high temperature structural materials can be designed. Throughout the study, the fundamental design strategies for oxidation-induced self-healing ceramics are proposed.

References

1) Ministry of the Environment, Japan Greenhouse Gas Inventory Office of Japan (GIO), CGER, NIES. (2016). National Greenhouse Gas Inventory Report of JAPAN 2016: Available from: http://www-gio.nies.go.jp/aboutghg/nir/2016/NIR-JPN-2016-v3.0_rev_web.pdf
2) Ministry of Land, Infrastructure, Transport and Tourism. (2014). CO_2 emissions from transportation sector in Japan. (In Japanese): Available from: http://www.mlit.go.jp/sogoseisaku/environment/sosei_environment_tk_000007.html
3) Ministry of Economy, Trade and Industry. (2016). Jidōsha sangyo wo meguru kōzō henka to sono taiō ni tsuite [Structural change in automotive industry and the countermeasure]. (In Japanese): Available from: http://www.meti.go.jp/policy/economy/keiei_innovation/sangyokinyu/GB/04.pdf
4) Ibuki, H. (2016). Jidōsha sangyo wo meguru kōzō henka to sono taiō ni tsuite [Structural change in automotive industry and the countermeasure]. *Monthly Report of Japan Foreign Trade Council*, (745), 7-11. (In Japanese).
5) Japan Automobile Manufacturers Association, (2009). Sekai no dōro kōtsu sector ni okeru CO_2 sakugen torikumi no teigen [Proposal on approach for CO_2 reduction at world road traffic sector]. (In Japanese): Available from: http://www.jari.or.jp/Portals/0/resource/uploads/b2948d8b2dfb705c6d47ab668a2c9d62.pdf
6) Arthur D. Little Japan, New Energy and Industrial Technology Development Organization. (2015). Shatai keiryōka ni kakawaru kōzō zairyō, kōzō gijyutsu ni kansuru kadai to kaihatsu shishin no kentō [Issues in structural materials and technologies for weight reduction of automotive and their development strategy]. (In Japanese): Available from: http://www.nedo.go.jp/content/100751047.pdf
7) Taka, Y. (2014). Automobiles and Materials (2nd Report) Reduction of Automobile Weight *Journal of Nakanihon Automotive College*, (44), 19-33. In Japanese.
8) Noda, S. (2003). Saisentan no jitsuyō tainetsu zairyō – jidōsha oyobi hatsuden yō turbine de mochi'irareru tainetsu zairyō [Advanced practical high-temperature materials: high-temperature materials in automotive and Power generation turbine]. *Materia Japan*, *42*(4), 271-275.
9) Hagiwara, Y., Ishida, M., Oka, T., Watanabe, R., & Koji, S. (1991). Development of nickel-base superalloy for exhaust valves (No. 910429). *SAE Technical Paper*.
10) Tominaga, K., Shimizu, T. & Ueda, S. (2007). Development of heat-resistant nickel-based super alloy for exhaust valve. *Honda R&D technical review*, *19*(2), 55-60. (In Japanese)
11) Suzuki, A., Noda, S. & Okabe, M. (2002). Corrosion and Heat Resistant Materials. Effect of Microstructures on Mechanical Properties of a Heat Resistant Titanium Alloy Ti-6242S at Elevated Temperatures. *Denki Seiko*, *73*(2), 107-112. (In Japanese).
12) Wu, X. (2006). Review of alloy and process development of TiAl alloys. *Intermetallics*, *14*(10), 1114-1122.
13) Yamaguchi, M., Inui, H., & Ito, K. (2000). High-temperature structural intermetallics. *Acta materialia*, *48*(1), 307-322.
14) Inoue, Y., & Kikuchi, M. (2003). Present and future trends of stainless steel for automotive

exhaust system. *High-temperature*, *950*, 750.

15) Matsumoto, K., Tojo, M., Jinnai, Y., Hayashi, N., & Ibaraki, S. (2008). Development of compact and high-performance turbocharger for 1,050 C exhaust gas. *Mitsubishi Heavy Industries Technical Review*, *45*(3).
16) Airbus. (2013). Global market forecast 2013-2032: Available from: http://www.airbus.com/company/market/global-market-forecast-2016-2035/
17) Boeing. (2015). Current market outlook 2015-2034: Available from: http://www.boeing.com/resources/boeingdotcom/commercial/about-our-market/assets/downloads/Boeing_Current_Market_Outlook_2015.pdf
18) Airbus. (2016). Global market forecast 2016-2035: Available from: http://www.airbus.com/company/market/global-market-forecast-2016-2035/
19) International Civil Aviation Organization. (2013). Global Air Transport Outlook to 2030 and Trends to 2040 (ICAO Cir 333): Short summary is available from: http://www.icao.int/Meetings/Regional-Symposia/LCC-China2013/Documents/Presentations/YWang_Global.pdf
20) Group on International Aviation and Climate Change (GIACC). (2009). Global aviation CO_2 emissions projections to 2050. *Fourth Meeting of the Group on International Aviation and Climate Change (GIACC/4)*: Available from: http://www.icao.int/environmental-protection/GIACC/Giacc-4/Giacc4_ip01_en.pdf
21) International Civil Aviation Organization. (2010). ICAO Environment report 2010: Available from: http://www.icao.int/environmental-protection/Pages/EnvReport10.aspx
22) International Civil Aviation Organization. (2016). ICAO Environment report 2016: Available from: http://www.icao.int/environmental-protection/Pages/env2016.aspx
23) International Civil Aviation Organization. (2009). ICAO Programme of Action on International Aviation and Climate Change. *High-Level Meeting on International Aviation and Climate Change*: Agenda is available from: http://www.icao.int/environmental-protection/Pages/programme-of-action.aspx
24) Miura, N. (2012). Trend of heat resistant alloys for aero engine applications. *Denki Seiko*, *83*(1), 36.
25) Sato, A., Harada, H., Yeh, A. C., Kawagishi, K., Kobayashi, T., Koizumi, Y., ... & Zhang, J. X. (2008). A 5th generation SC superalloy with balanced high temperature properties and processability. Superalloys, 131-138.
26) Koizumi, Y., Kobayashi, T., Yokokawa, T., Osawa, M., Harada, H., Hino, T., & Yoshioka, Y. (2003). Creep strengths of a Ni-base single crystal superalloy TMS-82+ and its tie-line alloys. Journal of the Japan Institute of Metals, 67(4), 205-208.
27) Padture, N. P., Gell, M., & Jordan, E. H. (2002). Thermal barrier coatings for gas-turbine engine applications. Science, 296(5566), 280-284.
28) Han, J. C. (2004). Recent studies in turbine blade cooling. International Journal of Rotating Machinery, 10(6), 443-457.

29) Guedou, J. Y., & Villaroche, S. (2010). Materials Evolution in Hot parts of aero-turbo-engines. *Proceedings of the 27th International Congress of the Aeronautical Sciences*.
30) Okada, A., Kameyama, T., Hojo, J. (2008). Technological Innovation in Ceramics: Silicon Nitride for Automotive Technology. *Proceedings of the 4th International Symposium "Technological Innovations in Japan–Research on the History of Technology by Engineers–"*. (In Japanese).
31) Hatano, K. (1954). Senjika Doitsu no turbine yō yōgyō seihin no kenkyū – PB kagaku report ni yoru [Study on ceramics for turbine blades developed in Germany during WW2 – from PB chemical report]. Yogyo-Kyokai-Shi, 62(701), 674-678. (In Japanese). doi:10.2109/jcersj1950.62.701_674
32) Jack, K. H. (1986). Ceramics and Civilization, Vol. III: High-Technology Ceramics. *American Ceramic Society*, Columbus, OH, 259.
33) Deeley, G. G., Herbert, J. M., & Moore, N. C. (1961). Dense silicon nitride. Powder metallurgy, 4(8), 145-151.
34) Van Reuth, E. C. (1974). The Advanced Research Projects Agency's Gas Turbine Program. Ceramics for High Performance Applications, Brook Hill Inc, Chestnut Hill, Mass, 1-8.
35) Industrial Technology Council. (1999). "Ceramic gas turbine kēkaku" saishū hyōka hōkoku sho ["Ceramic gas turbine project" Final evaluation report]. *Sangyo gijyutsu shingikai hyoka bukai ceramic gas turbine gijyutsu kaihatsu hyōka i'inkai*. (In Japanese).
36) Iki, N., Matsunuma, T., Yoshida, H., Sodeoka, S., Inoue, T., Suzuki, M. (2010). Tests and Future Tasks of a Small Gas Turbine with Ceramic Parts. *Journal of Gas Turbine Society of Japan*, 38(4), 259-264. (In Japanese).
37) Yoshida, Y. (2002). Current Status and Future Outlook of Micro Gas Turbine Technologies. *Journal of the Japan Society of Mechanical Engineers*, 105(1007), 693-697. (In Japanese).
38) Yoshida, T. (2001). Micro gas turbine no kaihatsu dōkō to shōrai tenbō [Development trend and future vision of macro gas turbine]. *NTS Inc*. (In Japanese).
39) Takata, H. (2003). Kogata ceramic gas turbine [Micro ceramic gas turbine]. *NTS Inc*.
40) Ogasawata, T. (2004). Recent Research Activities regarding SiC-Based Ceramic Composites for Aerospace Applications (<Special Topic Article>Perspectives of SiC-Based Ceramic Composites and Their Applications to Fusion Reactors). *Journal of Plasma and Fusion Research*, 80(1), 36-41.
41) Ceramic gas turbine gijyutsu kaihatsu hyōka i'inkai. (1999). "Chō onsoku yusōki yō suishin system kaihatsu project" ["Project on development of propulsion system for supersonic transport"]. *Sangyo gijyutsu shingikai hyoka bukai*. (In Japanese).
42) New Energy and Industrial Technology Development Organization. (2004). "Kankyō tekiō gata jisedai chō onsoku suishin system no kenkyū kaihatsu" jigo hyōka houkoku sho [Final evaluation report on the project "Development of environmentally considerate next generation supersonic propulsion system"] : (In Japanese): Available from: http://www.nedo.go.jp/introducing/iinkai/kenkyuu_bunkakai_16h_jigo_9_1_index.html
43) Ishizaki, M. (2007). Koukū uchū yō kō'on buzai muke ceramic ki fukugō zairyō [Ceramic matrix composite for high-temperature material in aerospace engineering]. *Ceramics*, 42(12), 967-969. (In Japanese).
44) Japan Science and Technology Agency. (2014). Warenai ceramics de jet engine wo tsukuru

[Development of jet engine parts with unbreakable ceramic]. *JST News*. (In Japanese).

45) Koga, K. (2007). Dan'netsu diesel engine [Adiabatic diesel engine]. *Ceramics*, 42(9), 668-671. (In Japanese).

46) Harada, H., Yokokawa, T., Sato, A., Kawagishi, K., GU, Y. (2007). High Temperature Turbine Materials Development in NIMS: The Present and Future (<Special Issue>"New Developments in Japanese-made Aeroengines". *Journal of High-Temperature Society*, 33(5), 237-243.

47) Zwaag, S. (Ed.). (2008). Self-healing materials: an alternative approach to 20 centuries of materials science. Springer Science+ Business Media BV.

48) Lange, F. F. (1989). Powder processing science and technology for increased reliability. Journal of the American Ceramic Society, 72(1), 3-15.

49) Lewis, J. A. (2000). Colloidal processing of ceramics. Journal of the American Ceramic Society, 83(10), 2341-2359.

50) Sigmund, W. M., Bell, N. S., & Bergström, L. (2000). Novel Powder-Processing Methods for Advanced Ceramics. Journal of the American Ceramic Society, 83(7), 1557-1574.

51) Messing, G. L., Zhang, S. C., & Jayanthi, G. V. (1993). Ceramic powder synthesis by spray pyrolysis. Journal of the American Ceramic Society, 76(11), 2707-2726.

52) Harmer, M. P., Chan, H. M., & Miller, G. A. (1992). Unique opportunities for microstructural engineering with duplex and laminar ceramic composites. Journal of the American Ceramic Society, 75(7), 1715-1728.

53) Clegg, W. J. (1992). The fabrication and failure of laminar ceramic composites. Acta metallurgica et materialia, 40(11), 3085-3093.

54) Chartier, T., Merle, D., & Besson, J. L. (1995). Laminar ceramic composites. Journal of the European Ceramic Society, 15(2), 101-107.

55) Chan, H. M. (1997). Layered ceramics: processing and mechanical behavior. Annual review of materials science, 27(1), 249-282.

56) Bao, G., & Wang, L. (1995). Multiple cracking in functionally graded ceramic/metal coatings. International Journal of Solids and Structures, 32(19), 2853-2871.

57) Jha, D. K., Kant, T., & Singh, R. K. (2013). A critical review of recent research on functionally graded plates. Composite Structures, 96, 833-849.

58) Niihara, K., Nakahira, A., & Sekino, T. (1992). New nanocomposite structural ceramics. In MRS Proceedings (Vol. 286, p. 405). Cambridge University Press.

59) Sternitzke, M. (1997). Structural ceramic nanocomposites. Journal of the European Ceramic Society, 17(9), 1061-1082.

60) Ibrahim, I. A., Mohamed, F. A., & Lavernia, E. J. (1991). Particulate reinforced metal matrix composites—a review. Journal of materials science, 26(5), 1137-1156.

61) Wei, G. C., & Becher, P. F. (1985). Development of SiC-whisker-reinforced ceramics. Am. Ceram. Soc. Bull.;(United States), 64.

62) Becher, P. F. (1991). Microstructural design of toughened ceramics. Journal of the American Ceramic Society, 74(2), 255-269.

63) Brennan, J. J., & Prewo, K. M. (1982). Silicon carbide fibre reinforced glass-ceramic matrix composites exhibiting high strength and toughness. Journal of Materials Science, 17(8),

2371-2383.

64) Prewo, K. M., Brennan, J. J., & Layden, G. K. (1986). Fiber reinforced glasses and glass-ceramics for high performance applications. American Ceramic Society Bulletin, 65(2), 305-322.

65) Evans, A. G., & Marshall, D. B. (1989). Overview no. 85 The mechanical behavior of ceramic matrix composites. Acta Metallurgica, 37(10), 2567-2583.

66) Wu, D. Y., Meure, S., & Solomon, D. (2008). Self-healing polymeric materials: a review of recent developments. Progress in Polymer Science, 33(5), 479-522.

67) Blaiszik, B. J., Kramer, S. L. B., Olugebefola, S. C., Moore, J. S., Sottos, N. R., & White, S. R. (2010). Self-healing polymers and composites. Annual Review of Materials Research, 40, 179-211.

68) Thakur, V. K., & Kessler, M. R. (2015). Self-healing polymer nanocomposite materials: A review. Polymer, 69, 369-383.

69) Hautakangas, S., Schut, H., Van Dijk, N. H., del Castillo, P. R. D., & van der Zwaag, S. (2008). Self-healing of deformation damage in underaged Al–Cu–Mg alloys. Scripta Materialia, 58(9), 719-722.

70) He, S. M., Van Dijk, N. H., Schut, H., Peekstok, E. R., & Van der Zwaag, S. (2010). Thermally activated precipitation at deformation-induced defects in Fe-Cu and Fe-Cu-BN alloys studied by positron annihilation spectroscopy. Physical Review B, 81(9), 094103.

71) Wu, M., Johannesson, B., & Geiker, M. (2012). A review: Self-healing in cementitious materials and engineered cementitious composite as a self-healing material. Construction and Building Materials, 28(1), 571-583.

72) Van Tittelboom, K., & De Belie, N. (2013). Self-healing in cementitious materials—A review. Materials, 6(6), 2182-2217.

73) Joseph, C., Gardner, D., Jefferson, T., Isaacs, B., & Lark, B. (2010). Self-healing cementitious materials: a review of recent work. Proceedings of the Institution of Civil Engineers-Construction Materials, 164(1), 29-41.

74) Zwaag, S. (Ed.). (2008). Self-healing materials: an alternative approach to 20 centuries of materials science. Springer Science+ Business Media BV.

75) Van der Zwaag, S., Van Dijk, N. H., Jonkers, H. M., Mookhoek, S. D., & Sloof, W. G. (2009). Self-healing behaviour in man-made engineering materials: bioinspired but taking into account their intrinsic character. Philosophical Transactions of the Royal Society of London A: Mathematical, Physical and Engineering Sciences, 367(1894), 1689-1704.

76) Ghosh, S. K. (Ed.). (2009). Self-healing materials: fundamentals, design strategies, and applications. John Wiley & Sons.

77) Hager, M. D., Greil, P., Leyens, C., van der Zwaag, S., & Schubert, U. S. (2010). Self-Healing Materials. Advanced Materials, 22(47), 5424-5430.

78) van der Zwaag, S., & Brinkman, E. (Eds.). (2015). Self-Healing Materials: Pioneering Research in the Netherlands. IOS Press.

79) White, S. R., Sottos, N. R., Geubelle, P. H., Moore, J. S., Kessler, M., Sriram, S. R., ... & Viswanathan, S. (2001). Autonomic healing of polymer composites. Nature, 409(6822),

794-797.

80) Jonkers, H. M., Thijssen, A., Muyzer, G., Copuroglu, O., & Schlangen, E. (2010). Application of bacteria as self-healing agent for the development of sustainable concrete. Ecological engineering, 36(2), 230-235.

81) Shinya, N., Kyono, J., & Laha, K. (2006). Self-healing effect of boron nitride precipitation on creep cavitation in austenitic stainless steel. Journal of intelligent material systems and structures, 17(12), 1127-1133.

82) Samadzadeh, M., Boura, S. H., Peikari, M., Kasiriha, S. M., & Ashrafi, A. (2010). A review on self-healing coatings based on micro/nanocapsules. Progress in Organic Coatings, 68(3), 159-164.

83) García, Á., Schlangen, E., van de Ven, M., & van Bochove, G. (2012). Optimization of composition and mixing process of a self-healing porous asphalt. Construction and Building Materials, 30, 59-65.

84) Kim, Y. H., & Wool, R. P. (1983). A theory of healing at a polymer-polymer interface. Macromolecules, 16(7), 1115-1120.

85) Takeda, K., Unno, H., & Zhang, M. (2004). Polymer reaction in polycarbonate with Na2CO3. Journal of applied polymer science, 93(2), 920-926.

86) Kalista Jr, S. J., Ward, T. C., & Oyetunji, Z. (2007). Self-healing of poly (ethylene-co-methacrylic acid) copolymers following projectile puncture. Mechanics of advanced materials and structures, 14(5), 391-397.

87) Varley, R. J., & van der Zwaag, S. (2008). Towards an understanding of thermally activated self-healing of an ionomer system during ballistic penetration. Acta Materialia, 56(19), 5737-5750.

88) Chen, X., Dam, M. A., Ono, K., Mal, A., Shen, H., Nutt, S. R., ... & Wudl, F. (2002). A thermally re-mendable cross-linked polymeric material. Science, 295(5560), 1698-1702.

89) Park, J. S., Darlington, T., Starr, A. F., Takahashi, K., Riendeau, J., & Hahn, H. T. (2010). Multiple healing effect of thermally activated self-healing composites based on Diels–Alder reaction. Composites Science and Technology, 70(15), 2154-2159.

90) Liu, Y. L., & Chen, Y. W. (2007). Thermally reversible cross-linked polyamides with high toughness and self-repairing ability from maleimide-and furan-functionalized aromatic polyamides. Macromolecular Chemistry and Physics, 208(2), 224-232.

91) Cordier, P., Tournilhac, F., Soulié-Ziakovic, C., & Leibler, L. (2008). Self-healing and thermoreversible rubber from supramolecular assembly. Nature, 451(7181), 977-980.

92) Herbst, F., Döhler, D., Michael, P., & Binder, W. H. (2013). Self-Healing Polymers via Supramolecular Forces. Macromolecular rapid communications, 34(3), 203-220.

93) Heuer, A. H., & Roberts, J. P. (1966). The influence of annealing on the strength of corundum crystals. In Proc. Br. Ceram. Soc, 6, 17-27.

94) Lange, F. F., & Radford, K. C. (1970). Healing of surface cracks in polycrystalline Al2O3. Journal of the American Ceramic Society, 53(7), 420-421.

95) Davies, L. M. (1966). The effect of heat treatment on the tensile strength of sapphire. In Proc.

Brit. Ceram. Soc, 6(1), 29-35.

96) Evans, A. G., & Charles, E. A. (1977). Strength recovery by diffusive crack healing. Acta Metallurgica, 25(8), 919-927.

97) Matsuo, Y., Ogasawara, T., Kimura, S., Sato, S., Yasuda, E. (1991). The Effects of Annealing on Surface Machining Damage of Alumina Ceramics. Journal of the Ceramic Society of Japan, 99(1149), 384-389.

98) Gupta, T. K. (1976). Kinetics of Strengthening of Thermally Shocked MgO and Al2O3. Journal of the American Ceramic Society, 59(9-10), 448-449.

99) Lange, F. F., & Gupta, T. K. (1970). Crack healing by heat treatment. Journal of the American Ceramic Society, 53(1), 54-55.

100) J. T. A. Roberts, B. J. Wrona, "Crack Healing in UO_2," Journal of the American Ceramic Society, Vol.56, No. 6 (1973), pp. 297-299.

101) G. Bandyopadhyay, J. T. A. Roberts, "Crack Healing and Strength Recovery in UO_2," Journal of the American Ceramic Society, Vol.59, No. 9-10 (1976), pp. 415- 419.

102) Ohya, Y., Nakagawa, Z. E., & Hamano, K. (1988). Crack healing and bending strength of aluminum titanate ceramics at high temperature. Journal of the American Ceramic Society, 71(5).

103) Mitomo, M., Nishimura, T., & Tsutsumi, M. (1996). Crack healing in silicon nitride and alumina ceramics. Journal of materials science letters, 15(22), 1976-1978.

104) Song, G., Pei, Y., Sloof, W., Li, S., De Hosson, J. T. M., & Van der Zwaag, S. (2008). Oxidation-induced crack healing in Ti_3AlC_2 ceramics. *Scripta Materialia, 58*(1), 13-16.

105) Chen, G., Zhang, R., Zhang, X., Zhao, L., & Han, W. (2009). Oxidation-induced crack healing in $Zr_2Al_4C_5$ ceramic. *Materials & Design, 30*(9), 3602-3607.

106) Li, S., Song, G., Kwakernaak, K., van der Zwaag, S., & Sloof, W. G. (2012). Multiple crack healing of a Ti_2AlC ceramic. *Journal of the European Ceramic Society, 32*(8), 1813-1820.

107) Yang, H., Pei, Y., Rao, J., & De Hosson, J. T. M. (2012). Self-healing performance of Ti_2AlC ceramic. *Journal of Materials Chemistry, 22*(17), 8304-8313.

108) Li, S., Xiao, L., Song, G., Wu, X., Sloof, W. G., & van der Zwaag, S. (2013). Oxidation and Crack Healing Behavior of a Fine-Grained Cr_2AlC Ceramic. *Journal of the American Ceramic Society, 96*(3), 892-899.

109) Yang, H., Pei, Y., & De Hosson, J. T. M. (2013). Oxide-scale growth on Cr_2AlC ceramic and its consequence for self-healing. *Scripta Materialia, 69*(2), 203-206.

110) Farle, A.-S., Kwakernaak, C., van der Zwaag, S., & Sloof, W. G. (2015). A conceptual study into the potential of $M_{n+1}AX_n$-phase ceramics for self-healing of crack damage. *Journal of the European Ceramic Society, 35*(1), 37-45.

111) Li, S., Bei, G., Chen, X., Zhang, L., Zhou, Y., Mačković, M., Greil, P. (2016). Crack healing induced electrical and mechanical properties recovery in a Ti_2SnC ceramic. *Journal of the European Ceramic Society, 36*(1), 25-32.

112) Li, S., Li, H., Zhou, Y., & Zhai, H. (2014). Mechanism for abnormal thermal shock behavior of Cr_2AlC. *Journal of the European Ceramic Society, 34*(5), 1083-1088.
113) Thompson, A. M., Chan, H. M., Harmer, M. P., & Cook, R. E. (1995). Crack healing and stress relaxation in Al_2O_3 SiC "nanocomposites". *Journal of the American Ceramic Society, 78*(3), 567-571.
114) Chou, I. A., Chan, H. M., & Harmer, M. P. (1998). Effect of annealing environment on the crack healing and mechanical behavior of Silicon Carbide-reinforced alumina nanocomposites. *Journal of the American Ceramic Society, 81*(5), 1203-1208.
115) Ando, K., Kim, B. S., Chu, M. C., Saito, S., & Takahashi, K. (2004). Crack-healing and mechanical behaviour of Al_2O_3/SiC composites at elevated temperature. *Fatigue & Fracture of Engineering Materials & Structures, 27*(7), 533-541.
116) Ono, M., Nakao, W., Takahashi, K., Nakatani, M., & Ando, K. (2007). A new methodology to guarantee the structural integrity of Al_2O_3/SiC composite using crack healing and a proof test. *Fatigue & Fracture of Engineering Materials & Structures, 30*(7), 599-607.
117) Osada, T., Nakao, W., Takahashi, K., & Ando, K. (2009). Kinetics of Self-Crack-Healing of Alumina/Silicon Carbide Composite Including Oxygen Partial Pressure Effect. *Journal of the American Ceramic Society, 92*(4), 864-869.
118) Chu, M. C., Sato, S., Kobayashi, Y., & Ando, K. (1995). Damage healing and strengthening behaviour in intelligent mullite/SiC ceramics. *Fatigue & Fracture of Engineering Materials & Structures, 18*(9), 1019-1029.
119) Ando, K., Chu, M.-C., Tsuji, K., Hirasawa, T., Kobayashi, Y., & Sato, S. (2002). Crack healing behaviour and high-temperature strength of mullite/SiC composite ceramics. *Journal of the European Ceramic Society, 22*(8), 1313-1319.
120) Ando, K., Ikeda, T., Sato, S., Yao, F., & Kobayasi, Y. (1998). A preliminary study on crack healing behaviour of Si_3N_4/SiC composite ceramics. *Fatigue & Fracture of Engineering Materials & Structures, 21*(1), 119-122.
121) Ando, K., Chu, M., Yao, F., & Sato, S. (1999). Fatigue strength of crack-healed Si_3N_4/SiC composite ceramics. *Fatigue & Fracture of Engineering Materials & Structures, 22*(10), 897-903.
122) Houjou, K., Ando, K., & Takahashi, K. (2010). Crack-healing behaviour of ZrO_2/SiC composite ceramics. *International Journal of Structural Integrity, 1*(1), 73-84.
123) Houjou, K., & Takahashi, K. (2012). Crack-healing behavior of ZrO_2/SiC composite ceramics and strength properties of crack-healing specimens. *International Journal of Structural Integrity, 3*(1), 41-52.
124) Takahashi, K., Yokouchi, M., Lee, S. K., & Ando, K. (2003). Crack-healing behavior of Al_2O_3 toughened by SiC whiskers. *Journal of the American Ceramic Society, 86*(12), 2143-2147.
125) Nakao, W., Ono, M., Lee, S.-K., Takahashi, K., & Ando, K. (2005). Critical crack-healing condition for SiC whisker reinforced alumina under stress. *Journal of the European Ceramic Society, 25*(16), 3649-3655.

126) Nakao, W., Mori, S., Nakamura, J., Takahashi, K., Ando, K., & Yokouchi, M. (2006). Self-crack-healing behavior of Mullite/SiC particle/SiC Whisker multi-composites and potential use for ceramic springs. *Journal of the American Ceramic Society, 89*(4), 1352-1357.

127) Takahashi, K., Uchiide, K., Kimura, Y., Nakao, W., Ando, K., & Yokouchi, M. (2007). Threshold stress for crack healing of mullite reinforced by SiC whiskers and SiC particles and resultant fatigue strength at the healing temperature. *Journal of the American Ceramic Society, 90*(7), 2159-2164.

128) Nakao, W., Tsutagawa, Y., & Ando, K. (2008). Enhancement of in situ self-crack-healing efficient temperature region by SiC nanosizing. *Journal of Intelligent Material Systems and Structures, 19*(3), 407-410.

129) Wataru, N., & Shihomi, A. (2012). Enhancement of the self-healing ability in oxidation induced self-healing ceramic by modifying the healing agent. *Smart Materials and Structures, 21*(2), 025002.

130) Abe, O., Ohwa, Y., & Kuranobu, Y.-i. (2006). Possibility of enhanced strength and self-recovery of surface damages of ceramics composites under oxidative conditions. *Journal of the European Ceramic Society, 26*(4), 689-695.

131) Salas-Villaseñor, A. L., Lemus-Ruiz, J., Nanko, M., & Maruoka, D. (2009). Crack disappearance by high-temperature oxidation of alumina toughened by Ni nano-particles. *Advanced Materials Research,* 68, 34-43.

132) Maruoka, D., Sato, Y., & Nanko, M. (2010). Crack-Healing Effectiveness of Nano Ni+ SiC Co-Dispersed Alumina Hybrid Materials. *Advanced Materials Research.* 89(91), 365-370.

133) Maruoka, D., & Nanko, M. (2013). Recovery of mechanical strength by surface crack disappearance via thermal oxidation for nano-Ni/Al_2O_3 hybrid materials. *Ceramics International, 39*(3), 3221-3229.

Chapter 2

Methodology for Evaluating Healing Agents for Oxidation-induced Self-healing Ceramics[1]

The chapter deals with the methodology for evaluating lower limit temperatures of the healing temperature range ($T_{H\text{-}low}$). The methodology is proposed from the quantitatively evaluated relationship between oxidation behaviour of the healing agents and the strength recovery behaviour of self-healing ceramics. The estimated value of the lower limit ($T_{H\text{-}low}^{est}$) is determined from thermogravimetric analysis, and the experimental value ($T_{H\text{-}low}^{exp}$) is derived from strength recovery testing of self-healing ceramics. The estimated value ($T_{H\text{-}low}^{est}$) compares well with the experimental value ($T_{H\text{-}low}^{exp}$) in the case of the mullite/$TiSi_2$ composite and the alumina/SiC composite. It is shown that the proposed methodology is sufficient for evaluating the viability of healing agents.

[1]This chapter is based on:

Yoshioka, S., & Nakao, W. (2015). Methodology for evaluating self-healing agent of structural ceramics. *Journal of Intelligent Material Systems and Structures*, 26(11), 1395-1403.

2.1 Introduction

The lower limit of the healing temperature range ($T_{H\text{-}low}$) is one of the critical properties of oxidation-induced self-healing ceramics. As discussed in Chapter 1, the temperature $T_{H\text{-}low}$ is related to the active state and the transition state. This means that $T_{H\text{-}low}$ is the threshold temperature at which the self-healing ceramics induce the healing reaction and can maintain their structural integrity actively. If the operation temperature of a high temperature component is lower than $T_{H\text{-}low}$ of the self-healing ceramics, the composite cannot induce desirable self-healing, ultimately resulting in component strength degradation. Conversely, the self-healing ceramics which have low $T_{H\text{-}low}$ can be applied in a variety of high temperature components.

The lower limit of the healing temperature range, $T_{H\text{-}low}$, is strongly affected by the oxidation behaviour of the healing agent. This is because the self-healing of extrinsic self-healing ceramics can only be induced by the oxidation of healing agents. This study aimed to quantitatively evaluate the relationship between the oxidation behaviour of the healing agents and the strength recovery behaviour of self-healing ceramics. Based on the results, the methodology for evaluating the lower limit temperature of the healing temperature range, $T_{H\text{-}low}$, was established.

As a case study, this study attempted to develop advanced self-healing ceramics that can induce self-healing below 1000°C because that no attractive composite for such a low temperature range has been reported previously. The preselection of healing agents was conducted based on thermodynamic calculations such as reaction enthalpy upon oxidation. The estimated value of lower limit $T_{H\text{-}low}^{est}$ was determined from the thermogravimetric analysis of the healing agents. The experimental value $T_{H\text{-}low}^{exp}$ is derived from strength recovery testing of the self-healing ceramics containing the selected healing agents. By comparing the value of $T_{H\text{-}low}^{est}$ and $T_{H\text{-}low}^{exp}$, the viability of the proposed methodology was discussed.

2.2 Definition of $T_{H\text{-}low}$ in Extrinsic Oxidation-induced Self-healing Ceramics

In order to discuss $T_{H\text{-}low}$, the term must be clearly defined. In this study, $T_{H\text{-}low}$ is defined as, "the lowest annealing temperature where strength of self-healing ceramics having semi-elliptical pre-crack with surface length of 100 μm recovered to their original strength within certain annealing time of x h."

This definition of $T_{H\text{-}low}$ refers to the definition of, "self-healing in structural ceramics," proposed by Ando et al[1]. Ando et al. were the first to report in detail on the self-healing behaviour of SiC particles containing alumina matrix composites from the perspective of fracture mechanics. Self-healing in structural ceramics is often evaluated by qualitative index such as crack disappearance rate. However, considering that self-healing ceramics are expected to be implemented in structural components, it is appropriate to refer the definition of $T_{H\text{-}low}$ where quantitative indexes, such as strength of materials, are employed. Moreover, in this study, we fix the surface length of the semi-elliptical pre-crack as 100 μm. This is because it becomes difficult to fill and bond cracks using formed oxides in a set time as the crack volume increases.

2.3 Selection Methodology for Healing Agents Based on Thermodynamic Calculations

2.3.1 Matrix

Since oxidation-induced self-healing ceramics are exposed to high temperature atmospheres constantly, the oxide matrix of the composite should protect healing agents from undesirable reactions. As discussed in Chapter 1, internal oxidation of healing agents due to internal diffusion of oxygen can be considered a critical deterioration factor because healing agents with high oxidation activity lead to a large chemical potential gradient in the matrix, and the chemical potential drives internal diffusion of oxygen through the matrix. In this study, the oxygen diffusion coefficients as a function of temperature for several oxides were investigated as an index for the healing agent protectivity of the oxide matrix.

Figure 2.1 shows the oxygen diffusion coefficient in several oxides as a function of inverse of temperature[2-5]. Mullite exhibits a low oxygen diffusion coefficient in grain boundary diffusion and also in volume diffusion below 1400°C. Therefore, mullite was chosen as a matrix for self-healing ceramics in low-temperature applications.

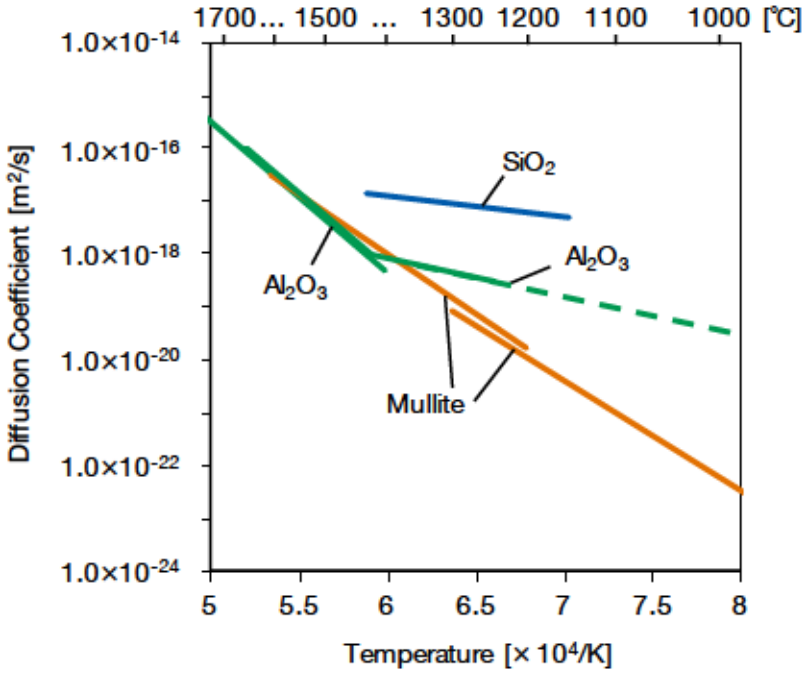

Figure 2.1 Oxygen Diffusion Coefficient in Several Oxides as a Function of Inverse of Temperature

2.3.2 Healing Agents

In this study, the focus was placed on silicon-based binary alloys as healing agent candidates because the alloys produce SiO_2 as an oxidation product. Since mullite has some composition range as shown in Figure 2.2, it can be expected that formed SiO_2 dissolves into mullite, resulting in strong adhesion between mullite matrices and SiO_2.

Figure 2.3 shows the procedure for selecting an attractive healing agent for mullite based self-healing ceramics. Once selected, healing agents are evaluated based on their high temperature

stability and reaction activity.

As discussed in Chapter 1, healing agents must have high temperature stability to avoid undesirable reactions in the dormant state. In this study, three reactions are considered undesirable during high temperature operation: phase transformations of healing agents (e.g. melting or evaporation), solution, oxidation or reduction reactions between healing agents and oxide matrices, and the internal oxidation of the healing agent. The deterioration factor of the internal oxidation of healing agents cannot be avoided by thermodynamic calculations because internal oxidation of the agents and the self-healing reaction are both induced by the oxidation reaction. Moreover, in order to avoid internal oxidation as much as possible, we have already selected mullite as a matrix as discussed in the previous section. In the present selection process, two possible reactions based on thermodynamics viz. were studied: phase transformations of healing agents and reactions between healing agents and the oxide matrices. Melting points of candidate alloys and Gibbs energy changes in the reaction between healing agents and the mullite matrix ($\Delta G°r$) were evaluated.

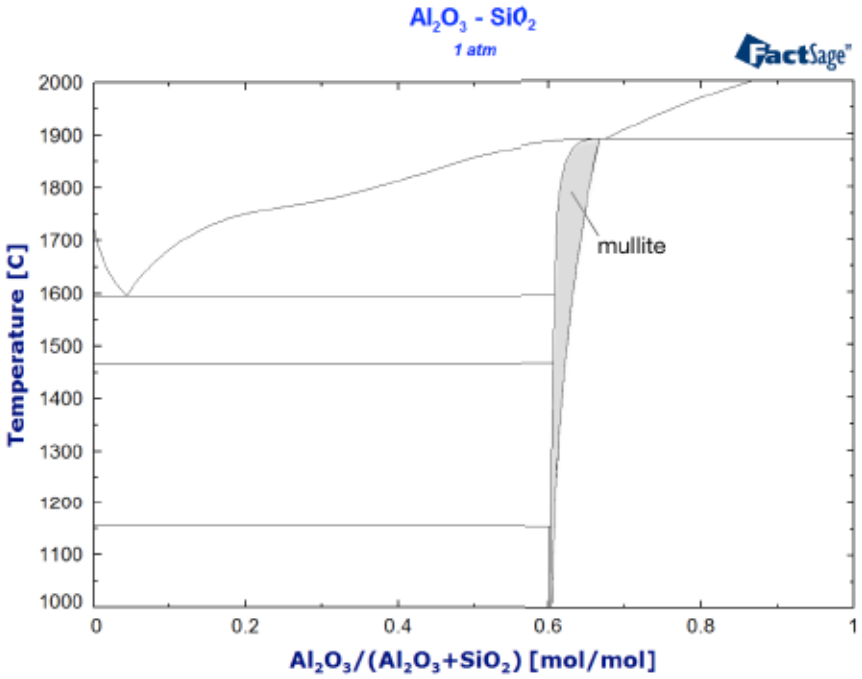

Figure 2.2 Pseudo-binary Phase Diagram for the Al_2O_3 and SiO_2 System Calculated by FactSage 7.0[6]

Mullite has some composition range.

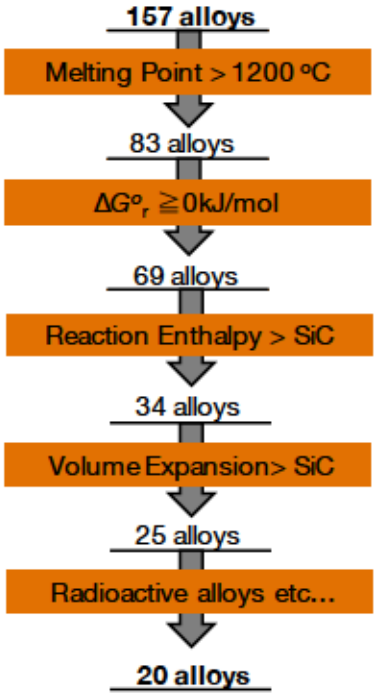

Figure 2.3 Procedure for Selecting an Attractive Healing Agent for Mullite-based Self-healing Ceramics

Healing agents should possess high reaction activity upon oxidation to produce the necessary volume of oxide to fill the introduced crack at low temperature ranges. In this study, three properties of healing agents were considered as an index of reaction activity: oxidation starting temperature, reaction heat and volume expansion upon oxidation. High reaction heat leads to an increase in local temperature at the crack's surface and promotes the oxidation of healing agents. Volumetric growth upon oxidation is required for successful crack filling. The reaction heat and the volumetric growth are calculated using the reaction enthalpy change upon oxidation and the relative volume expansion. Since kinetic analysis is required for determining the starting oxidation temperature of the healing agent, the evaluation was excluded in this section.

The practical evaluation process in the case of Si-based binary alloys is described below. First, all 157 silicon-based binary alloys were listed using the phase diagrams[7] of all Si-metal binary systems. Since high chemical stability of the advanced healing agent is required within the matrix at operating temperature, the melting point of the Si-based alloys and the Gibbs energy change of the reaction between element X and mullite, $\Delta G^{\circ}r$, were evaluated. Element X signifies the alternative element constituting the Si-based alloys, such as Zr in the Si-Zr alloy. The Si-based alloys having melting point below 1200°C were eliminated and 83 alloys remained as candidates. Subsequently, Si-based alloys showing a negative value of $\Delta G^{\circ}r$ were eliminated, because the alloys can reduce mullite to metallic Al and Si when $\Delta G^{\circ}r < 0$. The values of $\Delta G^{\circ}r$ were evaluated at room temperature using thermochemical tables[8] because $\Delta G^{\circ}r$ at high temperatures showed the same tendencies. For example, the reaction between Ti and mullite is expressed in Equation 2.1:

$$\frac{13}{2}\mathrm{Ti} + 3\mathrm{Al_2O_3 \cdot 2SiO_2} \rightarrow \frac{13}{2}\mathrm{TiO_2} + 6\mathrm{Al} + 2\mathrm{Si} \quad (2.1)$$

Thus, the ΔG^{o}r of the reaction is obtained using Equation 2.2.

$$\Delta G_r^o = \frac{13}{2}\Delta G_r^o(\mathrm{TiO_2}) - \Delta G_r^o(3\mathrm{Al_2O_3 \cdot 2SiO_2}) = 661.910\ [\mathrm{kJ/mol_{mullite}}] \quad (2.2)$$

From the value of ΔG^{o}r, it can be said that Ti will not reduce mullite. Moreover, Ti in Si-Ti binary alloys such as TiSi and $TiSi_2$ exhibits lower chemical potential than the elementary substance Ti, indicating that Ti-Si binary alloys are stable in mullite. Similar evaluations were conducted on whole metallic elements. The results are shown as a function of atomic number in Figure 2.4. Twenty metallic elements were found to satisfy the set criterion.

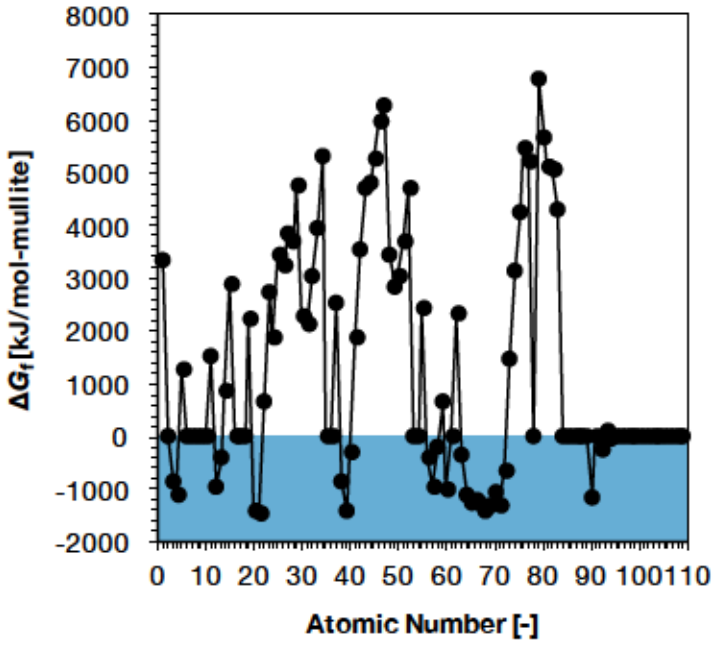

Figure 2.4 Values of ΔG^{o}_{r} of the Reaction Between Metallic Elements and Mullite at Room Temperature

Oxidation reaction activity of candidates was subsequently evaluated based on the reaction enthalpy and volume expansion upon oxidation. Volumetric growth is expressed as the relative volume expansion (RVE). In this work, the oxidation reaction of alloys is expressed by the following reaction. Equation 2.3 uses the oxidation of $TiSi_2$ as an example.

$$\mathrm{TiSi_2} + 3\mathrm{O_2} = \mathrm{TiO_2} + 2\mathrm{SiO_2} \quad (2.3)$$

Hence,

$$\mathrm{RVE}\ [\%] = \frac{V_{\mathrm{TiO_2}} + 2V_{\mathrm{SiO_2}} - V_{\mathrm{TiSi_2}}}{V_{\mathrm{TiSi_2}}} \times 100 \quad (2.4)$$

Here, V_x represents the molar volume of substance X. The value of V_x can be calculated based on the

following equation:

$$V_x\,[\mathrm{cm^3/mol}] = \frac{C\,[\text{Å}]\times 10^{-24}}{N\,[-]} \times N_A[\mathrm{mol^{-1}}] \tag{2.5}$$

Here, C represents the cell volume of substance X and N means the number of units in each cell. All crystal data was obtained from the crystallographic data[9].

The exothermic heat of the oxidation reaction increases the local temperature of the crack surface and promotes the establishment of desirable bonding between the crack surface and the formed oxide. Here, the reaction enthalpy upon oxidation, ΔH_r, is calculated using the change in Gibbs energies (ΔG_r)as defined by Equation 2.6.

$$\Delta G_r = \Delta H_r - T\Delta S \tag{2.6}$$

Here, ΔG_r represents the Gibbs energies change upon oxidation, ΔH_r represents the reaction enthalpy change upon oxidation, ΔS_r represents the reaction entropy change upon oxidation and T represents the absolute temperature. By plotting ΔG_r against T, ΔH_r can be obtained using the intercepts on axis Y. All thermochemical data was obtained from the datasets[8]. As an example, the Gibbs energy change in the reaction shown in Equation 2.4 can be presented as shown in Equation 2.7.

$$\Delta G_r = \Delta G_f(\mathrm{TiO_2}) + \Delta G_f(\mathrm{SiO_2}) - \{\Delta G_f(\mathrm{TiSi_2}) + 2\Delta G_f(\mathrm{O_2})\} \tag{2.7}$$

Here, ΔG_f: the Gibbs energy of formation. From the Y intercepts in the graph, the reaction enthalpy can be determined as 873.7 [kJ/mol-O_2] in the case of the oxidation of $TiSi_2$. It should be mentioned that all reaction enthalpies are calculated from the reaction balanced by 1 mole of O_2 because the value depends on the number of moles of reactants. Unfortunately, the thermochemical data[8] or the crystallographic data[9] of 11 alloys was unavailable, thus eliminating the alloys as candidates.

The alloys selected from the evaluation discussed above are listed in Table 2.1. All alloys listed in the table are attractive candidates for healing agents because they are expected to have both high temperature stability and high oxidation activity.

Table 2.1 Selected Si-based Binary Alloys as Healing Agents for Mullite-based Self-healing Ceramics

Element	Clarke number	Oxidation stability	Phase	Melting point [°C]	Reaction enthalpy [kJ/mol-O_2]	Volume expansion [%]
Fe	4.7	○	$FeSi_2$	1410	705	279
Ti	0.46	○	Ti_5Si_3	1920	855	217
			TiSi	1570	858.6	232
			$TiSi_2$	1480	873.7	252
Mn	0.09	○	MnSi	1275	675.9	278
Cr	0.02	○	Cr_3Si	1770	758.3	233
			CrSi	1413	801.7	251
			$CrSi_2$	1490	827.7	276
V	0.015	○	V_5Si_3	2010	655.0	321
			VSi_2	1677	743.5	314

The above evaluations were based on thermodynamics, meaning that kinetic characteristics such as oxidation starting temperature, growth of oxides and internal oxidation behaviour, were not considered as part of those evaluations. The oxidation kinetics of the ten selected candidates listed above are studied by means of thermogravimetric analysis in the following section.

2.4 Experiment

2.4.1 TG/DTA Analysis

The lower boundary of the available temperature range, $T_{H\text{-}low}^{est}$, was estimated from the oxidation behaviour of candidate powders analysed by means of thermogravimetry and differential temperature analyses (TG/DTA).

The analysed powders were $FeSi_2$, MnSi, $CrSi_2$, VSi_2, ZrSi (Kojundo Chemical Laboratory Co., Ltd., ø 0.1 μm), $TiSi_2$ #1 (GfE GmbH., ø 3.0 μm) and $TiSi_2$ #2 (Kojundo Chemical Laboratory Co., Ltd., ø 0.07 μm). Mullite powder (KM101, Kyoritsu Materials) was used as a reference. A TG/DTA analyser (TGD-9600, ULVAC-RIKO) with R-type thermocouple and alumina cells, having a 5mm diameter and a 5mm height, was used was used as an apparatus. Approximately 20mg of each sample powder and the mullite powder were put into alumina cells and heated to 1400°C in dried air with 10 ml/min. Exothermic heat and mass gain upon oxidation were recorded during the heating process using constant heating rate β. From the obtained mass gain curve, the oxidation peak temperature (T_p) was determined. The value of $T_{H\text{-}low}^{est}$ was estimated using the correlation between T_p and β and analysed based on the Kissinger-Sunose-Akahira equation.

2.4.2 Strength Recovery Behaviour

The lower boundary of the available temperature range ($T_{H\text{-}low}^{exp}$) was experimentally

determined using strength recovery testing of the self-healing ceramic. The strength recovery rate was evaluated using the strength of previously cracked specimens healed at several temperatures for 1h and 10h, abbreviated here as crack-healed specimens. The value of $T_{H\text{-}low}^{exp}$ was determined to be the lowest temperature at which the strength of self-healing ceramics having a semi-elliptical pre-crack with surface length of 100 μm recovered to their original strength as discussed in Section 2.2.

In this study, the $T_{H\text{-}low}^{exp}$ of two composites, which are mullite/15 vol. % -$TiSi_2$ #1 and mullite/15 vol. % -$TiSi_2$#2 and are abbreviated as Mu15$TiSi_2$#1 and Mu15$TiSi_2$#2, were determined experimentally. It was determined from the results of TG/DTA analysis shown below that $TiSi_2$ was the most attractive alloy for use as a healing agent. The raw powders of mullite (KM101, Kyoritsu Materials) and Y_2O_3 (RU-P, Shin-Etsu Chemical Co., Ltd.) have a mean particle size of 0.78 μm and 1.19 μm, respectively. $TiSi_2$#1 and $TiSi_2$#2 indicate the same powders used in the previous section. Mullite and each $TiSi_2$ powder was mixed using the volume ratio of 85 vol. % and 15 vol. % utilizing an alumina pot and 5mm alumina balls for 24h in isopropanol. During mixing, Y_2O_3 at 10 wt. % and acrylic emulsion (#7110, Sekisui Chemical Co., Ltd.) at 3 wt. % were added to the slurry as the sintering additive and the binding agent, respectively. After drying, the mixed powder was crushed via alumina mortar and sieved out below 250 μm. The sieved powder was formed to a rectangular plate (35×45×6mm) using uniaxial pressing at 100N and cold isostatic pressing (CIP) at 200MPa. The formed powder was sintered at 1450 ˚C for 10h in Ar. Subsequently, the sintered plate was cut into 4×3×22mm rectangular bar specimens.

The specimens were healed at temperatures from 400˚C to 1200˚C for 1h and 10h after being cracked at the centre of the specimens using a Vickers indentation. The introduced pre-crack had a surface length of 100 μm. As shown in Figure 2.5, the pre-crack was healed at 1200˚C for 10h.

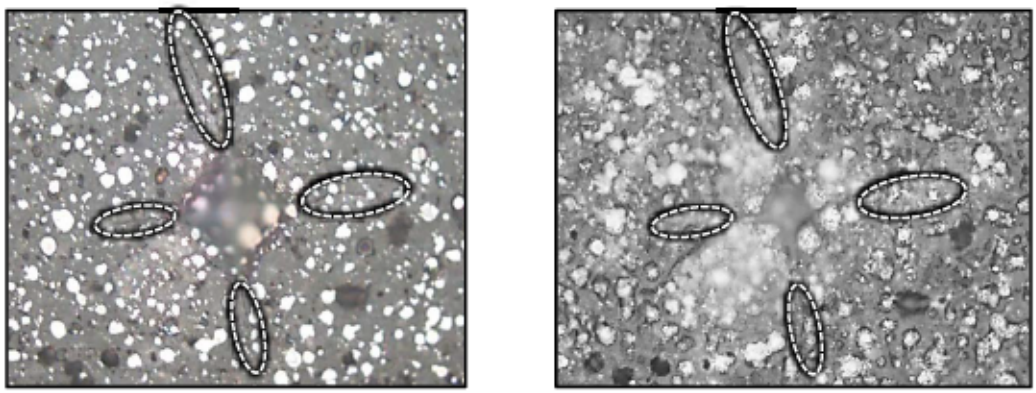

a) Pre-crack on the specimen before healing

b) Healed-crack on the specimen healed at 1200 ℃ for 10 h

Figure 2.5 Optical Micrograph of the Pre-crack Having Surface Length of 100 μm Before and After Healing

Strength testing was conducted on a three-point bending mechanism as shown in Figure 2.6. The span was 16 mm allowing the maximum tensile stress to be applied to the healed pre-crack. For comparison, the strengths of non-cracked and cracked specimens were measured using the same procedure.

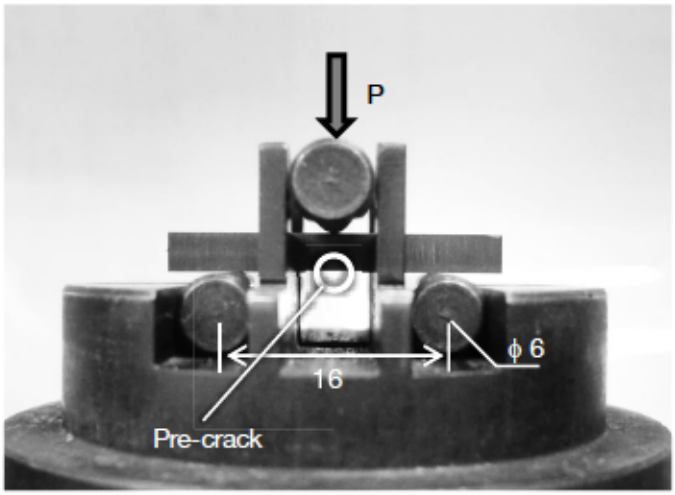

Figure 2.6 Photograph of Three Point Bending Test Set-up

2.5 Results

2.5.1 TG/DTA Analysis

Figure 2.7 shows TG and DTA curves for the oxidation of $TiSi_2$#2 particles at the constant heating rate of 5°C/ min. The green line, blue line and orange lines show the results of mass gain (TG), thermal difference (DTA) and differential of mass gain curve (DTG), respectively. At the temperature where the DTA curve exhibits a maximum, the differential of the mass gain curve also shows a maximum. Considering that the mass gain and the exothermic heat are corresponding to the oxidation of $TiSi_2$, it can be said that the rate of the oxidation reaction of $TiSi_2$ particles exhibits a maximum rate at this temperature. In this study, the oxidation peak temperature (T_p) is therefore defined as the on-peak temperature of the differential of the mass gain curve. For instance, the value of T_p for $TiSi_2$#2 is determined as 444°C when β= 5 °C/min. Similar analyses were conducted for all conditions of β.

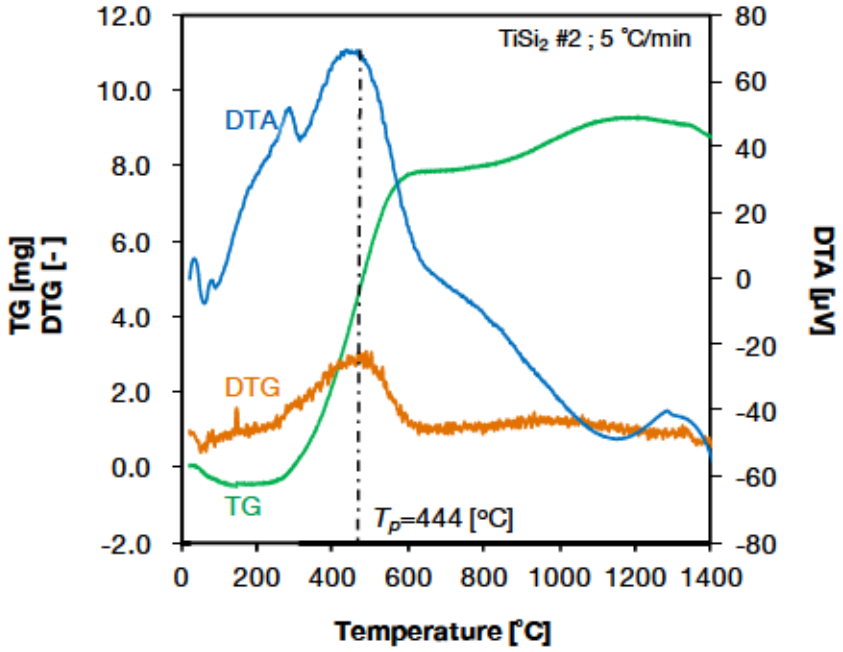

Figure 2.7 TG, DTA and DTG Curves Obtained By Thermogravimetric Analysis of $TiSi_2$#2 at the Constant Heating Rate of 5°C/ min

The oxidation peak temperature (T_p) is defined as the on-peak temperature of the DTG curve in this study.

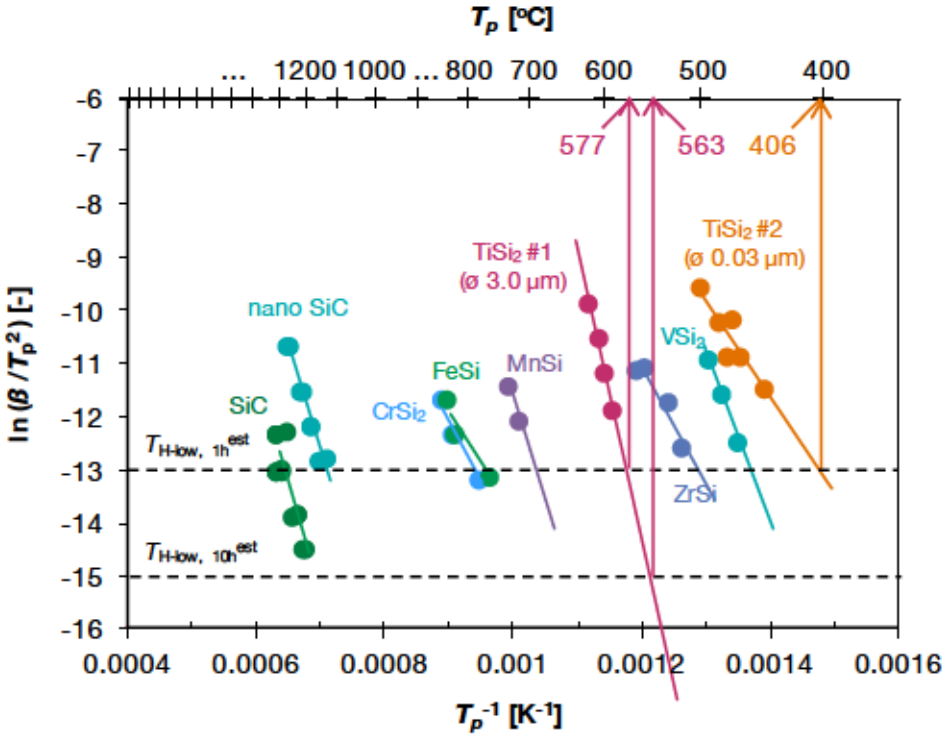

Figure 2.8 Temperature Dependence of the Rate of Oxidation Reaction Evaluated Based on the Kissinger-Sunose-Akahira Equation

Figure 2.8 shows the relationship between T_p and the value of the logarithm of β devised by T_p^2 for $TiSi_2$ oxidation with the referenced data of the oxidations of SiC and nano-SiC[10]. The value of ln (β/T_p^2) as the vertical axis corresponds to the reaction rate constant according to Equation 2.8.

$$\ln\left(\frac{\beta}{T_p^2}\right) + \frac{E_a}{RT_p} = \text{constant} \tag{2.8}$$

Equation 2.8, known as the Kissinger-Sunose-Akahira equation[11], is based on the Arrhenius equation. The righter plots in the figures indicating that the rate of oxidation exhibits a maximum at lower temperatures. From Figure 2.8, it can be expected that the self-healing ceramics containing $TiSi_2$ as a healing agent can induce the desirable self-healing at lower temperatures compared to those previously reported in self-healing ceramics.

Furthermore, T_H^{est} can be estimated by inserting the semi-empirical oxidation rate constant into Equation 2.8. The value of the oxidation rate constant was derived based on the experimental equation for the crack-healing rate of self-healing ceramics proposed by Osada et al.[12]. Osada et al. proposed Equation 2.9, which indicates the dependence of the annealing temperature (T_H) and the oxygen partial pressure (P_{O2}) on the healing rate (V_H) of alumina/15 vol.% SiC composite where the healing rate (V_H) corresponds to the inverse of the minimum healing time(t_{Hmin}).

$$V_H = \frac{1}{t_{Hmin}} = 6.95\times10^5 \cdot \exp\left(\frac{-4.65\times10^4}{T_H}\right) P_{O_2}^{0.835} \tag{2.9}$$

Based on the equation, it can be determined that the annealing temperature (T_H) of 1279°C is required for achieving self-healing within 1 h in air. Conversely, the representative reaction rate constant of the oxidation for 1.0h healing can be determined to be -12.96, corresponding to the value of ln (β/T_p^2) of SiC oxidation at T_p = 1279°C. By inserting those values into the approximation line of each candidate material, one can determine the value of 577°C as $T_{H\text{-}low,1\,h}^{est}$ and 563°C as $T_{H\text{-}10\,h}^{est}$ for the self-healing ceramics containing $TiSi_2$#1 particles as healing agents. Similarly, $T_{H\text{-}low,1\,h}^{est}$ is determined to be 406°C for $TiSi_2$#2.

2.5.2 Strength Recovery Behaviour

The results of strength recovery tests for Mu15'$TiSi_2$#1 and Mu15'$TiSi_2$#2 are shown in Figure 2.9. The orange and blue plots represent the results of strength recovery test of Mu15'$TiSi_2$#1 and Mu15'$TiSi_2$#2, respectively. The green plots represent the results of alumina/ SiC composite reported previously[3]. The open symbols represent the fracture was initiated from the introduced pre-crack and the closed symbols represent the fracture origin was the other defects. For comparison, the strength recovery behaviour was standardized by the strength recovery rate (R_s) using Equation 2.10.

$$R_S = \frac{\sigma_{healed} - \sigma_{pre-cracked}}{\sigma_{smooth} - \sigma_{pre-cracked}} \tag{2.10}$$

The averaged strength of smooth specimens of Mu15'$TiSi_2$#1 at room temperature was 183MPa, and that of pre-cracked specimens was 113MPa. The averaged strength of smooth

specimens of Mu15TiSi$_2$#2 was 238MPa, and that of pre-cracked specimens was 129MPa. In the case of Mu15TiSi$_2$#1, annealing at 400°C and 500°C leads to some preliminary strength recovery. Since annealing at 600°C led to a complete recovery of strength for Mu15TiSi$_2$#1, the value of $T_{\text{H-low,1 h}}^{\text{exp}}$ was determined to be 600°C. The value of $T_{\text{H-low,10 h}}^{\text{exp}}$ for Mu15TiSi$_2$#1 was also determined to be 600°C. No difference between $T_{\text{H-low,1 h}}^{\text{exp}}$ and $T_{\text{H-low,10 h}}^{\text{exp}}$ is directly influenced by the small difference between $T_{\text{H-low,1 h}}^{\text{est}}$ and $T_{\text{H-low,10 h}}^{\text{est}}$.

Mu15TiSi$_2$#2 shows different strength recovery behaviour. Annealing at 400°C and 500°C also leads to some strength recovery, similar to Mu15TiSi$_2$#1. However, complete strength recovery was attained at 1000°C. The value of $T_{\text{H-low,1 h}}^{\text{exp}}$ was determined to be 1000°C for Mu15TiSi$_2$#2.

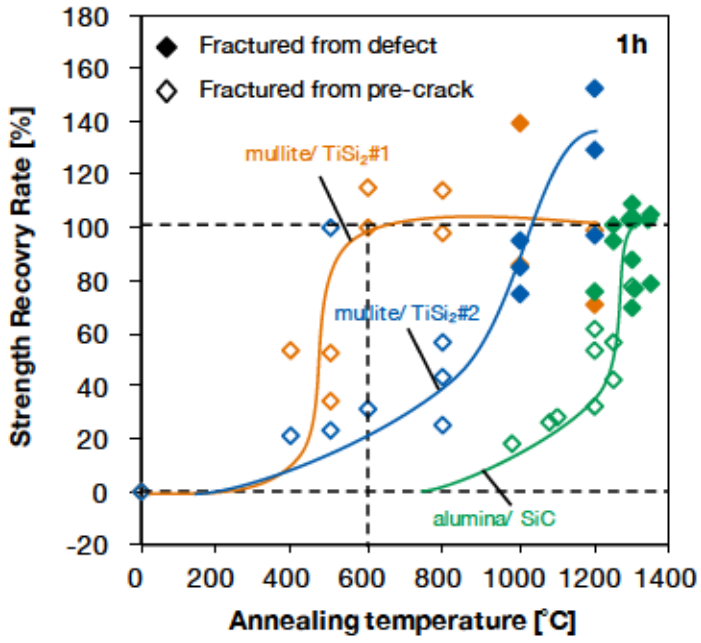

Figure 2.9 Strength Recovery Rate of Mullite/TiSi$_2$ Composite Compared to That of Alumina/SiC Composite Healed at Multiple Temperatures for 1h

2.6 Discussion

2.6.1 Consistency Between Estimated and Experimental Values of $T_{\text{H-low}}$

Figure 2.10 shows the consistency between the values of $T_{\text{H-low}}^{\text{est}}$ and $T_{\text{H-low}}^{\text{exp}}$ for Mu15TiSi$_2$#1 and Mu15TiSi$_2$#2, comparing to the values of the fibre-reinforced self-healing ceramics containing TiSi$_2$ as a healing agent, alumina/SiC composite[1] and alumina/ nano-SiC composite[10]. The direct proportion line indicates that the value of $T_{\text{H-low}}^{\text{est}}$ corresponds to the value of $T_{\text{H-low}}^{\text{exp}}$. In the cases of the composites containing SiC particles as healing agents, the values of $T_{\text{H-low}}^{\text{est}}$ accords well with $T_{\text{H-low}}^{\text{exp}}$. While most of the values of $T_{\text{H-low}}^{\text{est}}$ agree with the values of $T_{\text{H-low}}^{\text{exp}}$ in self-healing ceramics containing TiSi$_2$ as a healing agent, there is a huge difference between the value of $T_{\text{H-low}}^{\text{exp}}$ and $T_{\text{H-low}}^{\text{est}}$ in Mu15TiSi$_2$#2. The initial strength of the composite and effects of Ti cation are two factors that can

be considered as the cause of the mismatch between $T_{H\text{-}low}^{est}$ and $T_{H\text{-}low}^{exp}$ in this case.

In contrast to the average strength of smooth specimens of Mu15TiSi$_2$#1 at room temperature (183MPa), the average strength of Mu15TiSi$_2$#2 was 238MPa. This means that the internal defects in smooth Mu15TiSi$_2$#2 are smaller than those of Mu15TiSi$_2$#1. It becomes difficult to recover specimen strength completely as the strength of the smooth specimen becomes higher, because the introduced pre-crack should be diminished as small as internal defects by crack-filling by formed oxide upon oxidation. In fact, the strength of Mu15TiSi$_2$#2 annealed at 600°C for 1h recovered to 162MPa, which is comparable to the strength of Mu15TiSi$_2$#1 annealed in the same conditions. This indicates that the introduced pre-cracks in both samples have been diminished as the same level. In conclusion, the potential of TiSi$_2$ as a healing agent was evaluated sufficiently by means of the proposed method.

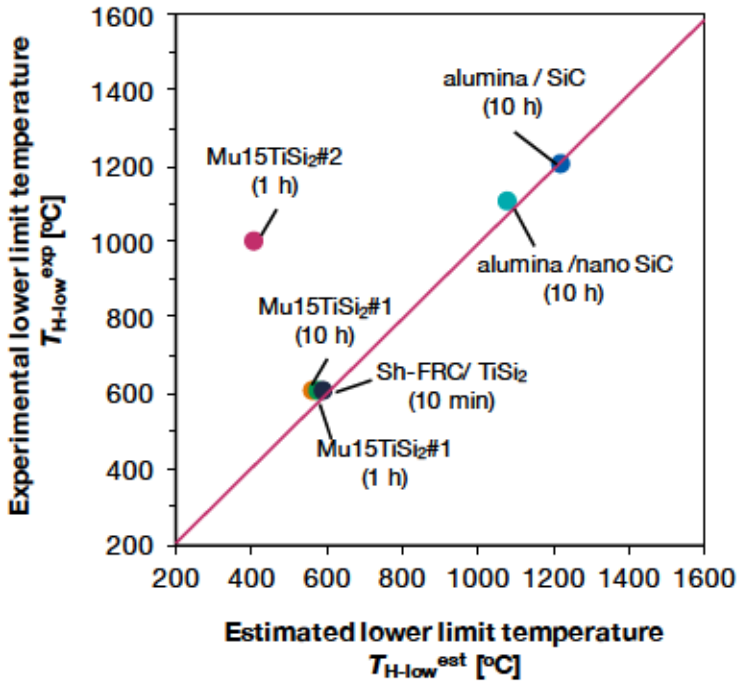

Figure 2.10 Consistency Between the Values of T_H^{est} and T_H^{exp} for Mu15TiSi$_2$#1 and Mu15TiSi$_2$#2 Compared to Those of Alumina/SiC Composite[1] and Alumina/nano-SiC Composite[10]

As shown above, the proposed method is sufficient to evaluate the healing potential of healing agents. However, the proposed methodology cannot predict the exact value of $T_{H\text{-}low}$ at which complete strength recovery is achieved. The alternative factor of the mismatch between $T_{H\text{-}low}^{est}$ and $T_{H\text{-}low}^{exp}$, i.e., the effect of Ti cation will be discussed in Chapter 3.

2.7 Conclusion

In this chapter, we aimed to derive the simple methodology for evaluating availability of self-healing agent. From this study, the following results were obtained:

I. The theoretical framework to predict the healing ability of non-oxides was proposed on the basis

of thermodynamics. In the proposed selection process, high temperature stability and reaction activity of the healing agents candidates were evaluated based on their melting point, the Gibbs energy change of the reaction with the matrix, reaction enthalpy and volume expansion upon oxidation.

II. The proposed methodology was applied to Si-based binary alloys. As a result, ten alloys including $FeSi_2$, MnSi, $CrSi_2$, VSi_2, ZrSi and $TiSi_2$ were selected as the attractive candidates.

III. Oxidation behaviour of selected Si-based binary alloys was evaluated based on the thermogravimetric analysis and Kissinger-Sunose-Akahira analysis. $TiSi_2$ showed the highest oxidation reaction activity. The lower limits of the available temperature range ($T_{H\text{-}low}^{est}$) of Mu15′$TiSi_2$#1 and Mu15′$TiSi_2$#2 were estimated using the correlation between the heating rate and the oxidation peak temperature. The values of $T_{H\text{-}low,\ 1h}^{est}$ were determined to be 577°C for Mu15′$TiSi_2$#1 and 406°C for Mu15′$TiSi_2$#2.

IV. The lower boundary of the available temperature range ($T_{H\text{-}low}^{exp}$) was experimentally determined from the strength recovery testing of the mullite/TiSi composites. $T_{H\text{-}low,\ 1h}^{exp}$ values were determined to be 600°C for Mu15′$TiSi_2$#1 and 1000°C for Mu15′$TiSi_2$#2.

V. The estimated values for $T_{H\text{-}low}^{est}$ align with the experimental value $T_{H\text{-}low}^{exp}$ in the case of self-healing ceramics containing SiC particles as a healing agent. However, some mismatch was found in case of the composite containing $TiSi_2$ particles as a healing agent. The cause of mismatch will be discussed in Chapter 3.

References

1) Ghosh, S. K. (Ed.). (2009). Self-healing materials: fundamentals, design strategies, and applications. John Wiley & Sons.
2) Kingery, W. D. (1960). Introduction to ceramics.
3) Mubhlenbachst, K., & Schaeffer, H. (1977). OXYGEN DIFFUSION IN VITREOUS SILICA-UTILIZATTON OF NATURAT ISOTOPIG ABUNDANCES.
4) Fielitz, P., Borchardt, G., Schmücker, M., Schneider, H., & Willich, P. (2004). Oxygen Grain-Boundary Diffusion in Polycrystalline Mullite Ceramics. *Journal of the American Ceramic Society*, *87*(12), 2232-2236.
5) Heuer, A. H. (2008). Oxygen and aluminum diffusion in α-Al2O3: How much do we really understand? Journal of the European Ceramic Society, 28(7), 1495-1507.
6) FactSage7.0, CRCT-ThermFact inc. & GTT-Technologies.
Available from: http://www.factsage.com/
7) Massalski, T. B., Murray, J. L., Bennett, L. H., & Baker, H. (1986). Binary Alloy Phase Diagrams. American Society for Metals: Metals Park, OH, 1986.
8) Barin, I., Platzki, G. (1995). Thermochemical Data of Pure Substances, Thermochemical Data of Pure Substances. Wiley-VCH.
9) ICSD-Inorganic Crystal Structure Database-web. 1998. FIZ Karlsruhe GmbH.
Available from: http://www.fiz-karlsruhe.de/icsd_home.html.
10) Nakao, W., Abe, S. (2012). Enhancement of self-healing ability in oxidation induced self-healing ceramic by modifying the healing agent. *Smart Materials and Structures*, 21(2):25002.
11) Akahira, T., Sunose, T. (1971). 1969 Research Report. *Chiba Institute of Technology*, 16 (22):246.
12) Osada, T., Nakao, W., Takahashi, K., Ando, K. (2009). Kinetics of Self-Crack-Healing of Alumina/Silicon Carbide Composite Including Oxygen Partial Pressure Effect. *Journal of the American Ceramic Society*, 92 (4):864-869.

Chapter 3

Effect of Cation in Healing Agents on Self-Healing Behaviour[1]

In this chapter, the presence of Ti cation in healing agents and its effect on self-healing behaviour is studied. The effect is clarified through strength recovery tests and direct observation of the crack-healing area in the alumina/TiC composite. The selection of TiC is based on the proposed method described in Chapter 2. The introduced crack is sufficiently filled with TiO_2 and the strength of the composite returns to its original strength within 1h by annealing at 800°C. This result clearly shows the viability of healing agent containing Ti cation for lower temperature applications. The outward diffusion of Ti cation is observed at the higher temperature of 1000°C. The outward diffusion induces crack-healing for wider cracks, but also leads to strength deterioration.

[1]This chapter is based on:

Yoshioka, S., Boatemaa, L., van der Zwaag, S., Nakao, W., & Sloof, W. G. (2016). On the use of TiC as high-temperature healing particles in alumina based composites. *Journal of the European Ceramic Society*, 36(16), 4155-4162.

3.1 Introduction

In Chapter 2, the methodology for evaluating the lower limit of the healing temperature range ($T_{H\text{-}low}$) was introduced. Based on the proposed method, it is easy to estimate whether the advanced self-healing ceramics containing a new healing agent are suitable for the corresponding applications. However, in order to develop a variety of self-healing ceramics, it is necessary to establish both the method for evaluating the potential of self-healing ability and the method for optimizing the self-healing ability in each application. In order to establish these methodologies, it is critical to control the oxidation behaviour of the self-healing agent. This is because the oxidation behaviour of healing agents directly affects strength recovery behaviour of extrinsic oxidation-induced self-healing ceramics, as shown in the previous chapter.

In this chapter, we will focus on the effect of Ti cation in healing agents on the self-healing behaviour of self-healing ceramics. In previous studies, extrinsic self-healing in ceramic matrix composites has been realized by embedding 15 vol.% to 30 vol.% SiC particles to produce a single oxide upon oxidation. From these studies, it was clarified that SiO_2 is an attractive crack-filling oxide[1-18]. However, the formation of SiO_2 for sealing and bonding the crack requires relatively high temperatures (above 1200°C). In contrast, Ti containing healing agents such as $TiSi_2$ show high oxidation activity and seem to have the potential to induce the desired self-healing at lower temperature ranges. In the composites, the resulting crack-filling substance is a mixture of two oxides: TiO_2 and SiO_2. In this case, the crack filling and strength recovery are affected by both the formation of SiO_2 and the presence of Ti cation in the healing agent, which produces TiO_2 upon oxidation.

To study the effect of Ti cation in the healing agent, the self-healing behaviour of composites containing TiC as a healing agent was studied. The availability of TiC as a healing agent was evaluated based on the method proposed in Chapter 2. The oxidation kinetics of the healing agent were determined with thermogravimetry analysis (TG-DTA). The strength recovery of pre-cracked alumina/TiC composites was investigated using three-point bending tests. The crack-filling kinetics of alumina/TiC composites was studied based on the direct observation of the healed area using a focused ion beam (FIB) and scanning electron microscopy.

3.2 Theoretical Analysis of the Healing Potential of TiC in an Alumina Matrix

The viability of TiC as a healing agent was evaluated based on the proposed method in Chapter 2, and additional mechanical properties were investigated based on the method recently proposed by Farle et al.[19]. Farle et al. presented a theoretical framework to predict the intrinsic healing ability of 59 MAX phases on the basis of chemical properties and mechanical parameters, including the adhesion between the reaction products and the matrix material and the CTE and modulus of the reaction products in relation to those of the parent phase.

3.2.1 Thermodynamic Stability of TiC

The thermodynamic stability of TiC in the presence of oxygen and that of its intended reaction product TiO_2 in the presence of Al_2O_3 is calculated using FACTSAGE (CRCT-ThermFACT Inc. & GTT-Technologies). In Figure 3.1, the thermodynamic stability of TiC in air as a function of temperature is shown. The figure shows that, thermodynamically speaking, TiC can transform into TiO_2 even at room temperature.

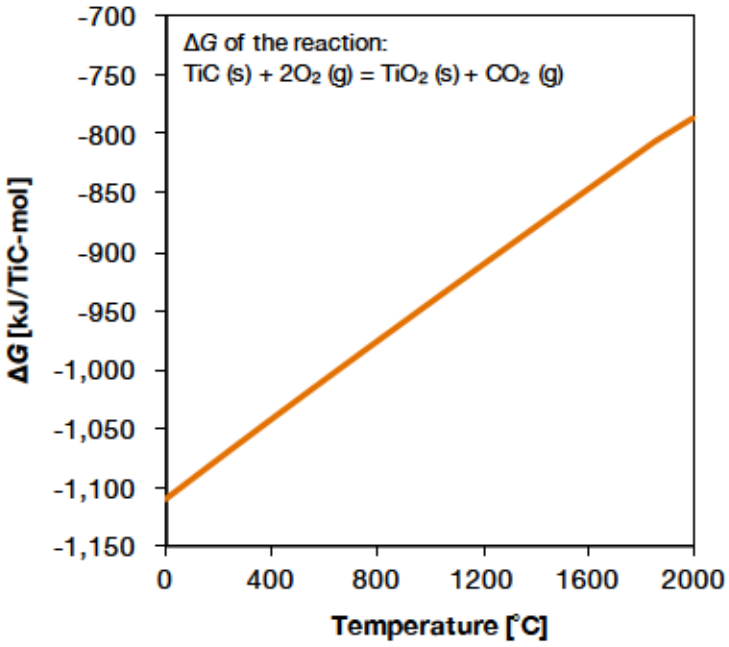

Figure 3.1 Thermodynamic Stability of TiC in Air Versus That of TiO_2 as a Function of Temperature

The calculated phase diagram for the TiO_2 and Al_2O_3 system for the temperature range 1000°C to 2000°C is shown in Figure 3.2. This figure shows that there are no deep eutectica and that the lowest temperature at which a liquid phase is present is about 1700°C. setting the upper healing temperature to be considered for this system.

According to the phase diagram, TiO_2 can react with Al_2O_3 and form the intermediate compound Al_2TiO_5 above 1270°C. Provided that the healing time is not extensive, temperatures below 1000°C could be viable for self-healing reactions because mullite/$TiSi_2$ can complete their self-healing process below 1000°C. Based on the pseudo phase diagram, there are no further reactions between TiO_2 and Al_2O_3 below 1270°C, indicating that, provided all other conditions are met, the temperature range below 1270°C is suitable for self-healing reactions and prolonged material usage.

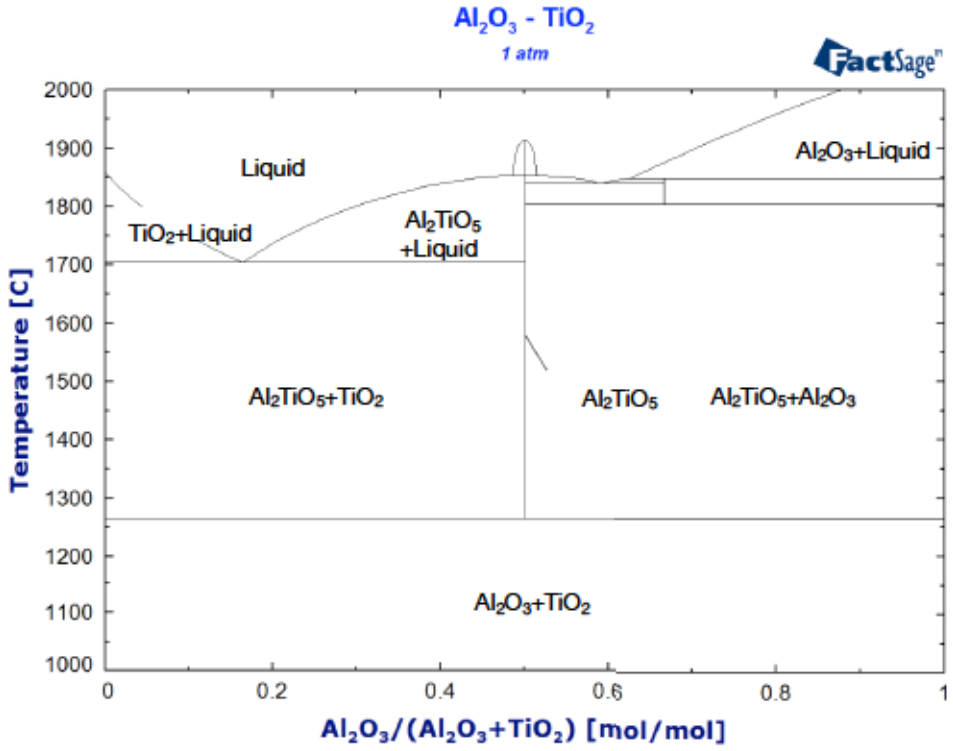

Figure 3.2 TiO_2-Al_2O_3 Pseudo Phase Diagram

3.2.2 Relative Volume Expansion (RVE)

Successful crack filling due to solid state chemical reactions requires that the molar volume of the reaction product is larger than that of the starting healing material in order to i) either fully or partially fill the crack, ii) locally reconnect opposing crack faces and iii) re-establish mechanical integrity. The volumetric growth is expressed as the relative volume expansion (RVE). In this study, the decomposition of a carbide into a metallic oxide is presented using Equation 3.1.

$$MC + 2O_2 = MO_2 + CO_2 \uparrow \tag{3.1}$$

Hence,

$$\text{RVE}\,[\%] = \frac{V_{MO_2} - V_{MC}}{V_{MC}} \times 100 \tag{3.2}$$

Here, V_x means molar volume of substance X. The value of V_x can be calculated based on Equation 3.3.

$$V_x\,[\text{cm}^3/\text{mol}] = \frac{C\,[\text{Å}] \times 10^{-24}}{N\,[-]} \times N_A[\text{mol}^{-1}] \tag{3.3}$$

Here, C means the cell volume of substance X and N means the number of unit in each cell. The

crystal data used are listed in Table 3.1.

Table 3.1 Reference Data Used for RVE Calculation

Compound	Cell Volume *C* [Å³]	Unit number *N* [-]	Molar volume *Vx* [cm³/mol]	Reference (PDF No.)
SiC	82.77	4	12.5	01-075-0254
TiC	81.07	4	12.2	04-004-2919
SiO_2 (Cristobalite)	176.54	4	26.6	01-082-0512
TiO_2 (Rutile)	62.43	2	18.8	00-021-1276

The calculated RVE of TiC is shown in Table 3.2. As seen in Table 3.2, the RVE of TiC is more than 0%, which means that TiC can indeed create the extra volume required for filling the crack gap upon oxidation.

Table 3.2 Calculated RVE Value of TiC and SiC

Reaction	Relative Volume Expansion (RVE) [%]
$SiC + 2O_2 \rightarrow SiO_2$ (Cristobalite)$+ CO_2$	113.3
$TiC + 2O_2 \rightarrow TiO_2$ (Rutile) $+ CO_2$	54.0

According to previous studies [3-4], a 15 vol.% of SiC was sufficient for filling surface cracks with 100 μm and attaining full strength recovery of alumina/SiC composites. Assuming the local crack facing distance of the induced indentation cracks to be equal, it can be argued that the optimal volume fraction of a TiC self-healing agent should be approximately 30 vol.% to realize a comparable level of self-healing in TiC/alumina composites and to compensate for the lower RVE value. Hence, the experimental studies presented here focus on 15 vol.% to 30 vol.% TiC-containing Al_2O_3 composites.

3.2.3 Work of Adhesion

To achieve complete strength recovery, the energy required to separate the crack-filling oxide from the alumina matrix should be comparable to or greater than the cohesion strength of the alumina matrix. The adhesion energy of the interface between matrix/crack-filling oxide interface is defined as the 'work of adhesion'. This work of adhesion can be expressed by Equation 3.4[20].

$$W_{ad} = -\left(\gamma_{matrix}^{surf} + \gamma_{oxide}^{surf}\right) + \gamma_{matrix/oxide}^{interface} \quad (3.4)$$

where, γ_{matrix}^{surf} and γ_{oxide}^{surf} mean the surface energy of the matrix and the oxide, and $\gamma_{matrix/oxide}^{interface}$ means the interface energy between the matrix and crack-filling oxide. The value for the interface energy has been estimated from the interaction energies of the atoms located at each site of the interface[21, 22]. The interaction energies were calculated from solution enthalpies of an element at one

site of interface dissolved in another element at the other site of the interface. Details of the calculations can be found elsewhere[23]. The calculated work of adhesion for relevant interfaces is shown in Figure 3.3.

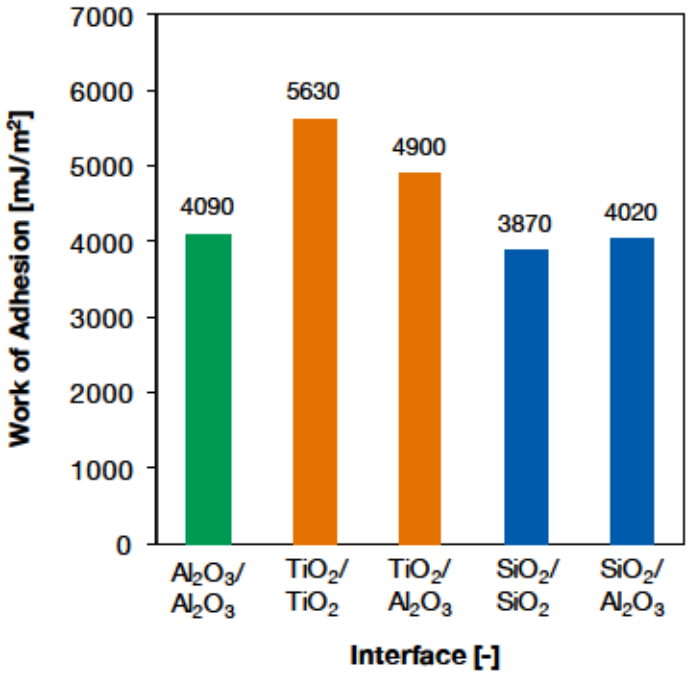

Figure 3.3 Calculated Work of Adhesion for Relevant Interfaces

As justified in Section 3.2.1, the formation of Al_2TiO_5 is ignored in the present analysis. The work of adhesion of the Al_2O_3/TiO_2 interface (4900 mJ/m²) and that of the TiO_2/TiO_2 interface (5630 mJ/m²) are both greater than that of the Al_2O_3/Al_2O_3 interface (4090 mJ/m²). The latter two values represent the cohesion of the crack filling and matrix phases, respectively. This means that the crack-healed section in alumina/TiC could be stronger than the alumina matrix itself. To put these values in perspective, the work of adhesion of the well-known self-healing ceramic system Al_2O_3/SiO_2 interface (4020 mJ/m²) is also reported.

From these calculations, it can be postulated that the alumina/TiC composites will attain full strength recovery once the crack is adequately filled with the formed TiO_2.

3.2.4 Comparison of Thermal Expansion Coefficients

Even if the crack is fully filled by the formation of an oxidic phase at the healing temperature, this is no guarantee that a strong and reliable bond is formed when the sample is exposed to a wider range of temperatures. Differences in the coefficient of thermal expansion (CTE) between the matrix and the material formed in the crack as a result of the healing reaction may lead to local stresses. Hence, it is important to compare the CTEs of the matrix (Al_2O_3), the healing agent (TiC) and the crack-filling oxides (TiO_2). Relevant average CTE values are listed in Table 3.3, together with the related values for alumina/SiC composites. The dependence of CTE on crystal orientation was not account for as the material deposited in the crack is polycrystalline.

Table 3.3 Thermal Expansion Coefficients of Relevant Compounds in Alumina/TiC and Alumina/SiC Composites

Compound	Temperature Range [°C]	CTE $\times 10^{-6}$ [°C^{-1}]	Reference
Al_2O_3	1000 - 1600	7.5 ± 0.4	24)
	20 - 2025	7.3 - 8.3	25)
TiC	23 - 848	6.99 ± 0.34 - 7.61 ± 0.20	26)
	1000 - 2600	8.31 ± 0.68	24)
SiC	25 - 1000	3.2 - 5.1	27)
	1000 - 1600	5.68 ± 0.11	24)
TiO_2 (rutile)	30 - 650	7.249 - 8.816	28)
	20 - 1610	8.9 - 11.1	25)
SiO_2(Cristobalite)	100 - 500	10.9	29)
	500 - 1000	1.7	29)

According to Table 3.3, the CTE values of the matrix, the unreacted healing agent and the relevant crack-filling oxides in the alumina/TiC system under consideration are in the range of 6.65×10^{-6} to 11.1×10^{-6} [°C^{-1}]. The maximum mismatch value is 4.45×10^{-6} [°C^{-1}] between TiC and TiO_2 at temperatures ranging from room temperature to 500°C. In contrast, the maximum mismatch value in the reference alumina/SiC system is 7.7×10^{-6} [°C^{-1}] between SiC and SiO_2 at temperatures ranging from room temperature to 500°C, and 6.6×10^{-6} [°C^{-1}] between the alumina matrix and SiO_2 at above 500°C. Considering that there are no reports on the spontaneous fracture of alumina/SiC self-healing ceramics due to a thermal expansion mismatch, it can be proposed that the effects of the CTE mismatch on structural integrity in the alumina/TiC composites can be ignored at this stage.

3.2.5 Comparison of Elastic Properties

A healed crack in a ceramic compound may be exposed to both thermal stresses induced by temperature excursions and to mechanical stresses due to external loading. In this case, it is important to compare the elastic moduli of the matrix, the healing agent and the decomposition product. The Young's moduli of relevant (polycrystalline) compounds in alumina/TiC and alumina/SiC composites are listed in Table 3.4.

Table 3.4 Young' Modulus of Related Compounds in Alumina/TiC and Alumina/SiC Composites

Compound	Specimen	Density [-]	Young's modulus [GPa]	Reference
Al_2O_3	Sintered bulk	≥ 99.6	380-410	30)
	Sintered bulk	≥ 99.8	380-405	30)
	Sintered bulk	≥ 99.5	398-400	30)
	Sintered bulk	≥ 99.6	340-380	30)
	Sintered bulk	≥ 99.0	340-380	30)
$TiC_{x\ (x<1)}$	Thin firm	-	< 460	31)
SiC	Sintered bulk	≥0.98	415	32)
TiO_2	Cristalized thin firm	-	85	33)
SiO_2(Cristobalite)	Natural single crystal	-	65.2	34)

Considering that Young's modulus of TiC_x is dependent on carbon levels[31], it can be stated that the Young's modulus of TiC_x is relatively comparable to that of the alumina matrix, as is the case for SiC. In contrast, the moduli of SiO_2 and TiO_2 are considerably lower than that of the matrix. Based on the values reported, and given that full strength recovery has been attained in alumina/SiC systems, it is expected that the alumina/TiC can also yield comparable self-healing levels. Early cracking along the healed interface is not likely to occur expect at higher macroscopic stress levels.

Based on the theoretical analysis presented above, it is to be expected that autonomous high temperature oxidative healing of the mechanical integrity of Al_2O_3 composites filled with 10 vol % to 30 vol % of TiC particles should theoretically be possible.

3.3. Experiment

Alumina matrix composites containing 30 vol.% TiC, named Al30TiC, were prepared and their strength recovery at room temperature as a function of the healing temperature was studied under the conditions described below. Furthermore, microstructural changes related to the strength recovery process were also examined.

3.3.1. Sample Preparation

Alumina raw powder (AKP-50, Sumitomo Chemical Co., Ltd.) and TiC powder (STD120, H.C. Starck GmbH) were used as starting materials. The initial average sizes were 0.2 and 2 μm, respectively. Ball-milling of TiC powder was conducted for 36h in isopropanol with a ø10 mm WC ball and a WC jar, resulting in an average particle size of 0.3 μm. Alumina powder and ball-milled TiC powder were mixed at 15 vol.% in isopropanol using ø 5mm alumina balls and a 1000 ml plastic bottle. After 12h mixing, the mixed powder was dried in the oven for 24h at 80°C. The dried powder was sieved with a ø 200 μm mesh powder sieve. The sieved powder was densified by means of spark plasma sintering (HP D 25-SD furnace, FCT System GmbH) with a ø 40mm carbon mould at 1500°C for 15 minutes in vacuum conditions under 35MPa. The heating rate was 10°C/min and natural cooling was used to cool down from the maximum temperature. The typical thickness of the

samples was about 5 mm. The relative density of the sintered bulk materials as measured by Archimedes' method was more than 99%. The sintered discs were cut into rectangular samples with a dimension of 3 x 4 x 23mm for four point bending tests. Samples were polished in various steps, with the final polish using a diamond paste with a particle size of 0.25 μm.

3.3.2 Strength Recovery Tests

In order to study the strength recovery of Al30TiC as a function of the annealing temperature, the strength values of three types of specimens (smooth specimen, pre-cracked specimen and healed specimen) were determined. Smooth specimens are samples without any induced damage prior to testing. Pre-cracked specimens are specimens with a standardized pre-crack at the centre of the surface introduced by a Vickers' indenter. The indentation force was 19.6N and the introduced crack had a surface length of about 100 μm for both sets of samples. The opening distance of these surface cracks could not be established with any real accuracy but was estimated to vary between 0.1 and 0.5 μm. The two sets of radial indentation cracks are either perpendicular to or parallel to the longest dimension of the bend test samples. No strong interaction between the indentation induced radial cracks and the healing particles was observed. The healed specimens were pre-cracked and were annealed for 1h in air at temperatures ranging from 400°C to 1000°C.

The strength of each sample was measured by means of three point bending test. The span between the supporting 5mm diameter steel rollers was 16mm. The specimen was mounted such that the maximum tensile stress was applied to the pre-crack or healed crack area. All tests were conducted at room temperature and with a cross-head displacement velocity of 0.5 mm/min.

3.3.3 Surface Characterisation

The crystal structure of the various phases in the samples prior to and after thermal annealing was determined using XRD (ULTIMA IV Rigaku Co.) operated with CuKα radiation. The external appearance of the healed cracks was observed with a laser microscope (KEYENCE, VK-X) and scanning electron microscope (JIB-4501, JEOL Ltd.). The chemical composition of the reaction product formed in the crack was determined using Electron Probe Micro Analysis (JXA-8530F JEOL Ltd microprobe). To enable such measurements, the surface oxidation layer was removed in advance by using a focused ion beam (JIB-4501, JEOL Ltd.).

3.3.4 Cross-section Analysis and Direct Observation of Crack-healed Area

The formed internal and external oxidation layer in the healed samples were analysed by using Electron Probe Micro Analysis (JXA-8530F JEOL Ltd microprobe). Prior to the analysis, the healed specimen was cut to rectangular samples with a dimension of 3 x 4 x 6 mm after the three-point bending test. The sample after annealing was embedded in a phenol resin (Phenolic powder, No. 203100080, Buehler Inc.), and the surface of 3 x 4mm was mechanically polished in various steps, with the final polish using a diamond paste with a particle size of 0.25 μm. After mechanical polishing, the sample was taken out of the resin and the cross-section was observed by EPMA.

The crack-filling behaviour of Al30TiC as a function of annealing temperature was studied by the direct observation of the crack-healed area in the samples after annealing. The sample preparation procedure for the direct observation is schematically shown in Figure 3.4. The sample had a dimension of 3 x 4 x 5mm for direct observations, and dozens of pre-cracks were introduced on the 4 x 5mm surface. This was annealed in the same conditions as the strength recovery tests described in Section 3.3.2. The 3 x 4mm surface of the sample was mechanically polished after annealing using the same method as the cross-section analysis. After mechanical polishing, the sample was removed from the resin and the exposed pre-crack was micromachined by FIB. The pre-crack was observed by SEM (JSM-7001F, JEOL Ltd.).

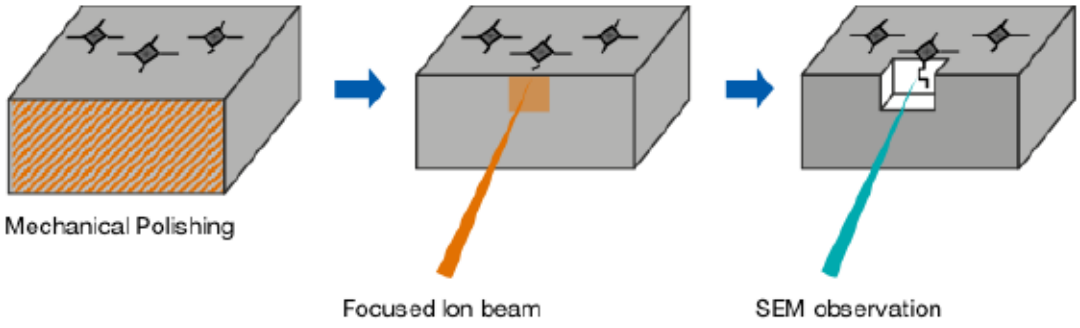

Figure 3.4: Schematic Illustration of Sample Preparation Procedure for Direct Observation

3.4 Results and Discussion

3.4.1 Strength Recovery

The results of the strength recovery tests for Al30TiC are shown in Figure 3.5. The green plots represent the results of strength recovery test of Al30TiC, and the red plots represents the results of alumina/SiC composite reported previously[]. The open symbols represent the fracture was initiated from the introduced pre-crack and the closed symbols represent the fracture origin was the other defects. The average strength of smooth Al30TiC specimens at room temperature was 715MPa, and that of pre-cracked specimens was 225MPa. Figure 3.5 shows that annealing at 400°C leads to some strength recovery. This is the lowest temperature at which partial strength recovery is observed, and is considerably lower than that observed for alumina/SiC composites. Annealing at 800°C led to a complete recovery of the strength for the Al30TiC samples. However, strength degradation was observed in the sample annealed at 1000°C. This degradation is due to the excess diffusion of Ti cation as discussed in the following sections.

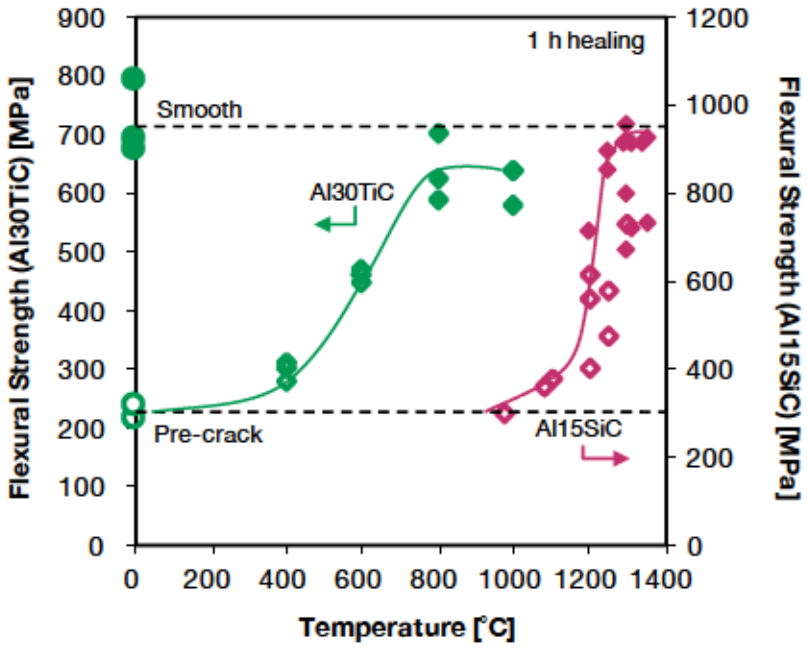

Figure 3.5 Flexural Strength Values of Al30TiC Samples and Al15SiC Samples After Healing for 1h in Air at the Reported Temperature

3.4.2 Surface Characterizations

Laser microscope images of pre-cracked areas before and after annealing are shown in Figures 3.6 through 3.9. These images show samples annealed at temperatures of 400°C, 600°C, 800°C and 1000°C, respectively.

Figure 3.6 (sample annealed at 400°C) shows no clear sign of surface oxidation and the cracks remain clearly visible. In contrast, Figures 3.7 and 3.8 (respective annealing temperatures of 600°C and 800°C) show clear signs of surface oxidation at the external surface intercept location of the TiC particles and the cracks are no longer clearly discernible. Figure 3.9 shows that the surface of specimen annealed at 1000°C is completely covered with formed oxides, and both the crack and the indentation are invisible.

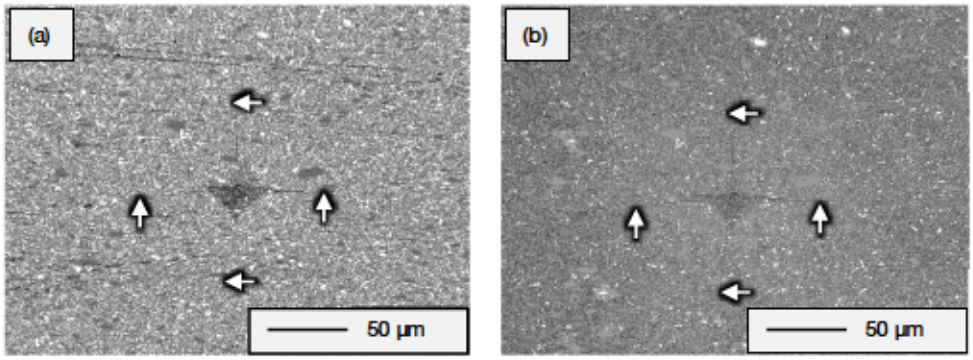

Figure 3.6 Laser Microscope Image of Pre-Cracked Area of Al30TiC Before (a) and After (b) Annealing at 400°C for 1h

Arrows indicate the end points of the radial cracks.

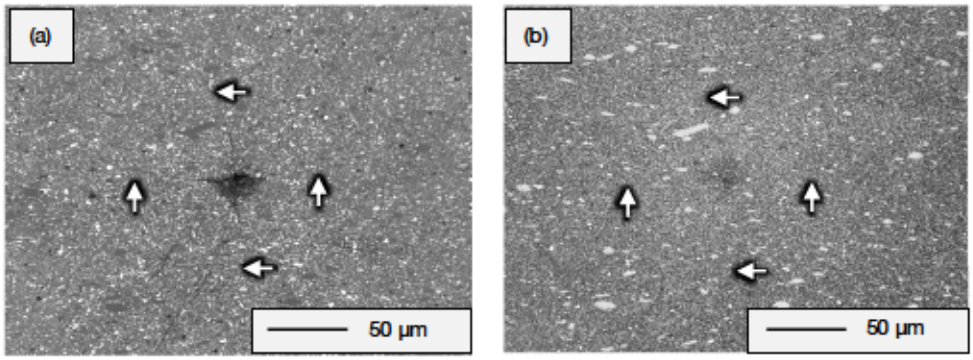

Figure 3.7: Laser Microscope Image of Pre-Cracked Area of Al30TiC Before (a) and After (b) Annealing at 600°C for 1h

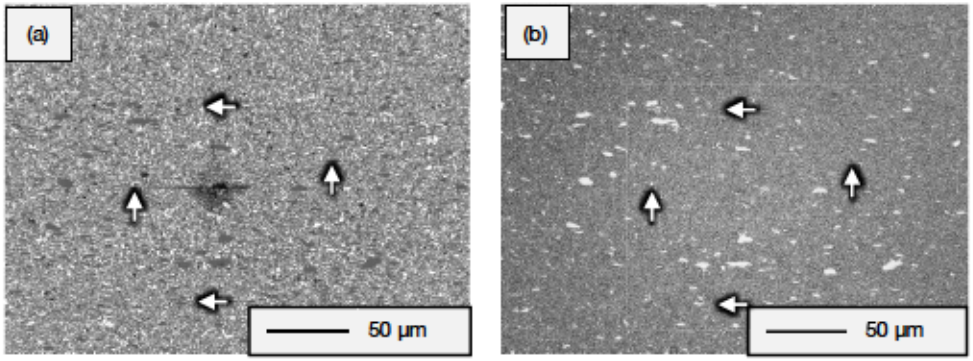

Figure 3.8: Laser Microscope Image of Pre-Cracked Area of Al30TiC Before (a) and After (b) Annealing at 800°C for 1h

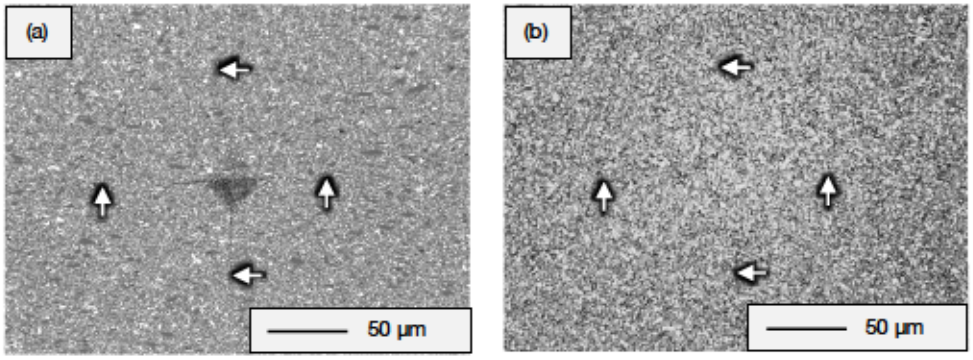

Figure 3.9 Laser Microscope Image of Pre-Cracked Area of Al30TiC Before (a) and After (b) Annealing at 1000°C for 1h

Figure 3.10 shows the results of surface observation by SEM on Al30TiC annealed at temperatures of 400°C, 600°C, 800°C and 1000°C, respectively.

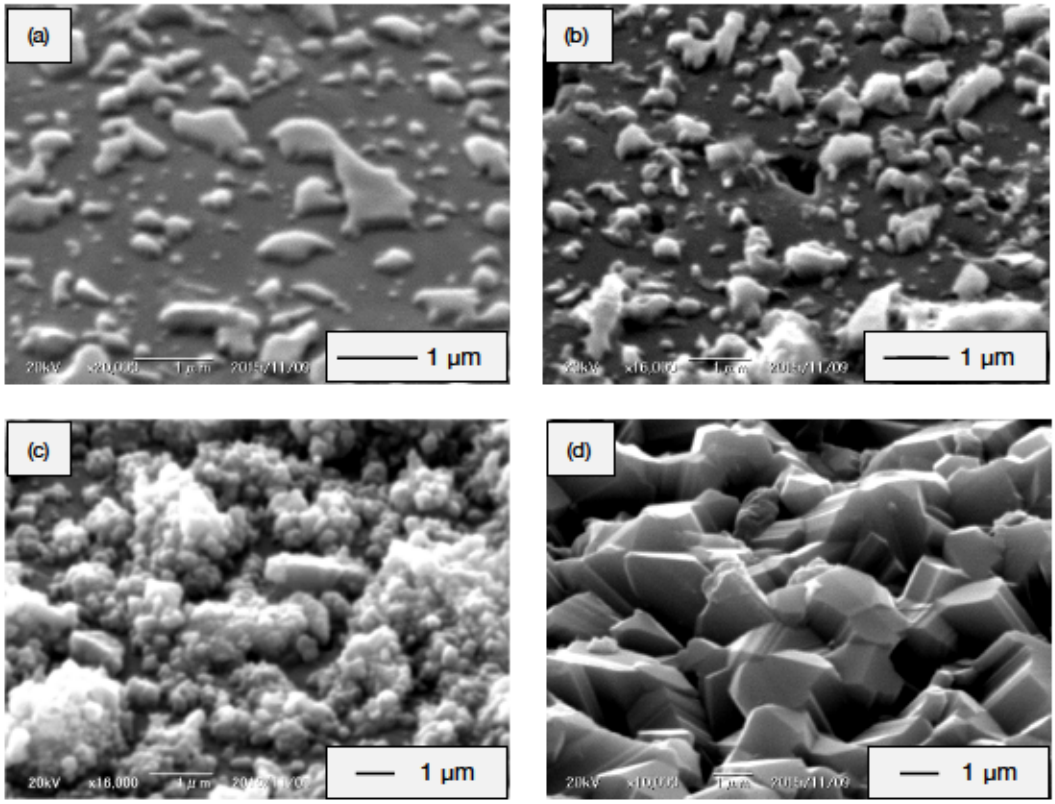

Figure 3.10 SEM Images of Al30TiC Surfaces Annealed at 400°C (a), 600°C (b), 800°C (c), and 1000°C (d) for 1h

As shown in Figure 3.10(a), the formed oxides are dispersed on the surface like islands and their shape looks like a droplet. When accounting for the Shimada et al.[35] report stating that TiC forms amorphous TiO_2 upon oxidation below 420°C, it can be deduced that the droplet-like oxides are also amorphous TiO_2. In Figure 3.10(b), the formed oxides are also dispersed, but their shape is rough. This corresponds to the crystallization of amorphous TiO_2. In Figure 3.10(c), it is clearly observed that the initial oxides have grown and the new nanoscale oxides are formed at the surface of the initial oxides. According to the previous report[35], this phenomenon can be expressed as following. The crystallization of the amorphous phase leads to volume expansion, and the surface of the TiC powder is cracked due to growth stress. Subsequently, new amorphous oxides are formed on the nascent surfaces and start the nucleation process. In contrast to the previous figures, the surface of the sample is completely covered with formed oxides and the grain growth of the formed oxides is observed. Figure 3.11 shows the backscattered electron image and Ti element mapping around the healed crack area of the specimen healed at 1000°C for 1h after removing the surface oxidation layer by focused ion beam. The healed crack is indicated by arrows in both figures. Taking the result of Energy Dispersive X-ray Spectrometry into account, it is clear that the crack is fully filled with the formed titanium oxide. It is interesting to note that the titanium oxide can also be found at locations in the crack well away from intersected TiC particles. This lateral spreading of the oxide along the crack is very advantageous to the efficiency of the healing process. It also should be noted that TiC healing agent particles near the crack surfaces are still intact.

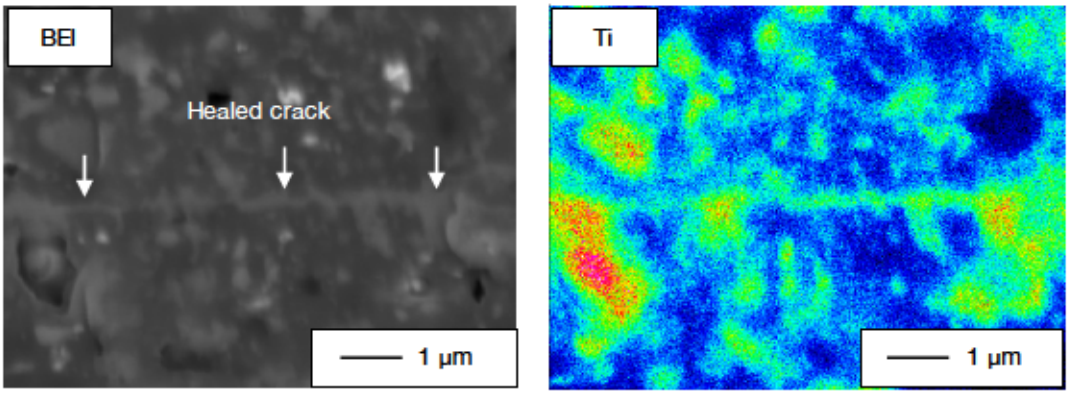

Figure 3.11 Backscattered Electron Image and Ti Element Mapping of Healed Crack Area of Al30TiC Annealed at 1000°C for 1h

The external oxidation layer was removed by FIB.

The results of the XRD analysis of the as-synthesized samples and the annealed samples are shown in Figure 3.12. Some contamination of TiC with WC was expected due to the ball milling treatment, but no traces of WC were detected. While it is expected from the surface observation of the annealed sample that the amorphous phase can be detected, the diffractogram did not differ from that of the as-synthesized specimen after 1h annealing at 400°C, possibly because the amount and the thickness of the formed oxides were too small to detect. At higher annealing temperatures, clear signs of rutile were observed, but anatase and brookite were not detected. TiC was still detectable in the sample annealed at 800°C. This corresponds to the results of the surface observation in Figure 3.10(c), where the surface is not fully covered with TiO_2. Figure 3.12 indicates that the crack is fully filled up with rutile.

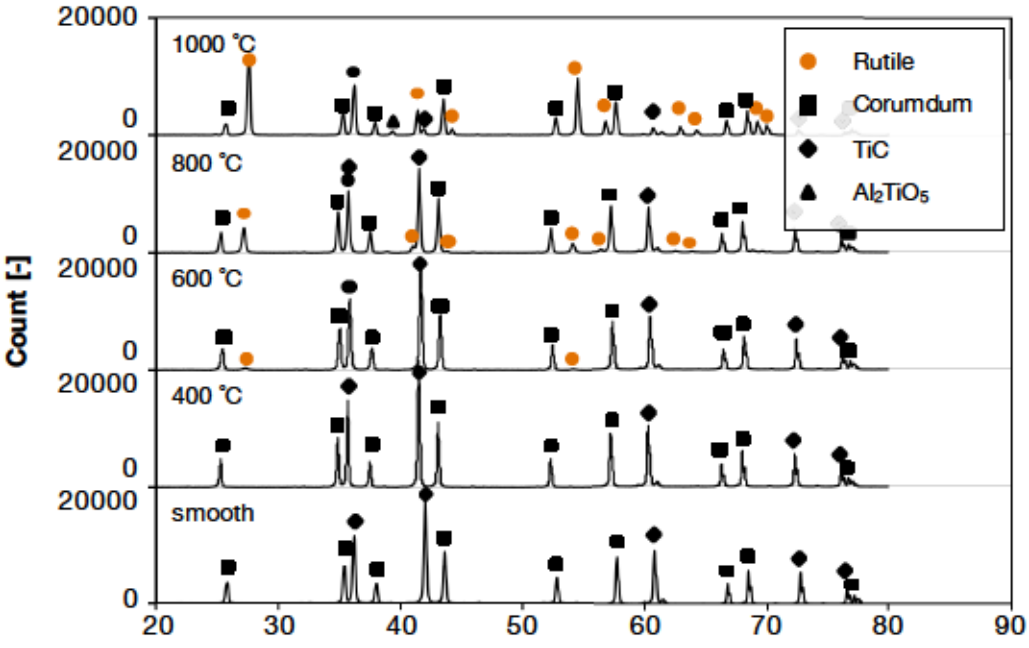

Figure 3.12 XRD Patterns of Al30TiC in the Pristine (smooth) State and After Annealing for 1h at the Indicated

Temperatures

3.4.3 Cross Section Analysis

Figure 3.13 shows the backscattered electron image and Ti element mapping of the cross section of the Al30TiC sample annealed at 1000°C for 1h. Elemental Ti is clearly concentrated around the surface and the depletion of Ti is observed below the surface. This indicates that the outward diffusion of Ti cation becomes significant at this temperature range. Owing to the outward diffusion, the crack gap can be filled without any defects. Moreover, a wider crack gap could also be filled because Ti will be supplied steadily by material near the crack. The outward diffusion of Ti cation leads to the counter-diffusion of micro-vacancies, resulting in the strength deterioration of the composite at 1000°C. However, the excess diffusion of Ti cation can be avoided by optimizing the volume fraction of the TiC content.

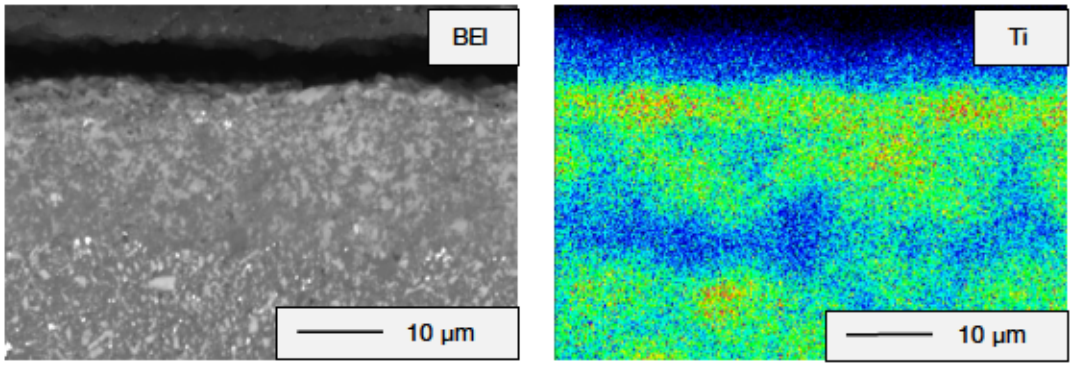

Figure 3.13 Backscattered Electron Image and Ti Element Mapping of Cross Section of Al30TiC Sample Annealed at 1000°C for 1h

Figure 3.14 shows the SEM images of the healed area in depth direction of Al30TiC annealed at the temperatures of 400°C, 600°C, 800°C and 1000°C for 1h, respectively. The figure shows backscattered electron images of the region underneath the indentation where the crack opening distance is largest (~150 μm). White particles and grey regions correspond to TiC particles and alumina matrices. The arrows at the centre of images indicate the introduced pre-crack.

Figure 3.14(a) shows that the pre-crack is remains completely visible and formed TiO_2 is barely observed. The slight strength recovery by annealing at 400°C may be due to the release of residual stress or the filling of the crack tip. In Figure 3.14(b), it can be seen that the pre-crack is partially bridged by formed TiO_2. The bridging of the pre-crack results in the partial strength recovery of the composite as shown in Figure 3.5. The introduced pre-crack is almost fully filled with TiO_2 in Figure 3.14(c), but small defects (less than 0.5 μm) remain in the healed area. However, when considering that the strength of the Al30TiC was completely recovered and the fracture origin in the sample was not the pre-crack but a separate defect, it can be said that the pre-crack is invalidated by annealing at 800°C. Figure 3.14(d) shows that the pre-crack is fully filled with TiO_2 and no vacancy is observed in the sample annealed at 1000°C. This perfect filling is achieved by the combination of the oxidation of TiC and the outward diffusion of Ti cation as discussed in Section 3.4.2. Considering the

classifications of self-healing ceramics discussed in Chapter 1, it can be said that Al30TiC demonstrates oxidation-induced self-healing below 800°C and diffusion induced self-healing above 1000°C.

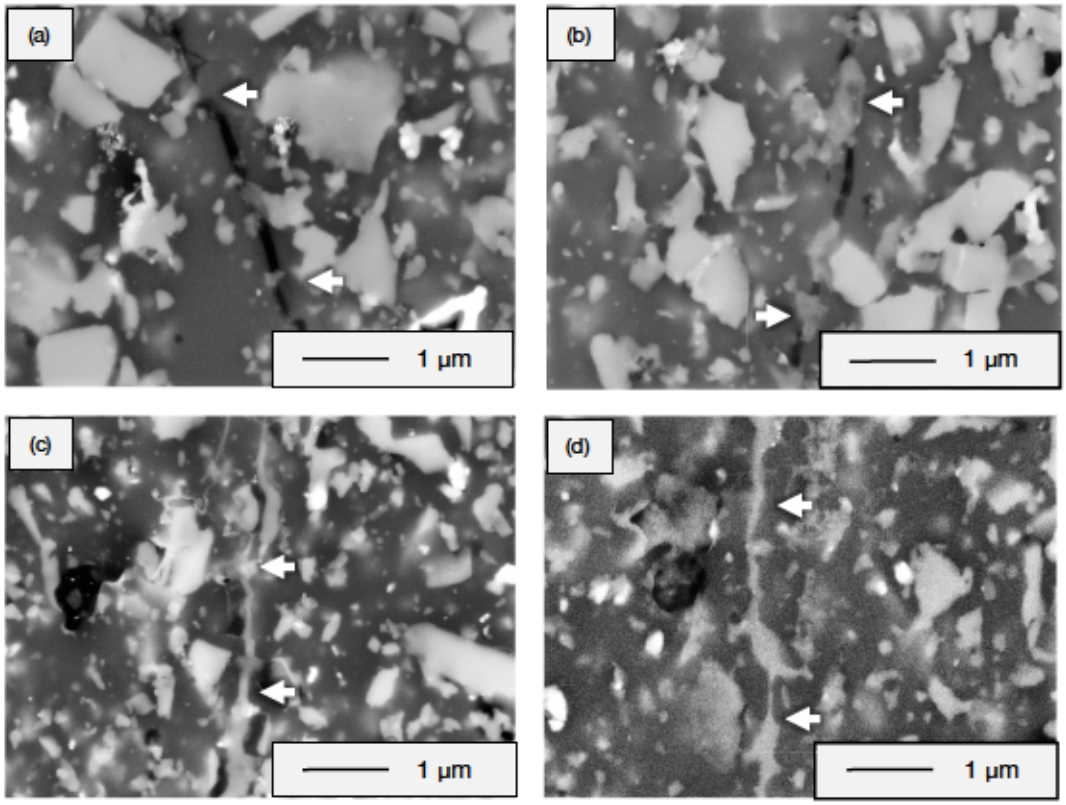

Figure 3.14 SEM Image of the Crack Healed Area in depth direction of Al30TiC Annealed at 400°C (a), 600°C (b), 800°C (c), 1000°C (d) for 1h

3.5 Conclusion

In this chapter, we studied the effect of Ti cation on the self-healing behaviour of extrinsic oxidation-induced self-healing ceramics. The effect is clarified through the experiments on strength recovery behaviour and micro-structural observation of the alumina/TiC composite. From this study, the following results were obtained:

I. The strength of the alumina/TiC composite was completely recovered when annealed at 800°C for 1h. The value of $T_{\text{H-low, 1h}}$ is 500°C lower than that of alumina/SiC composite ceramics.

II. The XRD analysis and elemental mapping via EPMA indicated that the crack-filling oxide is the rutile phase of TiO_2. Since the alumina/TiC showed complete strength recovery, it was also shown that TiO_2 is as attractive a crack-filling oxide as SiO_2.

III. The nature of TiO_2 formation and the crack-filling kinetics of alumina/TiC composites were

studied based on the surface observation by SEM and the direct observation of crack filled areas. The surface of the sample annealed at around 400°C, indicating that low-viscosity TiO_2 oxide was formed in the initial stage of oxidation. The initial oxide crystalized at 600°C. The submicron size of the TiO_2 was observed on the surface of the initial oxide at 800°C. Significant grain growth of the formed oxide was observed at 1000°C.

IV. Significant outward diffusion of Ti cation was observed by the cross-section analysis of the sample annealed at 1000°C for 1h. Due to outward diffusion, the crack gap was filled without any defects. Moreover, wider crack gaps can be filled because the Ti will be steadily supplied by material near the crack. The outward diffusion of Ti cation leads to the counter-diffusion of micro-vacancies, resulting in the strength deterioration of the composite at 1000°C.

V. The alumina/TiC composite shows a hybrid self-healing reaction. Oxidation-induced self-healing was observed at temperature ranges below 800°C, and diffusion induced self-healing was observed at temperature ranges above 1000°C.

References

1) Thompson, A. M., Chan, H. M., Harmer, M. P., & Cook, R. E. (1995). Crack healing and stress relaxation in Al_2O_3 SiC "nanocomposites". *Journal of the American Ceramic Society, 78*(3), 567-571.
2) Chou, I. A., Chan, H. M., & Harmer, M. P. (1998). Effect of annealing environment on the crack healing and mechanical behavior of Silicon Carbide-reinforced alumina nanocomposites. *Journal of the American Ceramic Society, 81*(5), 1203-1208.
3) Ando, K., Kim, B. S., Chu, M. C., Saito, S., & Takahashi, K. (2004). Crack-healing and mechanical behaviour of Al_2O_3/SiC composites at elevated temperature. *Fatigue & Fracture of Engineering Materials & Structures, 27*(7), 533-541.
4) Ono, M., Nakao, W., Takahashi, K., Nakatani, M., & Ando, K. (2007). A new methodology to guarantee the structural integrity of Al_2O_3/SiC composite using crack healing and a proof test. *Fatigue & Fracture of Engineering Materials & Structures, 30*(7), 599-607.
5) Osada, T., Nakao, W., Takahashi, K., & Ando, K. (2009). Kinetics of Self-Crack-Healing of Alumina/Silicon Carbide Composite Including Oxygen Partial Pressure Effect. *Journal of the American Ceramic Society, 92*(4), 864-869.
6) Chu, M. C., Sato, S., Kobayashi, Y., & Ando, K. (1995). Damage healing and strengthening behaviour in intelligent mullite/SiC ceramics. *Fatigue & Fracture of Engineering Materials & Structures, 18*(9), 1019-1029.
7) Ando, K., Chu, M.-C., Tsuji, K., Hirasawa, T., Kobayashi, Y., & Sato, S. (2002). Crack healing behaviour and high-temperature strength of mullite/SiC composite ceramics. *Journal of the European Ceramic Society, 22*(8), 1313-1319.
8) Ando, K., Ikeda, T., Sato, S., Yao, F., & Kobayasi, Y. (1998). A preliminary study on crack healing behaviour of Si_3N_4/SiC composite ceramics. *Fatigue & Fracture of Engineering Materials & Structures, 21*(1), 119-122.
9) Ando, K., Chu, M., Yao, F., & Sato, S. (1999). Fatigue strength of crack-healed Si_3N_4/SiC composite ceramics. *Fatigue & Fracture of Engineering Materials & Structures, 22*(10), 897-903.
10) Houjou, K., Ando, K., & Takahashi, K. (2010). Crack-healing behaviour of ZrO_2/SiC composite ceramics. *International Journal of Structural Integrity, 1*(1), 73-84.
11) Houjou, K., & Takahashi, K. (2012). Crack-healing behavior of ZrO_2/SiC composite ceramics and strength properties of crack-healing specimens. *International Journal of Structural Integrity, 3*(1), 41-52.
12) Takahashi, K., Yokouchi, M., Lee, S. K., & Ando, K. (2003). Crack-healing behavior of Al_2O_3 toughened by SiC whiskers. *Journal of the American Ceramic Society, 86*(12), 2143-2147.
13) Nakao, W., Ono, M., Lee, S.-K., Takahashi, K., & Ando, K. (2005). Critical crack-healing condition for SiC whisker reinforced alumina under stress. *Journal of the European Ceramic Society, 25*(16), 3649-3655.

14) Nakao, W., Mori, S., Nakamura, J., Takahashi, K., Ando, K., & Yokouchi, M. (2006). Self-crack-healing behavior of Mullite/SiC particle/SiC Whisker multi-composites and potential use for ceramic springs. *Journal of the American Ceramic Society, 89*(4), 1352-1357.

15) Takahashi, K., Uchiide, K., Kimura, Y., Nakao, W., Ando, K., & Yokouchi, M. (2007). Threshold stress for crack healing of mullite reinforced by SiC whiskers and SiC particles and resultant fatigue strength at the healing temperature. *Journal of the American Ceramic Society, 90*(7), 2159-2164.

16) Nakao, W., Tsutagawa, Y., & Ando, K. (2008). Enhancement of in situ self-crack-healing efficient temperature region by SiC nanosizing. *Journal of Intelligent Material Systems and Structures, 19*(3), 407-410.

17) Wataru, N., & Shihomi, A. (2012). Enhancement of the self-healing ability in oxidation induced self-healing ceramic by modifying the healing agent. *Smart Materials and Structures, 21*(2), 025002.

18) Abe, O., Ohwa, Y., & Kuranobu, Y.-i. (2006). Possibility of enhanced strength and self-recovery of surface damages of ceramics composites under oxidative conditions. *Journal of the European Ceramic Society, 26*(4), 689-695.

19) Farle, A.-S., Kwakernaak, C., van der Zwaag, S., & Sloof, W. G. (2015). A conceptual study into the potential of $M_{n+1}AX_n$-phase ceramics for self-healing of crack damage. *Journal of the European Ceramic Society, 35*(1), 37-45.

20) Howe, J. (1993). Bonding, structure, and properties of metal/ceramic interfaces: Part 2 Interface fracture behaviour and property measurement. *International materials reviews, 38*(5), 257-271.

21) Miedema, A., Niessen, A., De Boer, F., Boom, R., & Matten, W. (1989). Cohesion in metals: transition metal alloys. *Report, Philips Research Laboratories, Eindhoven, The Netherlands. FR de Boer, R. Boom, WCM Mattens, AR Miedema, AK Niessen: Cohesion in Metals. Transition Metals Alloys, North-Holland Publishing Co., Amsterdam*.

22) Vitos, L., Ruban, A., Skriver, H. L., & Kollar, J. (1998). The surface energy of metals. *Surface Science, 411*(1), 186-202.

23) Bennett, I. J., Kranenburg, J. M., & Sloof, W. G. (2005). Modeling the Influence of Reactive Elements on the Work of Adhesion between Oxides and Metal Alloys. *Journal of the American Ceramic Society, 88*(8), 2209-2216.

24) Engberg, C. J., & Zehms, E. H. (1959). Thermal Expansion of Al_2O_3, BeO, MgO, B_4C, SiC, and TiC Above 1000°C. *Journal of the American Ceramic Society, 42*(6), 300-305.

25) Fei, Y. (1995). Thermal expansion. *Mineral physics and crystallography: a handbook of physical constants, 2*, 29-44.

26) Elliott, R. O., & Kempter, C. P. (1958). Thermal expansion of some transition metal carbides. *The Journal of Physical Chemistry, 62*(5), 630-631.

27) Li, Z., & Bradt, R. (1986). Thermal expansion of the cubic (3C) polytype of SiC. *Journal of Materials Science, 21*(12), 4366-4368.

28) Rao, K. K., Naidu, S. N., & Iyengar, L. (1970). Thermal expansion of rutile and anatase. *Journal of the American Ceramic Society, 53*(3), 124-126.

29) Aumento, F. (1966). Stability lattice parameters and thermal expansion of beta-cristobllite. American Mineralogist, 51(7), 1167-1175.
30) Auerkari, P. (1996). *Mechanical and physical properties of engineering alumina ceramics*: Technical Research Centre of Finland Finland. (private communication)
31) Török, E., Perry, A. J., Chollet, L., & Sproul, W. D. (1987). Young's modulus of TiN, TiC, ZrN and HfN. *Thin Solid Films, 153*(1), 37-43.
32) Munro, R. (1997). Material properties of a sintered α-SiC. *Journal of Physical and Chemical Reference Data, 26*(5), 1195-1203.
33) Olofinjana, A. O., Bell, J. M., & Jämting, A. K. (2000). Evaluation of the mechanical properties of sol–gel-deposited titania films using ultra-micro-indentation method. *Wear, 241*(2), 174-179.
34) de Faoite, D., Browne, D. J., Chang-Díaz, F. R., & Stanton, K. T. (2012). A review of the processing, composition, and temperature-dependent mechanical and thermal properties of dielectric technical ceramics. *Journal of Materials Science, 47*(10), 4211-4235.
35) Shimada, S., & Kozeki, M. (1992). Oxidation of TiC at low temperatures. *Journal of materials science, 27*(7), 1869-1875.

Chapter 4

Methodology for Evaluating the Lifetime of Self-Healing Ability [1]

This chapter deals with the methodology for evaluating upper limit temperatures of the healing temperature range ($T_{\text{H-high}}$). Self-healing ceramics should maintain their self-healing ability even when constantly exposed to a high temperature atmosphere. However, in such severe conditions, healing agents embedded within the matrix can deteriorate due to inward diffusion of oxygen. In this chapter, it is shown that the self-healing ability has disappeared in the formed internal oxidation layer through the strength recovery test on alumina/SiC composite aged at 1200°C for 1000h. This indicates that the life span of self-healing ability can be evaluated as a function of the growth rate of the internal oxidation layer. Based on the results, the methodology for evaluating the upper limit temperature of the healing temperature range ($T_{\text{H-high}}$) is proposed.

[1]This chapter is based on:

Eto, S., Yoshioka, S., & Nakao, W. (2017). Self-healing behavior of aged self-healing ceramics. *Transactions of the JSME.* (manuscript in preparation).

4.1 Introduction

In contrast to previous chapters discussing the active state of oxidation-induced self-healing ceramics, this chapter focuses on the dormant state of the self-healing ceramics. In the real operating conditions of high temperature components, oxidation-induced self-healing ceramics are constantly exposed to a severely corrosive atmosphere. For example, middle pressure turbine blades in a jet engine are replaced after approximately 10000h or every 1000 flights[1-4]. This is equivalent to exposing the composite to a corrosive atmosphere at 1200°C for 1000h. Even in such severe conditions, the self-healing ceramics should maintain their self-healing ability to actively maintain their structural integrity.

As schematically shown in Figure 4.1, self-healing ability can deteriorate as a function of even if the ability is in dormancy state in such a severe condition. The structural integrity of self-healing ceramics will degrade as self-healing ability deteriorates, resulting in strength degradation of the composite as seen in conventional materials. Hence, it is critical to clarify the rate of deterioration of the composites' self-healing abilities and to establish a methodology for evaluating the self-healing lifespan to realize the implementation of the composites.

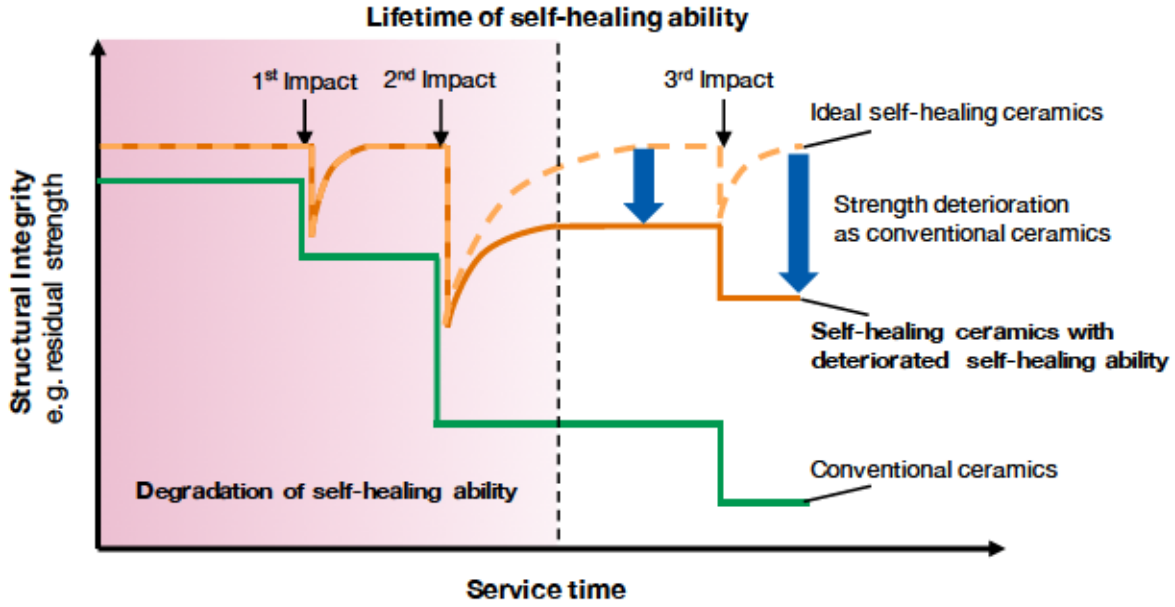

Figure 4.1 Schematic Illustration of Self-Healing Behaviour of Oxidation-Induced Self-Healing Ceramics With Deteriorated Self-Healing Ability

In the case of extrinsic oxidation-induced self-healing ceramics, degradation of self-healing ability corresponds to the deterioration of the healing agents. This is because the healing reaction in the composite can only be induced by the oxidation reaction of the healing agents. Phase transformations of healing agents, solution of healing agents into the matrix, and reactions between the matrix and the healing agents must be considered as contributing factors in the potential deterioration of healing agents. It is unnecessary, however, to discuss the phase transformation of

healing agents and the reaction between healing agents and the matrix, because undesirable reactions can be avoided by the theoretical calculations introduced in Chapter 2.

The deterioration factor of the internal oxidation of healing agents cannot be excluded by theoretical calculations because internal oxidation of the agents and self-healing reactions are both induced by the same oxidation reaction. In the previous study, Nanko et al.[5] reported that about 100 μm of internal oxidation layer was formed in Al_2O_3/Ni composites by annealing at 1300°C for 1h due to the external diffusion of Ni cation. On the other hand, Ando et al.[6] reported that the effect of the internal oxidation layer on the self-healing ability of Al_2O_3/SiC composites was negligible in the study and testing of the composites' high temperature creep. The lifetime of self-healing ability can be affected by the annealing conditions or the properties of the matrix, including the diffusion coefficient of the cation.

In this study, the internal oxidation of healing agents by the inward diffusion of oxygen was investigated as a main deteriorating factor of self-healing ability, as shown in Figure 4.2. It can be assumed that the cracking in the internal oxidation layer cannot be healed because the healing agents in the layer are already oxidized due to the internal diffusion of oxygen from the surrounding atmosphere. Moreover, as the internal oxidation layer grows as a function of service time and time, the unhealable region expands and new cracks in the region will remain. Consequently, the structural integrity of the composite can become deteriorated.

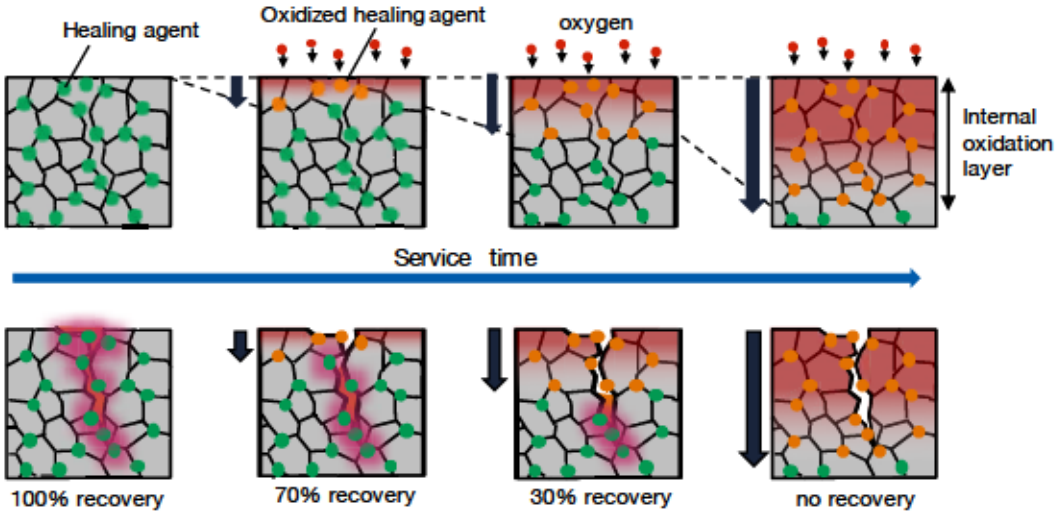

Figure 4.2 Degradation Model of Self-Healing Ability in Extrinsic Oxidation-Induced Self-Healing Ceramics

As the internal oxidation layer grows as a function of service time, the self-healing ability deteriorates as well. This is because crack-healing can be induced only in the areas where healing agents are still intact.

This study aims to establish a methodology for evaluating the durability of high temperature healing ability based on the quantitative evaluation of the effects of the internal oxidation layer on crack-healing ability in self-healing ceramics. The effect of the internal oxidation layer was studied based on the strength recovery behaviour of alumina/SiC composites having a certain internal oxidation layer thickness. Based on the results, a methodology for evaluating $T_{\text{H-high}}$ is proposed.

4.2 Definition of $T_{H\text{-}high}$ in Extrinsic Oxidation-induced Self-healing Ceramics

In this study, $T_{H\text{-}high}$ is defined as, "the maximum annealing temperature where strength of self-healing ceramics cannot be recovered completely by the ideal crack-healing condition due to deterioration of self-healing ability by aging for certain annealing time of x h." In the case of the alumina/SiC composites, the ideal crack-healing condition corresponds to annealing at 1300°C for 1h in air. When the strength of the alumina/SiC composite is not recovered completely by annealing at 1300°C for 1h in air after aging at T°C for Xh, we can conclude that $T_{H\text{-}high,\ X\,h}$=T °C.

4.3 Experiments

Alumina matrix composites containing 15 vol.% SiC, named Al15SiC, were prepared. The basic growth behaviour of the internal oxidation layer of the composite was studied by long-term annealing and cross-section analysis. The effect of the internal oxidation layer on self-healing ability was studied based on the strength recovery tests of Al15SiC aged at 1200°C for 1000 h. The aging conditions corresponded to the operation conditions of the middle pressure turbine blades of a jet engine.

4.3.1 Sample Preparation

Alumina raw powder (AKP-50, Sumitomo Chemical Co., Ltd.) and SiC powder (ULTRA FINE, IBIDEN Co., Ltd.) were used as starting materials. The initial average sizes were 0.2 and 0.35 μm, respectively. The alumina powder and the SiC powder were mixed at 15 vol.% in isopropanol using ø 5mm alumina balls and a 1000ml alumina pot. After 24h mixing, the mixed powder was dried on a heater for 3h at 120°C. The dried powder was sieved with a ø 250 μm mesh powder sieve. The sieved powder was densified by means of hot-pressing with a 50 mm x 50 mm carbon mould at 1700°C for 2h in Ar under 35MPa. The heating and cooling rate was 10°C/min. The typical thickness of the samples was about 5mm. The relative density of the sintered bulk materials as measured by Archimedes' method was more than 95%. The sintered discs were cut into rectangular bending specimens with a dimension of 3 x 4 x 48mm in accordance with JIS R1601. Samples were polished in various steps, with the final polish using a diamond paste with a particle size of 0.25 μm.

4.3.2 Growth Behaviour of the Internal Oxidation Layer

Growth behaviour of the internal oxidation layer in Al15SiC was evaluated based on the results of long-term annealing and cross-section analysis. The annealing was conducted in the temperature window of 1200°C to 1500°C for between 10h and 1000h. The depth of the internal oxidation layers was evaluated based on the backscattered electron images taken by SEM (JSM-7001F, JEOL Ltd.). Prior to the SEM observation, the cross-section of the aged samples was polished in various steps, with the final polish using a diamond paste with a particle size of 0.25 μm. As shown in Figure 4.3, the internal oxidation layer is clearly observed beneath the surface. The thickness of the layer was measured at each side of the specimen. Based on the obtained results, the growth behaviour of the

layer as a function of temperature was summarized by Arrhenius plots.

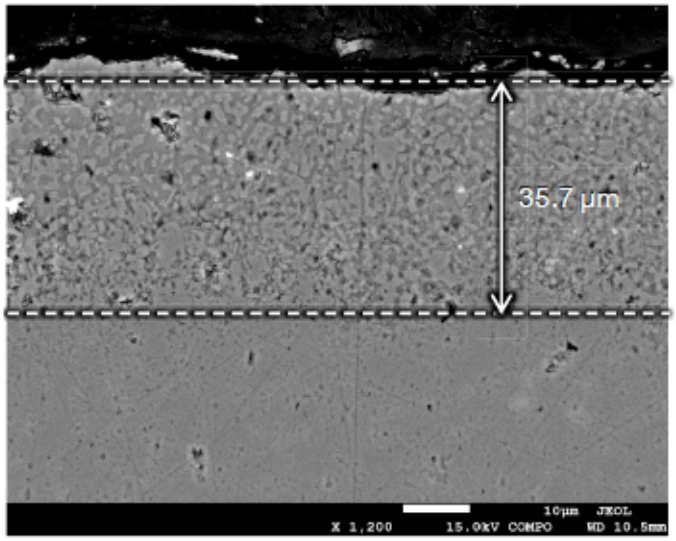

Figure 4.3 SEM Image of Cross-Section of Al15SiC Aged at 1400°C for 100h

4.3.3 Strength Recovery Behaviour of Aged Alumina/SiC Composite

Self-healing ability in the internal oxidation layer was evaluated based on the strength recovery tests of Al15SiC aged at 1200°C for 1000h, abbreviated as AGDAl15SiC. The aging conditions correspond to the operation conditions of the middle pressure turbine blades of a jet engine. The depth of the internal oxidation layer was evaluated by SEM observation (JSM-7001F, JEOL Ltd.). A semi-elliptical pre-crack with a 65 μm depth was introduced into the centre of the AGDAl15SiC specimens by using a Vickers indenter with a force of 10.8N. To heal the introduced pre-cracks, the aged specimens were annealed at 1300°C for 1h in air, following a previous study[6]. The strength recovery rate of the aged specimens was evaluated using Equation 4.1.

$$R_S = \frac{\sigma_{\text{healed}} - \sigma_{\text{pre-cracked}}}{\sigma_{\text{smooth}} - \sigma_{\text{pre-cracked}}} \tag{4.1}$$

Here, R_s [%]:strength recovery rate, σ_{smooth} [MPa]: fractural strength of specimen without pre-crack, $\sigma_{\text{pre-cracked}}$ [MPa]: fractural strength of specimen with introduced pre-crack, σ_{healed} [MPa]: fractural strength of pre-cracked specimen after annealing. The strengths were measured using the procedure in Section 4.2.2. The same evaluation of strength recovery was conducted on the specimens without the internal oxidation layer, called virgin specimens. By comparing the strength recovery behaviour of virgin Al15SiC and AGDAl15SiC, self-healing ability in the internal oxidation layer was studied.

4.3.4 Surface Analysis

The fracture surfaces of AGDAl15SiC after bending testing were analysed by laser microscope (VK-X, Keyence Corp.). The fracture initiation of AGDAl15SiC was determined from these

observations. The changes in the surface condition of Al15SiC aged at 1200°C for 1000h were observed, during which time annealing was observed in situ. The high temperature stage for an optical microscope (MS-TPS, Yonekura Inc.) was used as an apparatus. The sample dimensions were 3 × 4 × 1mm, with the pre-crack introduced on the 3 × 4mm surface. The sample was heated using an infrared heating method. The sample was heated to 1500°C with the heating rate of 10°C/min in open air.

4.4 Results

4.4.1 Growth Behaviour of the Internal Oxidation Layer

Figure 4.4 shows the growth behaviour of the internal oxidation layer at 1400°C in air as a function of annealing time. The growth behaviour of the layer clearly obeys Equation 4.2, known as Wagner's Parabolic Rate Law.

$$X^2 = k \cdot t \tag{4.2}$$

Here, X: thickness of internal oxidation layer [μm], k: parabolic rate constant [$\mu m^2 \cdot h^{-1}$]and t: annealing time [h]. The result indicates that the growth rate of internal oxidation behaviour is controlled by internal oxygen diffusion. The results obtained when annealing occurred at 1200°C, 1300°C and 1500°C also obeyed the parabolic rate raw. From Equation 4.2, the parabolic rate constant k can be determined at each annealing temperature.

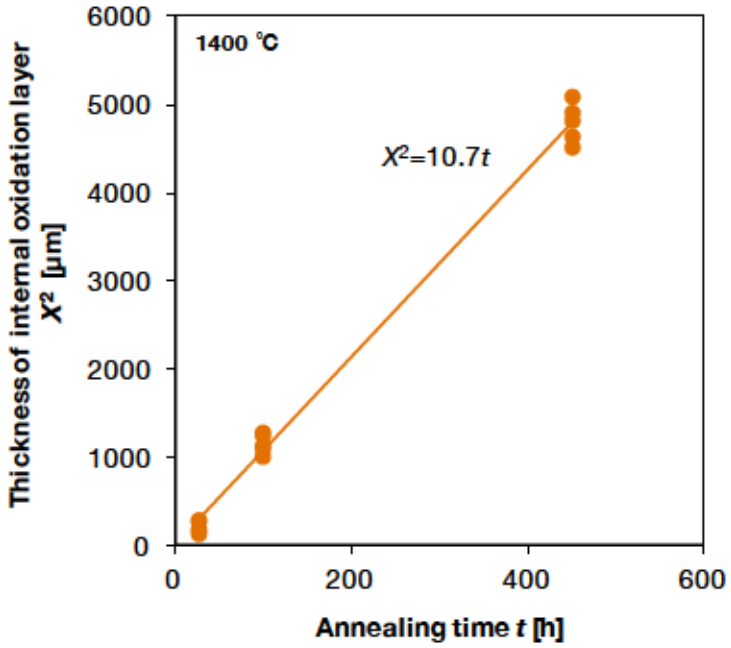

Figure 4.4 Growth Behaviour of the Internal Oxidation Layer in Al15SiC at 1400°C in Air as a Function of Annealing Time

The growth behaviour of the layer obeys Wagner's Parabolic Rate Law.

Figure 4.5 shows the temperature dependence of the parabolic rate constant k. The figure is

drawn based on Equation 4.3, known as the Arrhenius equation.

$$k = A \cdot \exp\left(-\frac{E_a}{RT}\right) \tag{4.3}$$

Here, k: parabolic rate constant [$\mu m^2 \cdot h^{-1}$], A: pre-exponential factor [$\mu m^2 \cdot h^{-1}$], E_a: activation energy [$kJ \cdot mol^{-1}$], R: gas constant[$J \cdot K^{-1} \cdot mol^{-1}$] and T: absolute temperature [K].

As shown in Figure 4.5, the parabolic rate constant k obtained from each annealing condition shows a linear relationship. This indicates that the internal diffusion of oxygen, which is the dominant chemical reaction in the growth of internal oxidation, can be assumed to be identical for all annealing conditions. By using Equation 4.3 and the least squares method, Equation 4.4 can be derived to describe the temperature dependence of the parabolic rate constant k:

$$\log k = -32551\frac{1}{T} + 20.589 \tag{4.4}$$

Based on Equation 4.4, the growth rate of the internal oxidation layer can be calculated at arbitrary annealing temperatures.

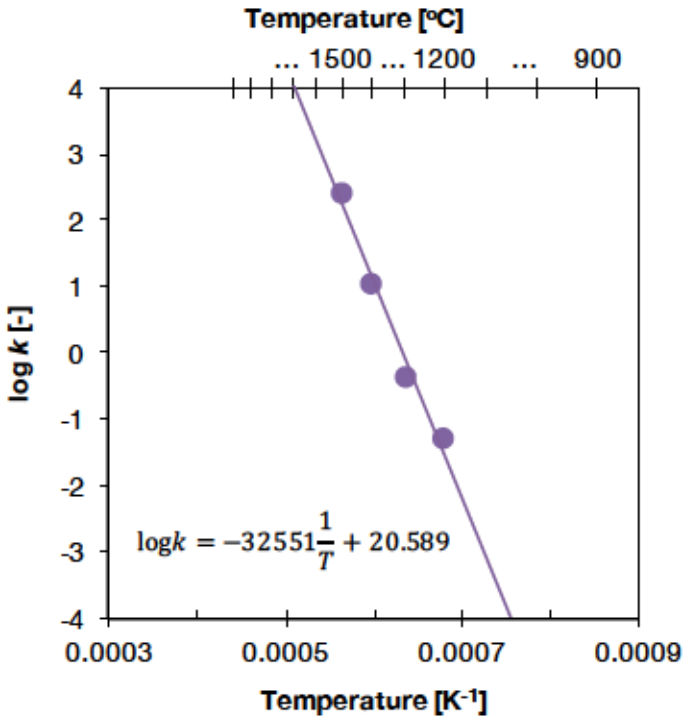

Figure 4.5 Temperature Dependence of Parabolic Rate Constant *k* Summarized by the Arrhenius Equation

4.4.2 Self-Healing Ability in Internal Oxidation Behaviour

Figure 4.6 shows the results of in situ surface observation of Al15SiC aged at 1200°C for 1000h during heating up to 1466°C in air with heating rate of 10°C/min. The introduced Vickers indent is located at the lower-left of the image and the pre-crack is indicated with arrows. The images

taken between room temperature and 1000°C are omitted because no changes in the surface due to oxidation of SiC were observed below 1000°C. The images in the temperature range between 1200°C and 1466°C became reddish because due to heat radiating from the sample. The surface of the sample before annealing is rough because of SiO_2 formed during the aging process at 1200°C for 1000h. For comparison, the in situ surface observation of virgin alumina/SiC composites reported by Ando et al.[8] is shown in Figure 4.7. The composition of the composites reported by Ando et al. is exactly same as Al15SiC used in this study, but was not aged prior to observation.

The surface condition of virgin alumina/SiC shown in Figure 4.7 changed drastically during annealing. The bubble formation due to the reaction in Equation 4.5, which corresponds to the self-healing reaction in alumina/SiC composite, was initially observed at 1247°C:

$$SiC + \frac{3}{2}O_2 = SiO_2 + CO\uparrow \tag{4.5}$$

The bubble formation intensified as the temperature increased, with the pre-crack disappearing at 1300°C.

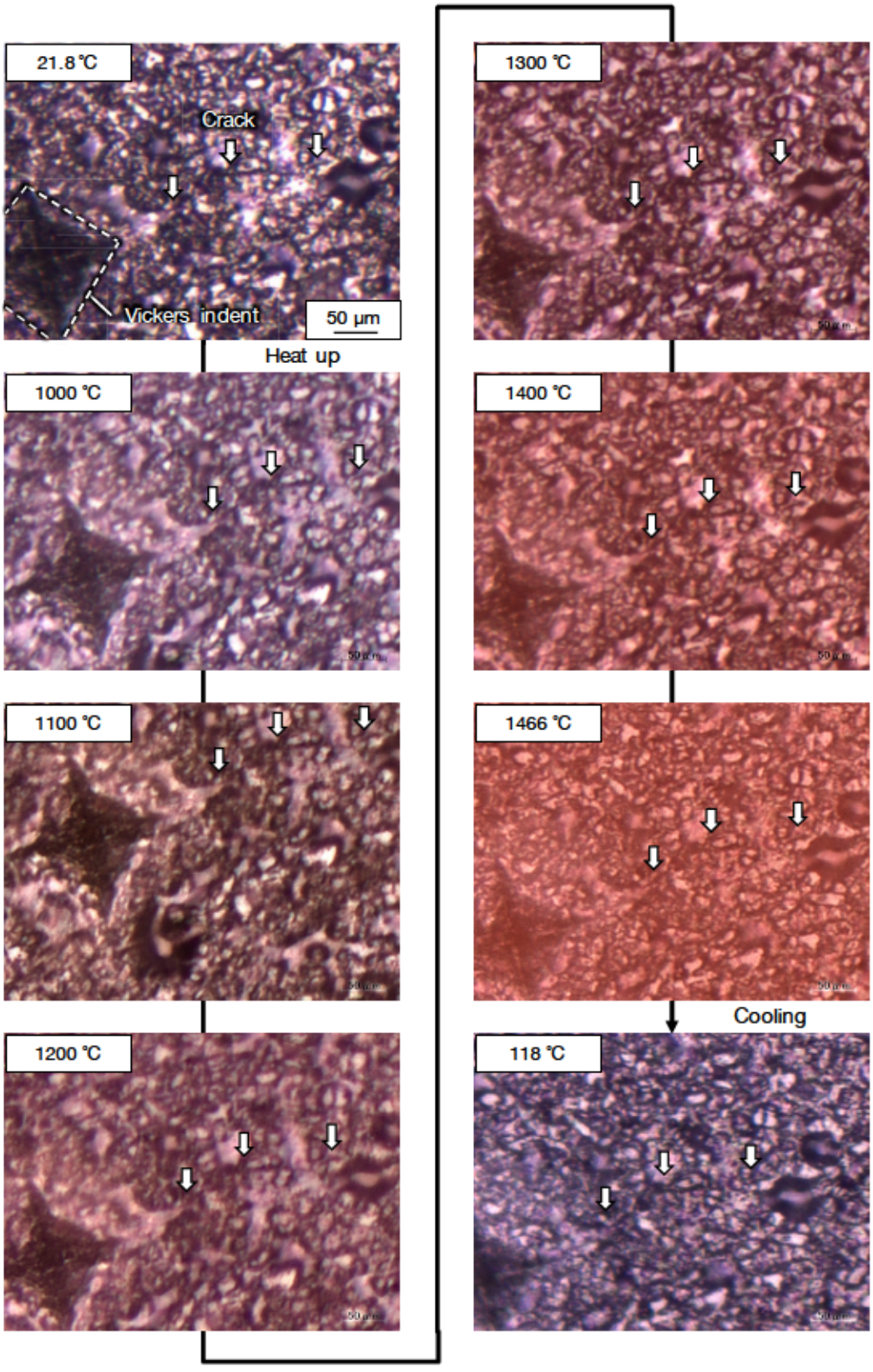

Figure 4.6 In Situ Surface Observation of Al15SiC Aged at 1200°C for 1000h

The aged Al15SiC is heated from room temperature to 1466°C at 10°C/min in air and then naturally cooled to 118°C.

The pre-crack is indicated with arrows.

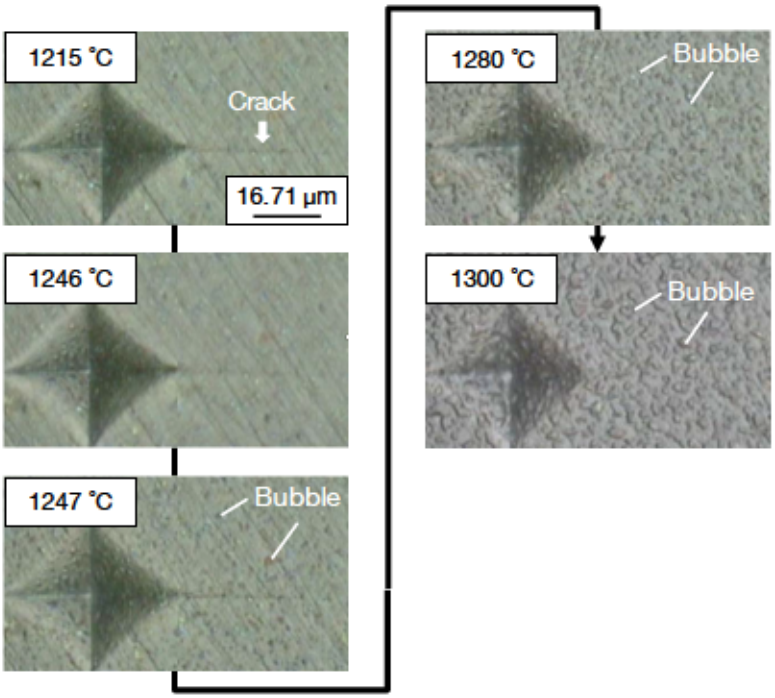

Figure 4.7 In Situ Surface Observation of Virgin Al15SiC as Reported by Ando et al.[8]

The virgin Al15SiC is heated from room temperature to 1300℃ at 10℃/min in air. The pre-crack is indicated with arrows. Bubble formation due to the formation of CO gas can be observed from 1246℃. The pre-crack has completely disappeared at 1300℃.

In contrast, the surface condition of the aged Al15SiC shown in Figure 4.6 is unchanged during annealing. Bubble formation is not observed even at 1300°C, and the pre-crack in the aged Al15SiC remains after annealing up to 1466°C. This suggests that the self-healing reaction shown as Equation 4.8 is not induced in the aged Al15SiC.

Figure 4.8 shows the fractured surface of the healed AGDAl15SiC and the pre-cracked AGDAl15SiC. The yellow region in the figure indicates the internal oxidation layer. From the SEM observation, the thickness of the internal oxidation layer is determined to be 7.1 μm. In the pre-cracked AGDAl15SiC, the semi-elliptical crack is indicated with a dashed line. This shape is same as the introduced indentation crack. In contrast, the shape of the fracture initiation in the healed AGDAl15SiC is different from the shape of the initial indentation crack. This indicates that most of the introduced crack is filled and bonded. However, considering that most of the fracture initiation is located in the internal oxidation layer and the fracture initiates from the indentation crack, the fracture initiation should be the unfilled part of the introduced crack.

Figure 4.9 shows the results of strength recovery tests on Al15SiC aged at 1200°C for 1000h, abbreviated as AGD15SiC. The average strength of smooth AGDAl15SiCis 701MPa. The strength of pre-cracked AGDAl15SiC is 241MPa. The strength of healed AGDAl15SiC, which has been pre-cracked and annealed at 1300°C for 1h, is between 637MPa and 655MPa. The results show that the strength of the healed specimens recovers to 88% of the smooth specimen's strength. The partial strength recovery of the AGDAl15SiC is due to the fact that most of the pre-crack was filled with SiO_2 formed by the oxidation of intact SiC located underneath the internal oxidation layer.

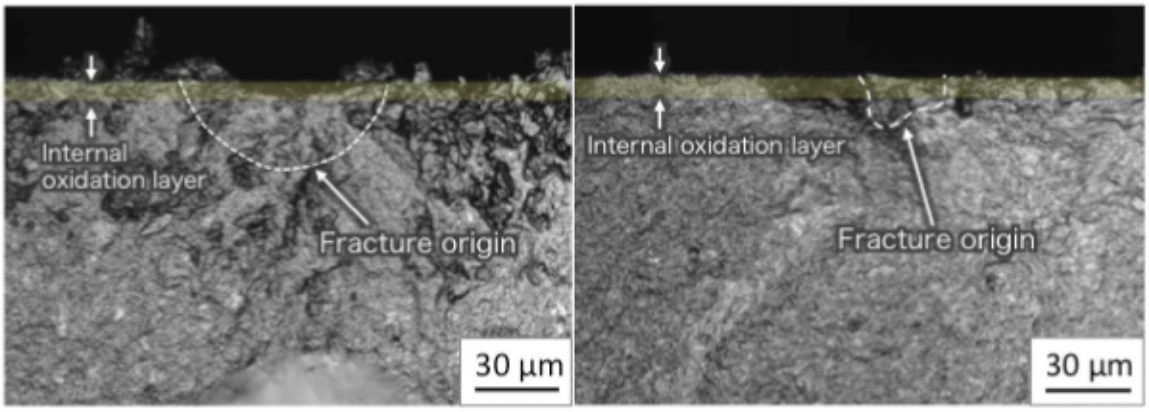

Figure 4.8 Fractured Surfaces of Pre-Cracked AGDAl15SiC (a) and Healed AGDAl15SiC (b)

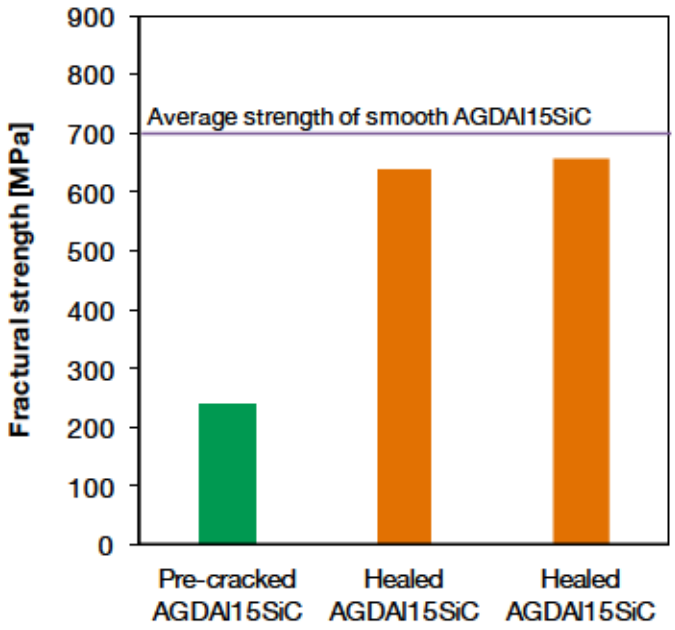

Figure 4.9 Strength Recovery Behaviour of AGDAl15SiC Aged at 1200°C for 1000h

In summary, the characteristic bubble formation related to the oxidation of SiC particles was not observed at the aged surface, and the strength of aged Al15SiC was not fully recovered even under ideal annealing conditions for crack-healing because the unfilled crack remained in the formed internal oxidation layer. From these results, it can be concluded that the self-healing ability in the internal oxidation layer has disappeared. This also suggests that the lifetime of the self-healing ability in extrinsic self-healing ceramics can be evaluated as a function of the internal oxidation layer thickness.

4.5 Discussion

4.5.1 Determination of Allowable Oxidation Layer Thickness X_c

As discussed above, the self-healing ability in extrinsic self-healing ceramics deteriorated as a function of the internal oxidation layer thickness because crack-healing could not be induced in the formed internal oxidation layer. The results indicate that the lifespan of self-healing ability can be quantitatively evaluated by determining the growth behaviour of the internal oxidation layer and the allowable oxidation layer thickness (X_c). In this study, X_c is defined by the thickness at which the crack-filling rate (f_{CH}) of the introduced pre-crack becomes less than 100% due to the presence of the internal oxidation layer.

The crack-filling rate (f_{CH}) can be calculated using the ratio between the volume of formed oxide (V_{CH}) and the crack volume (V_C) as shown in Equation 4.6

$$f_{CH}[\%] = \frac{V_{CH}}{V_C} \times 100 \tag{4.6}$$

The value of V_{CH} and V_C is calculated based on the model simulating the geometric structure of the semi-elliptical crack, as shown in Figure 4.10. C, C' and Δ_{max} represent the length, depth and crack opening distance of the introduced semi-elliptical crack, respectively. It is presumed that the process zone with a radius of a is formed underneath the indentation. In this study, the aspect ratio of the crack (C/C') is considered to be 1.

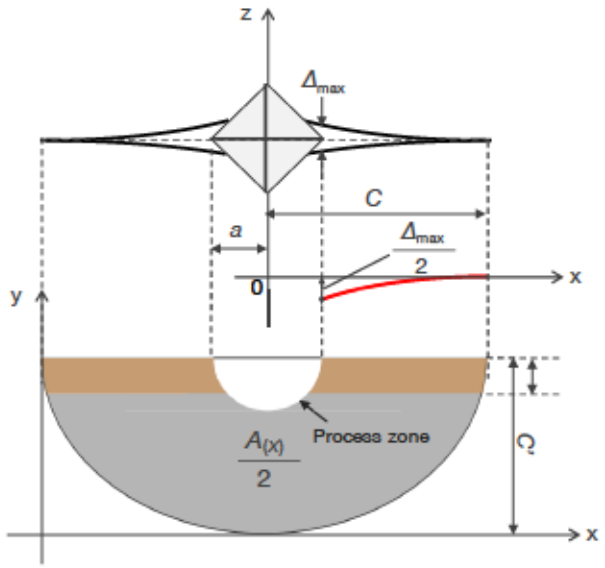

Figure 4.10 Schematic Illustration of the Geometric Structure of a Semi-Elliptical Crack Introduced by the Indentation Method

The value of V_{CH} is the extra volume produced by the formed oxide upon oxidation of intact healing agents on the crack surfaces, excluding the formed internal oxidation layer, as indicated by the grey colour zone shown in Figure 4.10. V_{CH} can be calculated as follows:

$$V_{CH} = A_{(X)} \cdot r_{SiC} \cdot f_V \left(\frac{d_{SiC}}{d_{SiO_2}} - 1 \right) \tag{4.7}$$

where A(x): crack surface area excluding internal oxidation layer, r_{SiC}: average particle diameter of SiC, f_v: volume fraction of SiC, and d_x: density of SiC and SiO_2. Based on the geometric structure of the crack surfaces, $A_{(x)}$ can be calculated using Equation 4.8.

$$A_{(X)} = 2\left\{ C^2 \cdot cos^{-1}\left(\frac{X}{C}\right) - X\sqrt{C^2 - X^2} \right\} \tag{4.8}$$

Assuming that the ridge line of the crack corresponds to a deflection curve, the value of V_C is calculated using Equation 4.9.

$$V_C = \frac{\pi \Delta_{max}}{40}(C - a)(4C + 11a) \tag{4.9}$$

Using Equations 4.6 through 4.9, volumetric crack-filling rate f_{CH} can be calculated as following:

$$f_{CH} = \frac{80\left\{C^2 \cdot \cos^{-1}\left(\frac{X}{C}\right) + X\sqrt{C^2 - X^2}\right\} \cdot r_{SiC} \cdot f_V \cdot \left(\frac{d_{SiC}}{d_{SiO2}} - 1\right)}{0.230 \cdot \pi (C - a)(4C + 11a)} \tag{4.10}$$

Figure 4.11 shows the relationship of the calculated crack-filling rate (f_{CH}) to both the thickness of the internal oxidation layer and the strength recovery rate of Al15SiC. Here, the experimental values of C=65 μm, a=15 μm, Δ_{max}=0.230 μm were used for the calculation. Orange line and green plots represent the calculated crack-filling rate and the results of strength recovery tests, respectively. Since the Al15SiC aged at 1200°C for 1000h has the internal oxidation layer thickness of 7.1 μm, the crack-filling rate calculated by Equation 4.10 is 96.5%. This indicates that the proposed model agrees with the experimental results. Based on the proposed model, an allowable internal oxidation layer thickness (X_c) of 5.5 μm the enables the crack-filling rate to reach 100%.

In addition to the determination of the allowable internal oxidation layer thickness (X_c), the proposed model shows the effect of the chemical reactions of the healing agents on the lifespan of the materials' self-healing abilities. Equation 4.10 indicates that the relative volume expansion directly affects the crack-filling rate of self-healing ceramics having an internal oxidation layer. This implies that a healing agent showing a high RVE value can elongate the lifetime of the materials' self-healing abilities.

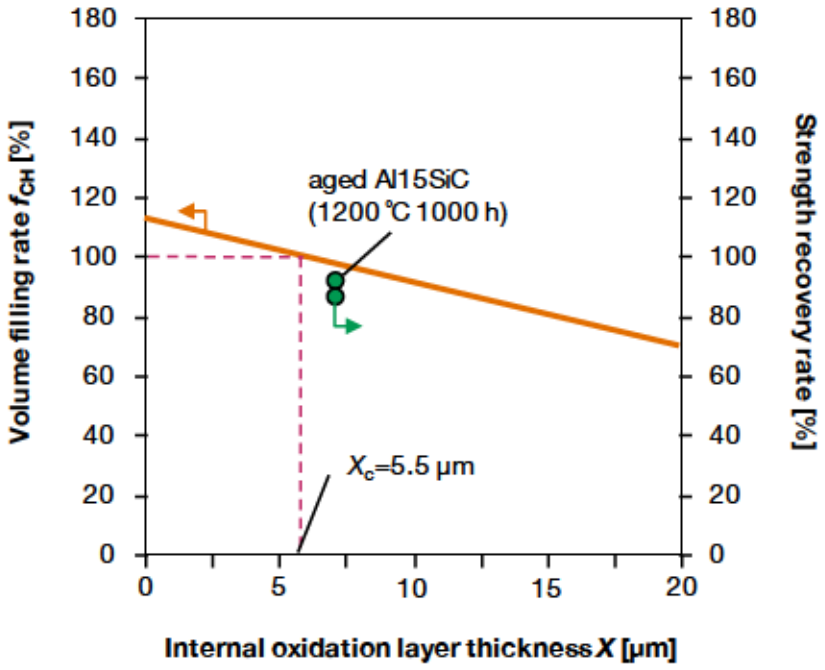

Figure 4.11 Internal Oxidation Layer Thickness Versus Crack-Filling Rate and Strength Recovery Rate

4.5.2 Methodology for Evaluating the Lifetime of Self-Healing Ability of Extrinsic Oxidation-Induced Self-Healing Ceramics

The allowable crack depth of Al15SiC was determined to be 5.5 μm based on the proposed model in Section 4.5.1. In the following, the methodology for evaluating the lifespan of the self-healing ability of extrinsic oxidation-induced self-healing ceramics is discussed in accordance with the definition of $T_{\text{H-high}}$ as presented in Section 4.2.

By inserting Equation 4.4 into Equation 4.2, we obtain the following equation.

$$X^2 = \exp\left(-32551 \cdot \frac{1}{T} + 20.589\right) \cdot t \tag{4.11}$$

Equation 4.11 indicates the dependence of the growth rate of internal oxidation layer thickness on temperature and annealing time. As previously discussed, the self-healing ability of the extrinsic self-healing ceramics reaches the end of its service life when the crack-filling rate drops below 100% due to the presence of the internal oxidation layer. By assigning the value of the allowable crack depth to Equation 4.11, the annealing time and temperature impact on the overall service life can be determined. Here, the annealing temperature corresponds to the upper limit of the healing temperature range ($T_{\text{H-high}}$), and the annealing time corresponds to the lifetime of the healing ability (t_L).

Figure 4.12 shows the relationship between the upper limit of the temperature range ($T_{\text{H-high}}$) and the lifetime of the healing ability (t_L). The orange line represents the result of the present Al15SiC. For comparison, the relationship on mullite/$TiSi_2$ and mullite/Y_2O_3/$TiSi_2$ composites, which are introduced in Chapter 2, are also indicated with green and purple line in the figure, respectively. The

t_L and $T_{H\text{-}high}$ of those composites are evaluated based on the same methodology as Al15SiC, but it was assumed that the allowable internal oxidation layer thicknesses in the mullite/$TiSi_2$ and mullite/Y_2O_3/$TiSi_2$ composites were equal to the Al15SiC. As shown in Figure 4.12, the lifetime (t_L) is shortened as $T_{H\text{-}high}$ increases, which can be paraphrased as the maximum operation temperature of the respective high temperature components. Conversely, as $T_{H\text{-}high}$ decreases the durability time of components becomes longer. The $T_{H\text{-}high}$- t_L line of Al15SiC is located to the right side of the figure, comparing this data to the other materials, ultimately indicating that Al15SiC has longer lifetime (t_L) and higher $T_{H\text{-}high}$ than the other composites.

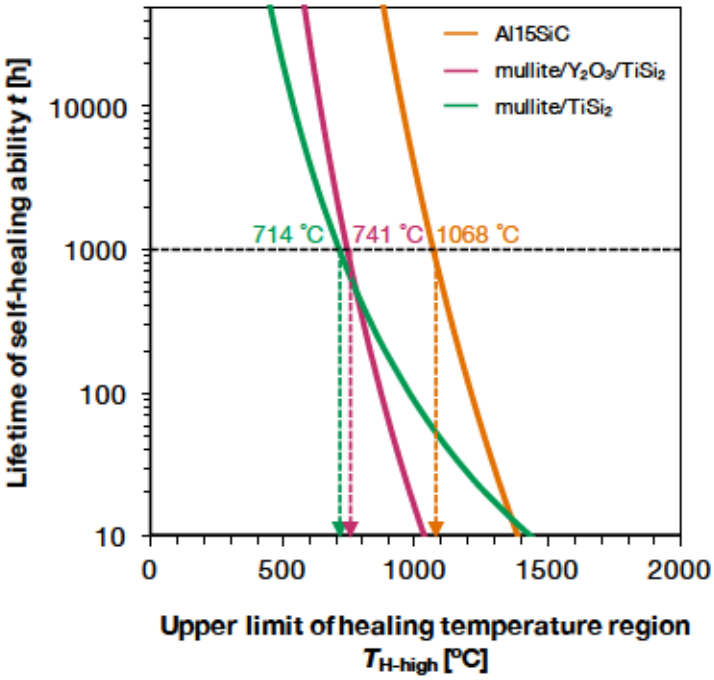

Figure 4.12 Relationship Between the Upper Limit of the Temperature Range ($T_{H\text{-}high}$) and the Lifespan of Self-Healing Ability (t_L)

By inserting the required lifespan of the self-healing ability of the composite, we can uniquely define the upper limit of temperature the range ($T_{H\text{-}high}$). For instance, the turbine blades of a jet engine should maintain their properties for 1000h at maximum operation temperature. Therefore, by inserting t_L=1000h into Figure 4.12, the $T_{H\text{-}high,\ 1000h}$ of each composite can be calculated as illustrated in Equation 4.10, clearly indicating that Al15SiC is more durable that the other composites.

$$\begin{aligned} &\text{Al15SiC:} && T_{H-high,1000h} = 1068\ ^{\circ}C \\ &\text{mullite/ } Y_2O_3\text{/ } TiSi_2\text{:} && T_{H-high,1000h} = 741\ ^{\circ}C \\ &\text{mullite/ } TiSi_2\text{:} && T_{H-high,1000h} = 714\ ^{\circ}C \end{aligned} \tag{4.10}$$

As shown above, the durability of extrinsic oxidation-induced self-healing ceramics can be evaluated as a function of the upper limit of the healing temperature range ($T_{H\text{-}high}$) or the lifespan of

the self-healing ability (t_L) on the basis of the proposed methodology.

4.6 Conclusion

In this chapter, the deterioration factor of the self-healing ability in extrinsic oxidation-induced self-healing ceramics was clarified, and a methodology for evaluating the upper limit of the healing temperature range ($T_{H\text{-}high}$) was proposed. From this study, the following results were obtained.

I. The growth behaviour of the internal oxidation layer in alumina/SiC composites was evaluated based on accelerated degradation tests at high temperatures and the Arrhenius equation. The growth behaviour of the internal oxidation layer obeyed Wagner's Parabolic Rate Law. The experimental equation for the growth law was determined to be as follows.

$$\log k = -32551\frac{1}{T} + 20.589$$

II. The strength of the alumina/SiC composite aged at 1200°C for 1000h recovered to 88% of that of the virgin specimen. The fracture origin of the aged composite was located in the internal oxidation layer. Those results suggest that pre-cracks have not been filled and bonded at the internal oxidation layer.

III. The changes in the surface condition of the aged alumina/SiC composite during annealing up to 1500°C were observed in situ. The typical signs of oxidation at the surface, such as formation of oxides or bubbles, were not observed. This result indicates that the desired oxidation reaction to achieve self-healing was not induced in the internal oxidation layer.

IV. Based on the proposed geometric model of the introduced crack, the allowable thickness of the internal oxidation layer in Al15SiC was determined to be 5.5 μm. The proposed model also suggests that high relative volume expansion in the healing agent can elongate the lifespan of the self-healing ability.

V. From the obtained results, the lifetime of the self-healing ability was evaluated as a function of the growth rate of the internal oxidation layer. The relationship between $T_{H\text{-}high}$ and lifespan of the self-healing ability (t_L) for the alumina/SiC composite was determined to be as follows.

$$5.5^2 = \exp\left(-32551 \cdot \frac{1}{T_{H-high}} + 20.589\right) \cdot t_L$$

VI. Based on the proposed evaluation method, the upper limit temperatures of several self-healing ceramics at 1000h operation ($T_{H\text{-}high,\,1000\,h}$) were determined to be as follows.

Al15SiC: $T_{H-high,1000h}$ =1068 °C

mullite/ Y_2O_3/ $TiSi_2$: $T_{H-high,1000h}$ =741 °C

mullite/ $TiSi_2$: $T_{H-high,1000h}$ =714 ℃

References

1) Wing, R., & McGill, I. R. (1981). The protection of gas turbine blades: a platinum aluminide diffusion coating. Aircraft Engineering and Aerospace Technology, 53(10), 15-21.
2) International Aircraft Development Fund. (2003). Kōkū engine no seibi ni kansuru genjyō to dōkō [Current status and trends on maintenance of jet engine]. (in Japanese): Available From: http://www.iadf.or.jp/8361/LIBRARY/MEDIA/H15_doukochosa/h15-4-4.pdf
3) Ackert, S. (2010). Engine maintenance concepts for financiers. *Macquarie AirFinance, Mar.*
4) Lane, C. (2014). Introduction. In The Development of a 2D Ultrasonic Array Inspection for Single Crystal Turbine Blades. Springer International Publishing.
5) Salas-Villaseñor, A. L., Lemus-Ruiz, J., Nanko, M., & Maruoka, D. (2009). Crack disappearance by high-temperature oxidation of alumina toughened by Ni nano-particles. *Advanced Materials Research,* 68, 34-43.
6) Nakao, W., Ono, M., Lee, S. K., Takahashi, K., & Ando, K. (2005). Critical crack-healing condition for SiC whisker reinforced alumina under stress. Journal of the European Ceramic Society, 25(16), 3649-3655.
7) Newman, J. C., & Raju, I. S. (1981). An empirical stress-intensity factor equation for the surface crack. Engineering fracture mechanics, 15(1-2), 185-192.
8) Ghosh, S. K. (Ed.). (2009). Self-healing materials: fundamentals, design strategies, and applications. John Wiley & Sons.

Chapter 5

Interface Design Between Matrices and Crack Filling Oxides [1]

This chapter deals with the effects of interface conditions between matrices and crack-filling oxides on the strength recovery behaviour of self-healing ceramics. The effect is discussed based on the results of strength recovery testing of the alumina/TiC composite as a function of annealing time. The strength recovery of the composite at 600°C shows an almost constant value of 50% regardless of annealing time, even though the pre-crack is totally filled with the formed oxide TiO_2. The intermediate compound, Al_2TiO_5, is not detected below 600°C where the value of strength recovery is saturated. The results imply that the formation of intermediate compounds at crack-healed area plays an important role in achieving a desirable bond at the point of interface between matrices and formed oxides, resulting in the complete strength recovery of self-healing ceramics. Based on those discussions, the methodology is proposed to allow for the evaluation of oxide matrices in which desirable interface bonding can be attained.

[1]This chapter is based on:

Yoshioka, S. & Nakao, W. Effect of interface condition between matrix and crack-filling oxide on strength recovery behavior of self-healing ceramics. *Journal of the European Ceramic Society* (manuscript in preparation).

5.1 Introduction

As discussed in Chapter 1, the first requirement for inducing self-healing in oxidation-induced self-healing ceramics is to bring the healing agent to its active state. In the active state, healing agents begin to oxidize intensely and formed crack-filling oxides indicate the presence of the mobile phase. The active state and proposed methodology for evaluating the lower limit of the healing temperature range ($T_{H\text{-}low}$) that would allow the composite to recover its original strength were the focus in Chapter 2.

In order to completely recover the mechanical integrity of self-healing ceramics, it is necessary to focus on both the active state and the transition state of self-healing. In the transition state, the formed mobile phase compounds become immobile, and the desired chemical bonding between formed oxides and the matrix is re-established. The complete strength recovery of the composite can be attained only after the completion of the transition state.

In this chapter, the focus is on the transition state of self-healing, aiming to clarify the effects of the interface conditions of crack-filled parts on the strength recovery behaviour of extrinsic oxidation-induced self-healing ceramics. A methodology for selecting an attractive matrix for respective healing agents is proposed based on the results, taking into account the properties of both the matrix and the healing compounds that are necessary to complete the transition phase.

The effect of the interface conditions of the crack-filled parts are studied based on the strength recovery behaviour of Al30TiC at a low temperature range as a function of annealing time. In Chapter 3, direct observation of crack-healed parts was used to confirm that the complete strength recovery of alumina/TiC composite was achieved at temperatures above 800°C owing to the complete filling of the crack by the formed TiO_2. This indicates that the transition phase has been completed at 800°C within 1h. However, despite the fact that the lower limit of the healing temperature range ($T_{H\text{-}low}^{est}$) of TiC-containing self-healing ceramics is estimated as 424°C by the method proposed in Chapter 2, the strength recovery rate of Al30TiC is only 14% when annealed at 400°C and 47% when annealed at 600°C. This suggests that the transition phase has not been completed within 1h at those temperatures. In this section, the strength recovery of Al30TiC as a function of annealing time was studied. Prior to testing, the oxidation behaviour of TiC was investigated using thermogravimetric analysis to confirm that the active state is completed at the specified temperature window. The crack-filled parts were directly observed by Focused Ion Beam and Scanning Electron Microscope (FIB/SEM). The formed oxides were also characterized by XRD analysis.

5.2 Experiments

5.2.1 Thermogravimetric Analysis of TiC Particles

A TG/DTA analyser (TGD-9600, ULVAC-RIKO) was used with an R-type thermocouple and an alumina cell having a 5mm diameter and a 5mm height. TiC powder (STD120, H.C. Starck GmbH) was used as a sample and alumina powder (AKP-50, Sumitomo Chemical Co., Ltd.) was used as a reference, with average particle sizes of 0.3 μm and 0.2 μm, respectively. About 20mg each of

TiC and alumina powders were put into the alumina cell and annealed at 600°C for 10h in dried air with 10 ml/min. The value of β was 10°C/min, corresponding to the heating rate used for the following strength recovery tests.

5.2.2 Strength Recovery Test of Al30TiC as a Function of Annealing Time

The Al30TiC was prepared using the same method described in Chapter 3. In order to study the strength recovery of Al30TiC as a function of the annealing time, the strength values of smooth specimens, pre-cracked specimens and healed specimens were determined. Smooth specimen refers to samples without induced damage prior to testing. Pre-cracked specimens are specimens with a standardized pre-crack introduced by Vickers' indenter at the centre of the surface. The indentation force was 19.6N and the introduced crack had a surface length of about 100 μm for both sets of samples. The two sets of radial indentation cracks are either perpendicular or parallel to the longest dimension of the bend test samples. The healed specimens are pre-cracked and have been annealed for between 10min and 300h in air at temperatures ranging from 600°C to 1000°C. The heating and cooling rates were standardized at 10°C/min.

The strength of each sample was measured by means of a three-point bending test. The span between the supporting 5mm diameter steel rollers was 16mm. The specimen was mounted to apply the maximum tensile stress to the pre-crack or healed crack part. All tests were conducted at room temperature and with a cross-head displacement velocity of 0.5mm/min.

5.2.3 Structure Characterisation

The crystal structure of the various phases in the samples prior to and after thermal annealing was determined using XRD (ULTIMA Ⅳ Rigaku Co.) operated with CuKα radiation. The crack-filled areas of the annealed specimens were directly observed by using a focused ion beam (JIB-4501, JEOL Ltd.) and SEM (JSM-7001F, JEOL Ltd.). The sample for direct observation was prepared using the same procedure introduced in Chapter 3.

5.3 Results

5.3.1 Thermogravimetric Analysis of TiC Particles

Figure 5.1 shows the result of thermogravimetric analysis at 600°C for 10h. Green, red and blue line represent the mass gain, the temperature profile and DTA, respectively. As shown in the figure, the mass gain corresponds to the oxidation reaction of the TiC powder and can be observed below 600°C. The reaction ends 9000s after reaching 600°C. When it is taken into account that alumina matrix composites containing 30 vol.% of TiC powder can fill the indentation crack as shown in Chapter 3, it can be expected that the present composite also has the potential for filling cracks by annealing at 600°C.

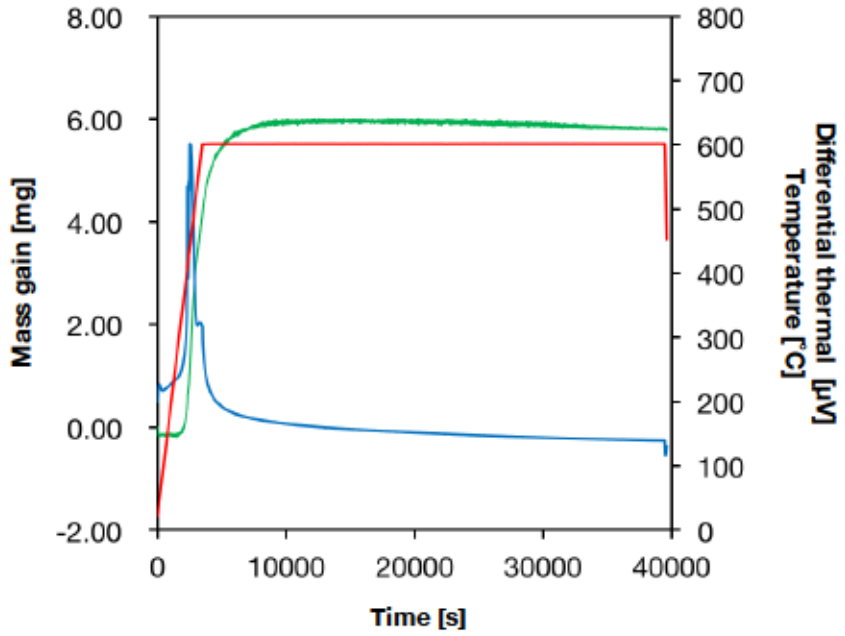

Figure 5.1 Result of Thermogravimetric Analysis of TiC Powder at 600°C for 10h in Dried Air

The oxidation reaction of TiC powder is completed 9000s after reaching at 600°C.

5.3.2 Direct Observation of Crack-Filled Area

Figure 5.2 shows the results of direct observations via FIB and SEM of the crack-filled parts of Al30TiC annealed at 600°C for 1h and 300h. Both images are backscattered electron images of the region underneath the indentation where the crack opening distance is largest (~150 μm). White particles and grey regions correspond to TiC particles and alumina matrices, respectively. Arrows at the centre of the images indicate the introduced pre-crack.

While the pre-crack in Al30TiC annealed for 1h is partially bridged by formed oxide, the crack is not fully filled. In the sample annealed for 300h, the pre-crack is fully filled with formed TiO_2 and no defects can be seen in the region. This result corresponds to the expectation that the pre-crack can be filled with the formed oxide as discussed based on the TGA analysis in the previous section.

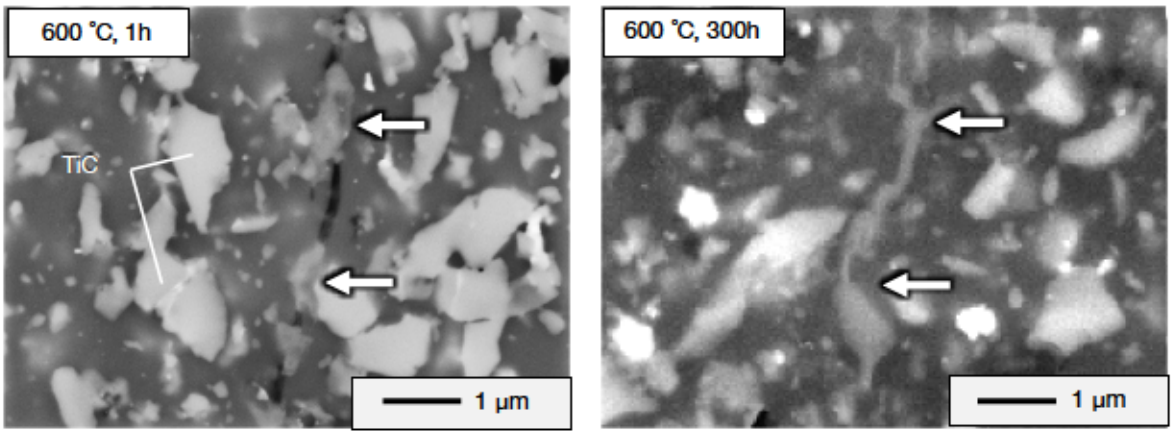

Figure 5.2 SEM Image of the Crack-Healed Area in the Depth Direction of Al30TiC Annealed at 600°C for 1h (a) and 300h (b)

5.3.3 Strength Recovery Test of Al30TiC as a Function of Annealing Time

The strength recovery behaviour of Al30TiC between 600°C and 1000°C as a function of annealing time is shown in Figure 5.3. The green, purple and orange plots indicate the strength of the sample annealed at 600 °C, 800 °C and 1000 °C, respectively. The open symbols represent the fracture was initiated from the introduced pre-crack and the closed symbols represent the fracture origin was moved to the other defects. The average strength of the smooth specimen is 715MPa and average strength of the pre-cracked specimen is 225MPa.

The strength of the sample healed at 1000°C is recovered within 10 min annealing, indicating that the active state and transition state of self-healing are completed within 10 min at 1000°C. While the strength of the specimen annealed at 1000°C for 1h is deteriorated because of the excess diffusion of Ti cation as discussed in Chapter 3, that of the specimen annealed for 10 min is higher than the average strength of the smooth specimen. This is because the outward diffusion of Ti cation does not progress in such a short annealing time, and the initial surface crack is invalidated by the healing reaction. In contrast, the strength recovery rate of the specimen annealed at 800°C for 10 min is only 50% of the strength of the smooth specimen and could be caused by insufficient filling of the crack.

The strength recovery rates of the specimens are 34% when annealing at 600°C for 10 min, and 49% when annealing at 600°C for 1h. The specimens annealed at 600°C for 50h and 300h show very little change in the strength recovery rate. These results are beyond the reasonable expectation based on the thermogravimetric analysis in Section 5.3.2, because it is expected that the recovery rate should increase as the amount of formed TiO_2 increases.

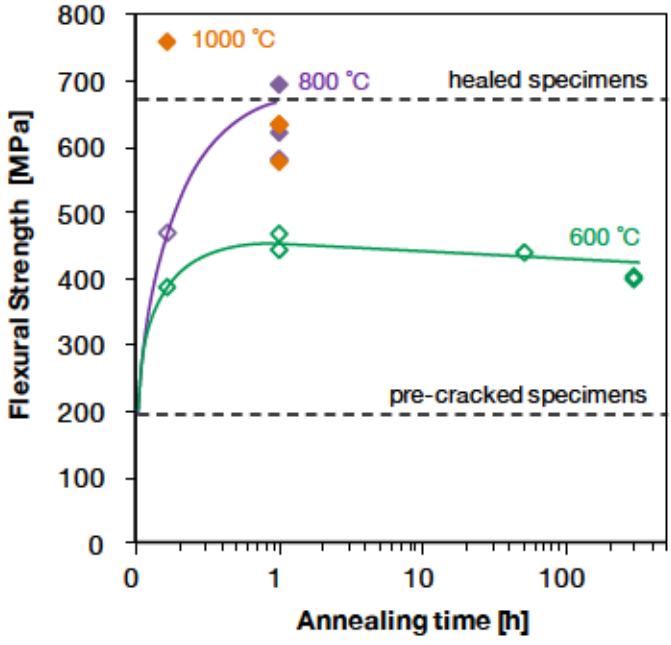

Figure 5.3 Strength Recovery Behaviour of Al30TiC as a Function of Time

5.3.4 XRD Surface Analysis of Annealed Al30TiC

Figure 5.4 shows the XRD surface analysis of Al30TiC annealed at several temperatures for 1h. The round, square, diamond and triangle symbols indicate rutile, corundum, TiC and Al_2TiO_5, respectively. Formed TiO_2 is not detected in the smooth specimens, but as annealing temperature is increased, the peak of the oxide becomes sharp. The noteworthy result is that Al_2TiO_5, the intermediate compound between Al_2O_3 and TiO_2, is detected only above 800°C. The temperature corresponds to the temperature at which complete strength recovery of Al30TiC is observed.

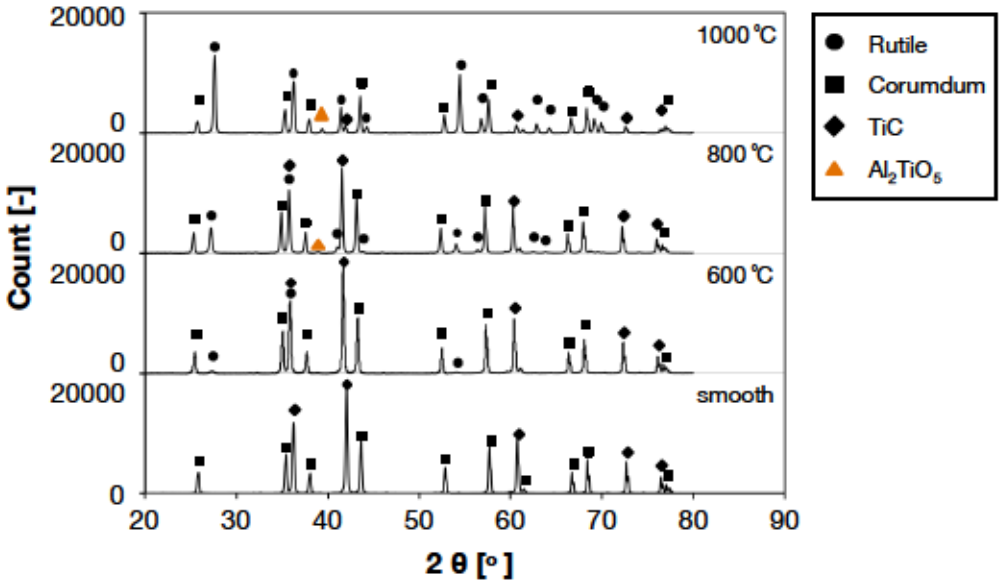

Figure 5.4 XRD Surface Analysis of Annealed Al30TiC at Several Temperatures

5.4 Discussion

5.4.1 Effect of Interface Conditions on Crack-Filled Parts

From the results above, it was revealed that both the oxidation of TiC particles and the filling of pre-cracks progress as annealing time increases. It was also shown that the full filling of the pre-crack did not lead to the strength recovery of the composite at lower temperatures (600 °C). From this data, there are two factors that must be considered. First, the bonding strength of the interface between the formed oxides (TiO_2//TiO_2 interface) is not sufficient. Second, the bonding strength of the interface between the formed oxide and the matrix (TiO_2//Al_2O_3 interface) is also not sufficient.

The first factor can be discussed in regards to the sintering of TiO_2. There are several previous reports on the sintering behaviour of TiO_2[1,2]. According to these reports, the densification of TiO_2 generally starts between 1100°C and 1300°C. In contrast, the densification of the submicron ordered TiO_2, such as the TiO_2 formed on TiC particles, starts in a lower temperature range. The density of sintered submicron TiO_2 reaches 99% of its theoretical value at around 850°C[1], and reaches 90% by annealing at 550°C for 15h to 20h[2]. Those reports did not discuss the mechanical strength of sintered TiO_2, but it is possible that the TiO_2 present could have been densified as well. The formed TiO_2 has

a diameter of less than 1 μm as shown in Figure 3.1, and an annealing time of 50h to 300h is much longer than the times in the previous reports. As a result, it was concluded that the sintering of TiO_2 was progressed enough to re-establish the chemical bonds and the mechanical strength of the TiO_2//TiO_2 interface.

The second factor can be discussed in regards to previous reports on the strength recovery behaviour of the alumina/SiC composite. The composite can recover its strength completely by annealing at 1200°C for 10h or 1300°C for 1h, and it is expected, based on XRD analysis, that a small amount of mullite is formed at the crack surfaces[3]. As shown in Figure 5.4, the intermediate compound Al_2TiO_5 is detected in the Al30TiC. By extension, it also can be expected that the intermediate compound has been formed at the alumina//TiO2 boundary by annealing above 800°C. It is noteworthy that the temperature at which the intermediate compound is detected corresponds to the temperature at which the strengths of both composites are completely recovered. Moreover, considering that the strength of the Al30TiC was not recovered by annealing at 600°C even though the pre-crack was fully filled with oxide, it can be argued that the formation of intermediate compounds plays an important role in attaining complete strength recovery of the composite, or in the completion of the transition phase of self-healing.

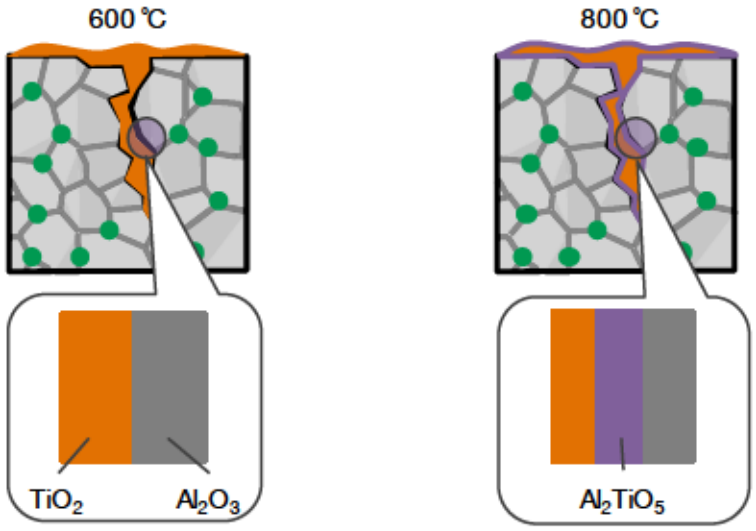

Figure 5.5 Schematic Illustration of the Interface Conditions in the Crack-Filled Area of Al30TiC

5.4.2 Methodology for Evaluating Matrices for Self-Healing Ceramics

The obtained results suggest that the formation of intermediate compound plays an important role in attaining desirable bonding interfaces in crack-filled areas, resulting in complete strength recovery of the oxidation-induced self-healing ceramics. In such a case, the chemical properties of both the healing agents and the matrix strongly affect the formation of intermediate compounds in the crack-filled area. The critical required properties of matrices necessary for forming intermediate compounds and a proposed methodology for evaluating an oxide matrices for extrinsic oxidation-induced self-healing ceramics are discussed.

Osada et al. suggest that the decrease in viscosity of formed SiO_2 enables the intermediate compound to form more easily, resulting in an increase in the strength recovery rate of alumina/SiC self-healing ceramics[4]. The study is based on the kinetic approach to optimizing the rate of self-healing and has yielded great results[4]. In case of this study, the proposed method is inapplicable because the crystallization of the formed TiO_2 is rapid and the formation of intermediate compounds is controlled by a solid-solid reaction, in contrast to the liquid-solid reaction present in the case of alumina/SiC. For the purposes of this study, an alternative selection methodology based on thermodynamics was used.

The proposed selection process of an oxide matrix for extrinsic oxidation-induced self-healing ceramics is shown in Figure 5.6. The proposed method is intended primarily for matrix selection, but the method is theoretically applicable for selecting additives for self-healing ceramics systems, which enable the systems to attain the desired bonding interfaces in the crack-filled areas.

The selection process was applied to oxides of 48 elements from Groups 1-14 and Periods 1-6 in the Periodic Table. Lanthanide metal is excluded in this study. Phase diagrams were primarily used to experimentally confirm information from the available literature[5-34]. Theoretical phase diagrams calculated by FactSage 7.0 were used when experimental phase diagrams were not available or the temperature window of the experimental phase diagrams was limited. Gibbs free energy of formation of intermediate compound values were all calculated by FactSage 7.0.

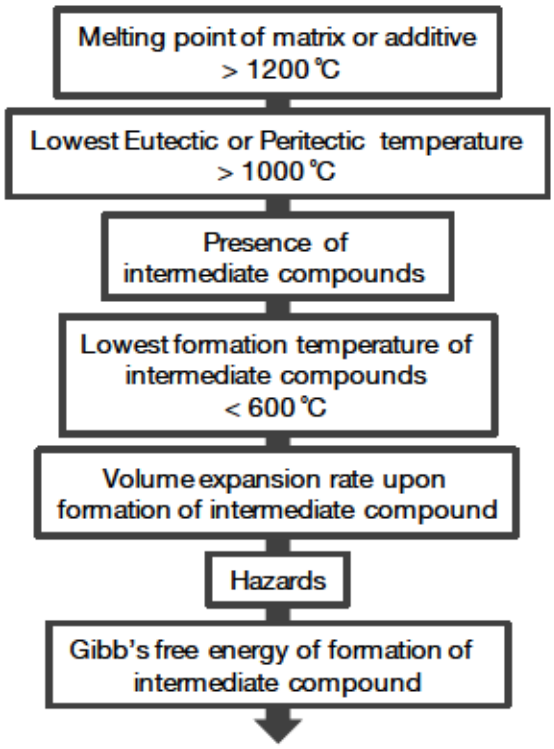

Figure 5.6 Selection Process of Matrices or Additives That Enable Complete Composite Strength Recovery Below 600°C

The results of the investigation of the phase diagrams are summarized in Table 5.1. The melting point of oxide candidates was evaluated to confirm their high temperature stability. Oxides having a melting

point below 1200°C were excluded. Subsequently, in order to confirm the high temperature strength of of the composite, the lowest eutectic or peritectic temperature listed in the pseudo-phase diagrams between TiO_2 and each oxide candidate were evaluated. The formation of a liquid phase could lead to the deterioration of the high temperature strength of the self-healing ceramic because a liquid phase has no mechanical strength. Assuming the operating temperature of the composite is below 1000°C, the oxides showing the lowest eutectic or peritectic temperature below 1000°C in the pseudo-system were also excluded. Furthermore, the oxides that can form intermediate compounds with TiO_2 below 600°C were selected based on the same pseudo-phase diagrams. Relative volume expansion (RVE) upon the formation of intermediate compounds was also evaluated, because excess volume expansion or shrinkage produces internal stress in crack-healed areas or leads to insufficient filling of an introduced crack. The values of RVE were small, meaning that the volumetric change upon the formation of intermediate compounds could be ignored. Finally, the hazards of oxides such as toxicity and radioactivity were evaluated and hazardous oxides were excluded. Seventeen oxides were selected and are shown in Table 5.1.

Table 5.1 Summary of Investigation of Phase Diagrams

Oxide	Melting Point [°C]	Intermediate compound	Lowest formation temperature of intermediate compound [°C]	Lowest formation temperature of liquid phase [°C]	Relative volume expansion [°C]
BaO	1923	Ba_2TiO_4	927>	1325	6.33
SrO	2430	$SrTiO_3$	227>	1439	-9.16
Li_2O	1570	Li_2TiO_3	600>	1030	-4.61
CaO	2613	$Ca_3Ti_2O_7$	200>	1417	-2.03
MgO	2852	$MgTiO_3$	200>	1620	2.85
MnO	1945	Mn_2TiO_4	200>	1369	8.49
CoO	1830	Co_2TiO_4	1050>	1430	2.35
FeO	1377	$FeTiO_3$	200>	1312	1.89
NiO	1955	$NiTiO_3$	200>	1573	2.72
ZnO	1975	Zn_2TiO_4	600>	1418	-3.78
ZrO_2	2715	$ZrTiO_4$	600>	1720	-0.71

The selection indexes above based on thermodynamic analysis and ignore kinetic aspects. If we ignore the effects of micro-structure on the material, the kinetic aspects can be discussed based on the Gibbs free energy change in the system, since every mass transfer phenomenon, including the densification process, is driven by the Gibbs energy change in the system. Since the Gibbs free energy change of formation of the intermediate compounds (ΔG_f) is calculated in the temperature window of 200°C to 2000°C in the study, it can be expected that the intermediate compound is stable and easily formed when the ΔG_f shows a large negative value. The results of these calculations are shown in

Figures 5.7 and 5.8.

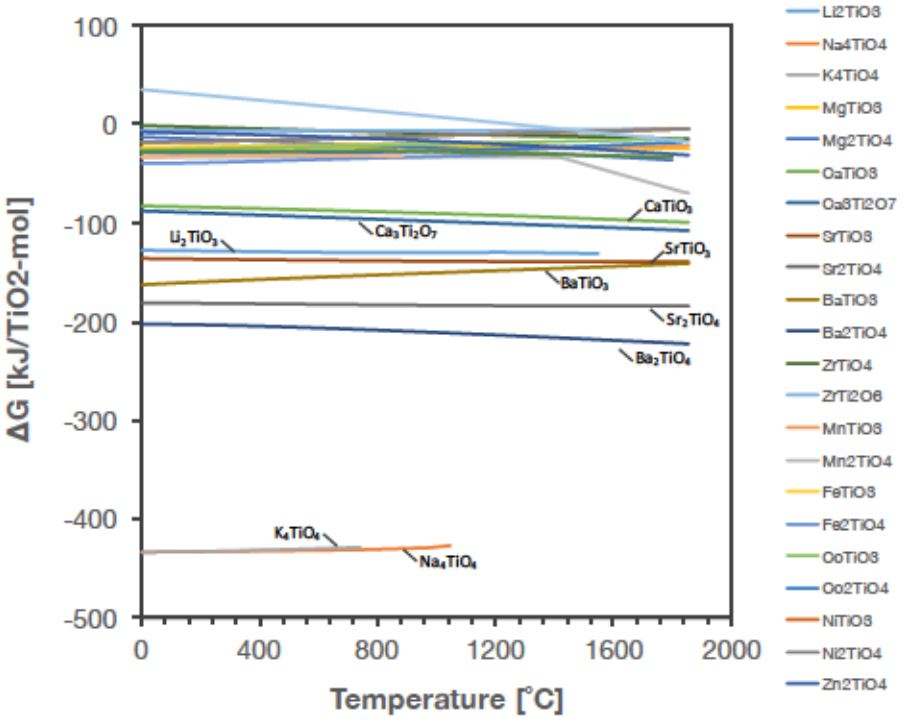

Figure 5.7 Calculated Gibbs Free Energy of Formation of Intermediate Compounds between TiO_2 and Oxide Candidates

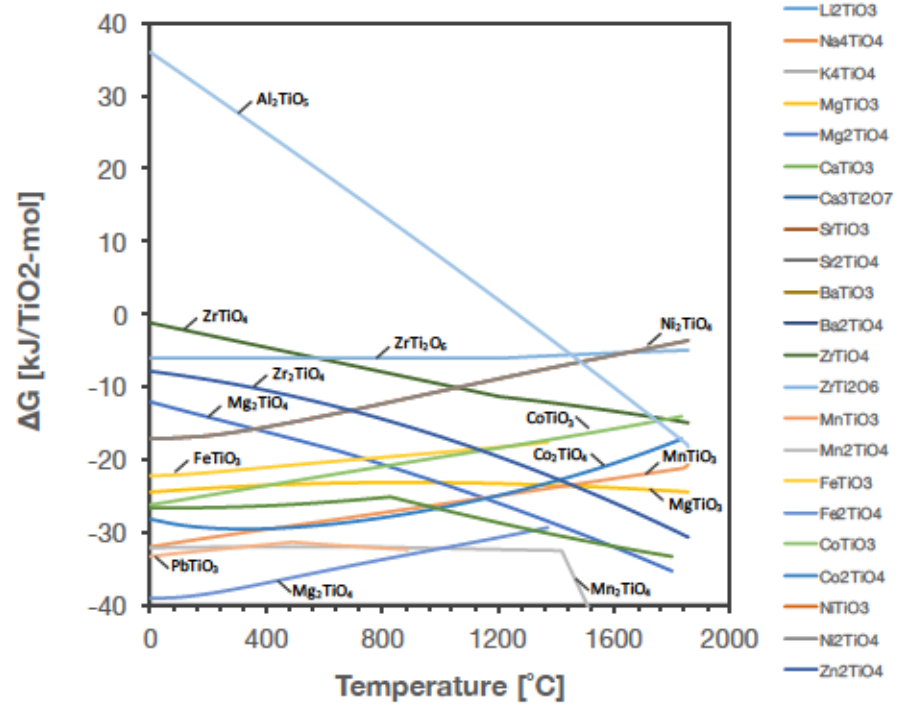

Figure 5.8 Enlarged View of Figure 5.7 Between ΔG= -40 to 40 [kJ/mol]

From the figures shown above, the stability of the intermediate compounds at 600°C was evaluated

and ordered as listed below:

Ba> Sr> Li> Ca> Mg> Mn> Co> Fe> Ni> Zn> Zr> Al

It should be mentioned that the ΔG_f of the reaction: $TiO_2+Al_2O_3=Al_2TiO_5$ shows a positive value under 1300°C. This suggests that the formation of Al_2TiO_5 cannot progress voluntarily below 600°C and that the bonding between the two oxides also cannot be attained. From the evaluations, it appears that the most attractive oxide to enable bonding of the interface in the crack-filled area is BaO. However, when taking into account that the selected oxides are used as the matrix, BaO, SrO, Li_2O, CaO, MnO, CoO, MgO and ZnO should be excluded due to their known difficulties as sinterable material or low mechanical strength. From there, it can be said that the only attractive matrix oxide candidate is ZrO_2.

As shown above, a methodology for evaluating an attractive matrix for self-healing ceramics has been proposed based on thermodynamics. It is suggested that ZrO_2 is the most attractive matrix for the TiC healing agent. It is thought that the ZrO_2/TiC composite may produce the desired bonding at the ZrO_2//TiO_2 interface in the crack-filled area at temperatures below 600°C, resulting in the complete strength recovery of the composite.

Figure 5.9 shows the results of the strength recovery testing of yttria-stabilized zirconia containing 30 vol.% of TiC particles as a healing agent (YZ30TiC). The detailed experimental conditions and discussion of the self-healing behaviour of the composite are available in Appendix I. Figure 5.9 clearly shows that the composite achieves complete strength recovery at 400°C for 1h. Moreover, based on multiple surface analyses, it was confirmed that the interfacial bonding at 400°C was achieved not by the formation of intermediate compounds, but by a solid solution of Ti ions in the matrix.

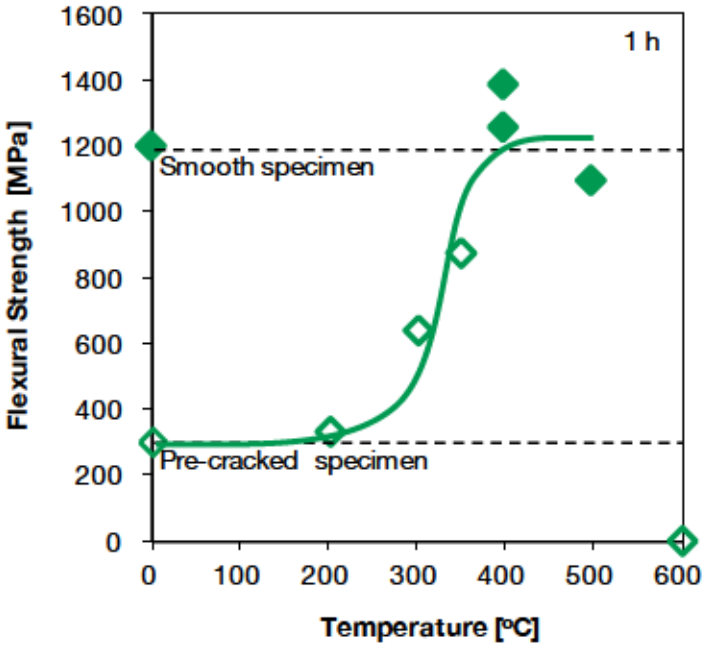

Figure 5.9 Strength Recovery Behaviour of YZ30TiC in Air Annealed for 1h

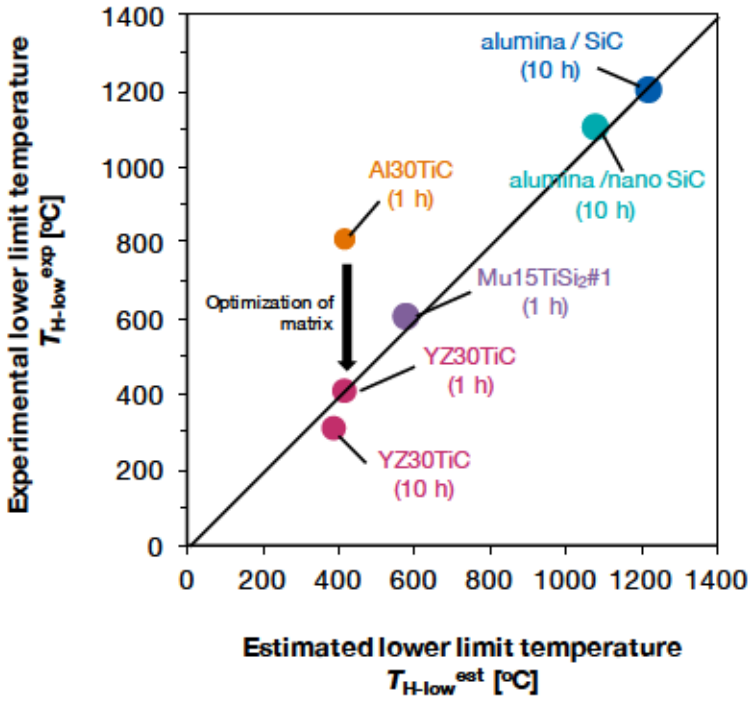

Figure 5.10 Consistency Between the Values of T_H^{est} and T_H^{exp} for YZ30TiC Compared to Previously Reported Self-Healing Ceramics

T_H^{est} and T_H^{exp} represent the estimated value and the experimental value of the lower limit of the healing temperature range (T_H), respectively. The derivation process for those values is shown in Chapter 2.

Figure 5.10 shows the comparison between the values of T_H^{cst} and T_H^{exp} for YZ30TiC alongside the values for several previously discussed oxidation-induced self-healing ceramics. In the case of Al30TiC, there is a difference of 400°C between the estimated and experimental values. The difference is caused by insufficient bonding between the formed oxide and the matrix in the crack-healed area, as discussed in Section 5.4.1. In contrast, the estimated value and the experimental value in the YZ30TiC system are relatively close, resulting from the optimization of the matrix for the TiC healing agent.

Though the desired interfacial bonding in the YZ30TiC system was attained not by the formation of intermediate compounds, but by a solid solution of Ti ions in the matrix, it is clearly shown that the reaction between a formed oxide and a matrix strongly influences the strength recovery behaviour of oxidation-induced self-healing ceramics. These results support the proposed concept of the transition state and confirm the viability of the methodology proposed in Chapter 2.

5.5. Conclusion

In this chapter, the effects of interface conditions between matrices and crack-filling oxides on

the strength recovery behaviour of self-healing ceramics were clarified. The effects were discussed based on the results of strength recovery testing of alumina/TiC composites as a function of annealing time. From this study, the following results were obtained.

I. The strength recovery of the composite at 600°C shows an almost constant value of 50% regardless of annealing time, despite the fact that the pre-crack is fully filled with formed TiO_2.

II. The intermediate compound (Al_2TiO_5) is not detected below 600°C, where the strength recovery value is saturated.

III. The obtained results clarify that there are cases in which the filling of the induced crack does not correspond to the strength recovery of the composite. The results also imply that the formation of intermediate compounds in crack-filled areas plays an important role in the achievement of the desired bonding of the interface between the matrix and the formed oxide that results in the complete recovery of strength in self-healing ceramics.

IV. The methodology for evaluating an attractive matrix for self-healing ceramics was proposed based on thermodynamic analysis. From these results, it is suggested that ZrO_2 is the most viable matrix for extrinsic oxidation-induced self-healing ceramics containing TiC as a healing agent. In the ZrO_2/TiC composite, it is expected that the desired bonding in the ZrO_2//TiO_2 interface in crack-filled areas can be achieved below 600°C due to the formation of the intermediate compound $TiZrO_4$, and that the formation of intermediate compounds results in the complete recovery of strength in the composite.

V. Yttria-stabilized zirconia/TiC composites show complete strength recovery at 400°C for 1h. The results of surface XRD analysis imply that the reestablishment of mechanical integrity in crack-healed areas was achieved by the presence of a solid solution of Ti ions in the YSZ matrix rather than the formation of the intermediate compound $TiZrO_4$. The new self-healing mechanism has been identified as "solid-solution induced" self-healing.

VI. Viability of the methodology for evaluating self-healing agents as proposed in Chapter 2 was reconfirmed.

Reference

1) Yan, M. F., & Rhodes, W. W. (1983). Low temperature sintering of TiO_2. *Materials Science and Engineering*, *61*(1), 59-66.
2) Hahn, H., Logas, J., & Averback, R. S. (1990). Sintering characteristics of nanocrystalline TiO 2. *Journal of Materials Research*, *5*(03), 609-614.
3) Nakao, W., Takahashi, K., & Ando, K. (2009). Self-healing of Surface Cracks in Structural Ceramics. *Self-healing materials: fundamentals, design strategies, and applications*.
4) Osada, T., & Kamoda, K. (2014). Prediction of Crack-healing Rate in Self-Healing Ceramics Using Oxidation Kinetics and Nonlinear Fracture Mechanics. *Proceedings of the Mechanical Engineering Congress 2014*.
5) Izquierdo, G., & West, A. R. (1980). Phase equilibria in the system Li_2O-TiO_2. Materials Research Bulletin, 15(11), 1655-1660.
6) Eriksson, G., & Pelton, A. D. (1993). Critical evaluation and optimization of the thermodynamic properties and phase diagrams of the MnO-TiO_2, MgO-TiO_2, FeO-TiO_2, Ti_2O_3-TiO_2, Na_2O-TiO_2, and K_2O-TiO_2 systems. *Metallurgical Transactions B*, *24*(5), 795-805.
7) Kaufman, L. (1988). Calculation of multicomponent ceramic phase diagrams. *Physica* B+C, 150(1-2), 99-114.
8) DeVries, R. C., Roy, R., & Osborn, E. F. (1955). Phase Equilibria in the System CaO-TiO_2–SiO_2. *Journal of the American Ceramic Society*, 38(5), 158-171.
9) Gong, W., & Jin, Z. (2002). Thermodynamic description of BaO-SrO-TiO_2 system. *Calphad*, 26(3), 403-418.
10) Rase, D. E., & Roy, R. (1955). Phase equilibria in the system BaO–TiO_2. *Journal of the American Ceramic Society*, 38(3), 102-113.
11) Wong-Ng, W., Roth, R. S., Vanderah, T. A., & McMurdie, H. F. (2001). Phase equilibria and crystallography of ceramic oxides. *Journal of research of the National Institute of Standards and Technology*, 106(6), 1097.
12) MIZUTANI, N., Tajima, Y., & KATO, M. (1976). Phase Relations in the System Y_2O_3-TiO_2. *Journal of the American Ceramic Society*, *59*(3-4), 168-168.
13) Stanek, C. R., Minervini, L., & Grimes, R. W. (2002). Nonstoichiometry in $A_2B_2O_7$ pyrochlores. *Journal of the American Ceramic Society*, 85(11), 2792-2798.
14) Schaedler, T. A., Fabrichnaya, O., & Levi, C. G. (2008). Phase equilibria in the TiO_2–$YO_{1.5}$–ZrO_2 system. *Journal of the European Ceramic Society*, 28(13), 2509-2520.
15) Habel, D., Stelzer, J. B., Feike, E., Schröder, C., Hösch, A., Hess, C., ... & Schubert, H. (2006). Phase development in the catalytic system V_2O_5/TiO_2 under oxidising conditions. *Journal of the European Ceramic Society*, 26(15), 3287-3294.
16) Roth, R. S., & Waring, J. L. (1970). Effect of oxide additions on the polymorphism of tantalum pentoxide III. Stabilization of the low temperature structure type. *Journal of Research of the National Institute of Standards and Technology A*: Phys Chem A, 74, 4.
17) Sōmiya, S., Hirano, S., & Kamiya, S. (1978). Phase relations of the Cr_2O_3–TiO_2 system. *Journal of Solid State Chemistry*, 25(3), 273-284.

18) Jacob, K. T., Shekhar, C., & Waseda, Y. (2008). Thermodynamic properties and phase diagram for the system MoO_2–TiO_2. *Journal of the American Ceramic Society*, 91(2), 563-568.
19) Chang, L. L. Y., Scroger, M. G., & Phillips, B. (1967). High-temperature, condensed-phase equilibria in the system Ti-WO. *Journal of the Less Common Metals*, 12(1), 51-56.
20) MacChesney, J. B., & Muan, A. (1961). Phase equilibria at liquidus temperatures in the system iron oxide-titanium oxide at low oxygen pressures. *American Mineralogist*, 46(5-6), 572-582.
21) Jacob, K. T., & Subramanian, R. (2008). Phase Diagram for the System RuO_2-TiO_2 in Air. Journal of Phase Equilibria and Diffusion, 29(2), 136-140.
22) Brežný, B., & Muan, A. (1969). Phase relations and stabilities of compounds in the system CoO–TiO_2. *Journal of Inorganic and Nuclear Chemistry*, 31(3), 649-655.
23) McDaniel, C. L., & Schneide. SJ. (1967). Phase Relations in the Systems TiO_2-IrO_2 and SnO_2-IrO_2 in air. *Journal of Research of the National Bureau of Standards Section A-Physics and Chemistry*, (2), 119.
24) Muan, A. (1992). Equilibrium Relations in the System NiO–TiO_2 in the Temperature Range 1300 to 1750 C. *Journal of the American Ceramic Society*, 75(6), 1357-1360.
25) Lu, F. H., Fang, F. X., & Chen, Y. S. (2001). Eutectic reaction between copper oxide and titanium dioxide. *Journal of the European Ceramic Society*, 21(8), 1093-1099.
26) Dulln, F. H., & Rase, D. E. (1960). Phase Equilibria in the System ZnO-TiO_2. *Journal of the American Ceramic Society*, 43(3), 125-131.
27) Hoffmann, S., Norberg, S. T., & Yoshimura, M. (2006). Melt synthesis of Al2TiO5 containing composites and reinvestigation of the phase diagram Al_2O_3–TiO_2 by powder X-ray diffraction. *Journal of electroceramics*, 16(4), 327-330.
28) EN Bunting. (1933). Phase Equilibria in the Systems TiO_2, TiO_2-SiO_2 and TiO_2-Al_2O_3. *Part of Bureau of Standards Journal of Research*, 11, 719-725.
29) Kamiya, S., & Tilley, R. J. D. (1977). Phase relations in the pseudobinary system TiO_2–Ga_2O_3. *Journal of Solid State Chemistry*, 22(2), 205-216.
30) Li, Z., Sun, J., You, L., Jiao, H., Li, G., Jing, X. & Lin, J. (2005). Phase Equilibrium of the In_2O_3-TiO_2-MO (M= Ca, Sr) Systems and the Structure of $In_6Ti_6CaO_{22}$. *Chemistry of materials*, 17(8), 2186-2192.
31) Sarver, J. F. (1961). Polymorphism and subsolidus equilibria in the system GeO_2-TiO_2. *American Journal of Science*, 259(9), 709-718.
32) Naidu, H. P., & Virkar, A. V. (1998). Low-Temperature TiO_2-SnO_2 Phase Diagram Using the Molten-Salt Method. *Journal of the American Ceramic Society*, 81(8), 2176-2180.
33) Park, M., Mitchell, T. E., & Heuer, A. H. (1975). Subsolidus Equilibria in the TiO_2-SnO_2 System. *Journal of the American Ceramic Society*, 58(1-2), 43-47.
34) Soh, J. R., Lee, H. M., & Kwon, H. S. (1994). Thermodynamic evaluation and phase diagram of PbO-TiO_2 system. *Calphad*, 18(3), 237-244.

Chapter 6

Conclusions

This chapter concludes this study and offers suggestions for further research. In Chapters 2 and 4, methodologies for evaluating the upper and lower limits of the healing temperature range (T_H) were proposed. Additional practical methodologies for customizing healing agents utilizing cation and interface design are described in Chapters 3 and 5. By integrating those proposed methods, an advanced self-healing ceramic can be designed that will demonstrate the desired self-healing under the specific operating conditions of high temperature structural materials. Throughout the study, fundamental design strategies for oxidation-induced self-healing ceramics are proposed.

The present study aims to clarify the correlation between the chemical reaction of healing agents and mechanical strength recovery of oxidation induced self-healing ceramics. Based on the obtained results, material design strategy for oxidation induced self-healing ceramics is proposed.

The oxidation-induced self-healing ceramics discussed in the study are the potential candidates for advanced high temperature structural materials. The oxidation-induced self-healing is an autonomous function enabling composites to fully restore mechanical properties in situ. This process is induced by the high temperature oxidation of non-oxide particles, called healing agents, that are embedded in oxide ceramics. Owing to this remarkable property, the ceramic matrix composites are able to avoid catastrophic failure and actively maintain their structural integrity during operation. Despite the fact that high temperature structural materials have various operating temperature ranges, the temperature range of self-healing ceramics in which the desired healing reaction can be observed is quite limited.

This temperature range, called the healing temperature range (T_H), is directly affected by the chemical properties of the healing agent. Methodologies for evaluating the upper and lower limits of the healing temperature range (T_H) were proposed by clarifying the effects of the chemical properties of the healing agent on self-healing behaviour. Additional practical methodologies for customizing healing agents (the use of cation and interface design) were proposed based on the discussion of the relationships between strength recovery behaviour and micro-structure changes in self-healing ceramics.

By integrating the proposed methodologies, an advanced self-healing ceramic that shows the desired self-healing behaviour under the specific operating conditions of high temperature structural materials can be designed. The conclusion of each chapter is briefly summarized below.

Chapter 1 Introduction

The chapter clearly described the impacts of the study on both scientific and industrial fields. Current development status and the practical issues of high temperature structural materials used in transportation were investigated, and social requirements in the materials development were discussed. The promise of implementing self-healing ceramics in replacement for their classical counterparts was also described. To expand the study's scientific context, previously proposed self-healing ceramics were organized using the research and development information of self-healing material. The current issues in the field of self-healing ceramics were extracted from those discussions, and the purpose of the study was described.

Chapter 2 Methodology for Evaluating Healing Agents for Oxidation-Induced Self-Healing Ceramics

The chapter dealt with the methodology for evaluating potential healing agents for oxidation-induced self-healing ceramics. The theoretical frame work for predicting the healing ability

of non-oxides was presented based on thermodynamic analysis. The methodology for estimating the lower limit temperature of the healing temperature range ($T_{H\text{-}low}$) was proposed by quantitatively evaluating of the relationship between the oxidation behaviour of the healing agents and the strength recovery behaviour of self-healing ceramics. The estimated value of the lower limit ($T_{H\text{-}low}^{est}$) was determined using thermogravimetric analysis, and the experimental value ($T_{H\text{-}low}^{exp}$) was derived from strength recovery tests of self-healing ceramics. The estimated value for $T_{H\text{-}low}^{est}$ was close to the experimental value $T_{H\text{-}low}^{exp}$ in the cases of the alumina/SiC composite and porous mullite/$TiSi_2$ composite. From the above studies, it was shown that the proposed methodology was sufficient for evaluating the self-healing potential of the healing agents.

Chapter 3 Effect of Cation in Healing Agents on Self-Healing Behaviour

In this chapter, the effect of cation in healing agents on self-healing behaviour was studied. The effect was clarified through the experiment on strength recovery behaviour and through micro-structural observation of the alumina/TiC composite. The selection of TiC was made based on the method described in Chapter 2. The strength of the material recovered to its original level within 1h by annealing at 800°C. Excess outward diffusion of Ti cation was observed at 1000°C. This result indicates that the cation could enhance the oxidation activity of the healing agent. This also shows the viability of healing agents containing Ti cation in lower temperature applications.

Chapter 4 Methodology for Evaluating the Lifespan of Self-Healing Ability

The chapter dealt with the methodology for evaluating the upper limit temperature of the healing temperature range ($T_{H\text{-}high}$). Self-healing ceramics should maintain their self-healing ability even when constantly exposed to high temperature atmospheres. In such severe conditions, healing agents embedded in the matrix can deteriorate due to inward diffusion of oxygen. It was shown that self-healing ability disappears due to internal oxidation through strength recovery tests on alumina/SiC composites aged at 1200°C for 1000h. This indicates that the lifespan of self-healing ability can be evaluated as a function of the growth rate of the internal oxidation layer. Based on this, a methodology for evaluating the upper limit temperature of the healing temperature range ($T_{H\text{-}high}$) was proposed.

Chapter 5 Interface Design Between Matrices and Crack Filling Oxides

The chapter dealt with the effects of interface conditions between matrices and crack-filling oxides on the strength recovery behaviour of self-healing ceramics. The effects were discussed based on the results of strength recovery testing of alumina/TiC composites as a function of annealing time. The strength recovery of the composite at 600°C showed an almost constant value of 50% regardless of annealing time, even though the pre-crack was fully filled with formed TiO_2. The intermediate compound Al_2TiO_5 was not detected below 600°C, where the strength recovery value was saturated. Those results imply that the formation of intermediate compounds at crack-healed area plays an

important role in achieving the desired bonding of the interface between the matrix and the formed oxide, which results in the complete strength recovery of the self-healing ceramic. A methodology was proposed on the basis of thermodynamics to evaluate oxide matrices and to determine which compounds can attain the desired bonding of the interface.

Appendix I

Self-Healing Behaviour of YSZ/30 vol.%-TiC Composite

1 Background

Based on the results in Chapter 5, it was suggested that improvement of the interfacial bonding strength in the crack-healed area was necessary to achieve complete strength recovery of the oxidation-induced self-healing ceramics. As a method for improvement, it is also suggested that an intermediate compound resulting from the reaction between the matrix and the formed oxide should be formed in the crack-healed area. Based on the discussion, potential candidates for an advanced oxide matrix for TiC healing agents were evaluated based on the binary phase diagrams between TiO_2 and oxide candidates. Consequently, twelve oxides, including BaO, were selected as potential candidates. Considering the mechanical strength of those oxides, ZrO_2 was selected as a matrix. It can be expected that the ZrO_2/TiC composite would show a complete strength recovery at approximately 600°C, resulting from the formation of the intermediate compound $ZrTiO_4$ in the crack-healed area.

When using ZrO_2 as a high temperature structural material, two characteristic properties of ZrO_2 must be considered: phase transformation and ionic conductivity. It is well known that ZrO_2 can be cracked upon cooling in the sintering process due to significant internal stress. The internal stress is caused by the volume change resulting from the structure's transition from tetragonal to monoclinic to cubic upon temperature changes. Thus, 'stabilized' ZrO_2 is generally used as a structural material. The tetragonal or cubic phases of ZrO_2 are stabilized by introducing another oxide, typically Y_2O_3. Hence, the reactions between ZrO_2 and TiO_2 and Y_2O_3 and TiO_2 should be equally considered. The yttria-stabilized ZrO_2 shows high ionic conductivity at high temperatures, resulting from the formation of oxygen vacancy as described in Equation 1.

$$Y_2O_3 \xrightarrow{ZrO_2} 2Y'_{Zr} + V_O^{\cdot\cdot} + 3O_O^{\times} \quad (1)$$

This means that oxygen ions can move freely through the crystal structure and oxidize the embedded TiC particles. The internal oxidation of the healing agent causes the deterioration of the self-healing function as discussed in Chapter 4, and sometimes leads to the catastrophic failure of a component due to induced internal stress upon formation of the oxide. Thus, the oxidation resistance of ZrO_2-based composites at high temperatures should also be discussed.

In the present appendix, the reactivity of yttria-stabilized zirconia (YSZ) against TiO_2 and oxygen diffusion in yttria-stabilized zirconia was investigated. Subsequently, the strength recovery behaviour of YSZ/ 30 vol.%-TiC was studied experimentally.

2 Theoretical Analysis of the Healing Potential of TiC in a Zirconia Matrix

2.1 Reactivity Between Yttria-Stabilized Zirconia and TiO_2

Several researchers have reported that TiO_2 can dissolve into zirconia or yttria-stabilized zirconia at a variety of temperatures[1-9]. Figures 1 and 2 show the binary phase diagram for ZrO_2 and TiO_2[1] and for Y_2O_3 and TiO_2[2], respectively. According to Figure 2, there is no solid-solution region in the TiO_2-Y_2O_3 system at any temperature. In contrast, Figure 1 shows that TiO_2 solutes into monolithic ZrO_2 from below 750°C to 1150°C at about 0-10 mol. % and tetragonal ZrO_2 from about 1100°C for 0 to <20 mol. %. Bannister et al. reported that the solubility of TiO_2 in tetragonal ZrO_2 is 13.8±0.3 mol% at 1300°C, 14.9±0.2 mol% at 1400°C, and 16.1±0.2 mol% at 1500°C[3]. In the TiO_2-Y_2O_3-ZrO_2 ternary system, Tsukuma et al. reported that 20 mol.% TiO_2 can dissolve into tetragonal ZrO_2 and cubic ZrO_2[4]. According to GAN et al., the solubility of TiO_2 in tetragonal ZrO_2 in partially stabilized zirconia with 3 mol.% yttria is about 14-16 mol.% at 1600°C[5].

Conversely, Tsukuma et al. reported that the volume fraction more than 20 mol. % was required for the formation of the intermediate compound $ZrTiO_4$ in the TiO_2-Y_2O_3-ZrO_2 ternary system at 1400°C[4]. McHale et al. reported that $ZrTiO_4$ was formed above ~1100°C, and that below that temperature stable low-temperature phase $ZrTi_2O_6$ was detected[6]. This result corresponds to the phase diagrams reported by Troitzsch et al.[1].

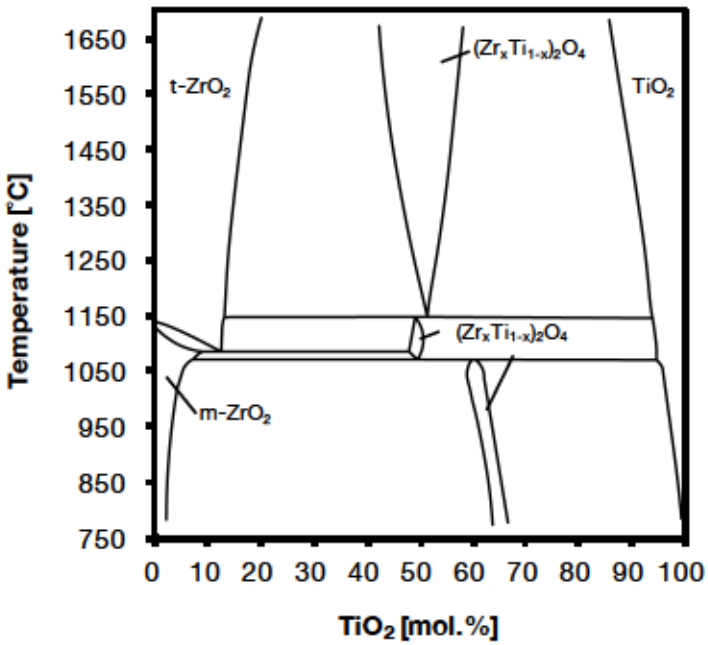

Figure 1 Binary Phase Diagram Between ZrO_2 and TiO_2 Traced From the Reference[1]

m-ZrO_2 and t-ZrO_2 represent monolithic ZrO_2 and tetragonal ZrO_2, respectively.

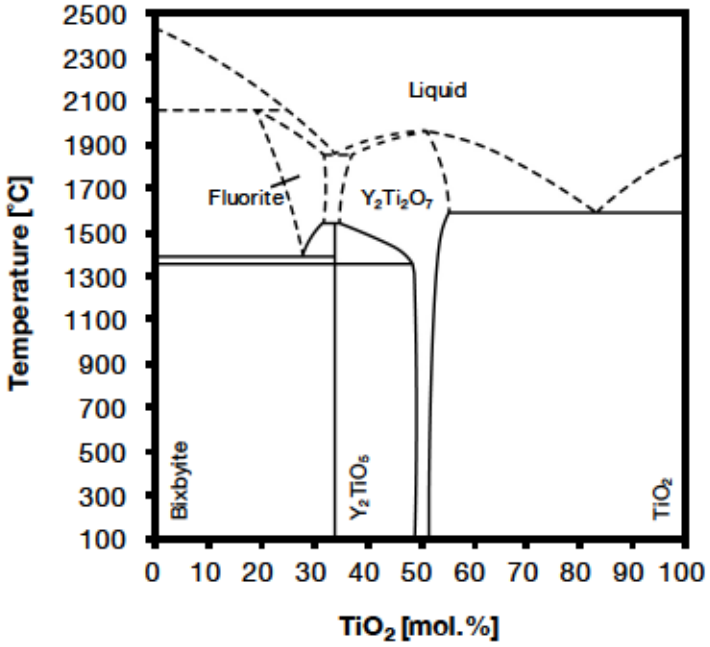

Figure 2 Binary Phase Diagram Between Y_2O_3 and TiO_2 Traced From the Reference[5]

In conclusion, it can be expected that TiO_2 can dissolve into zirconia or yttria-stabilized zirconia below 750°C. Despite the stable low-temperature phase, $ZrTi_2O_6$ is also expected to be formed below 1150°C. Relatively high concentrations of TiO_2 are required for the formation of intermediate compounds. In any case, the strength recovery of YSZ/TiC composites can be expected because both the solid solution of TiO_2 into YSZ and the formation of intermediate compounds leads to the strong interaction between the formed oxide and the matrix.

In order to verify the crack-healing in YSZ/TiC composites and their self-healing mechanisms, the strength recovery behaviour of the YSZ/TiC composite was examined experimentally.

3 Experiment

YSZ matrix composites containing 30 vol.% TiC, named YZ30TiC, were prepared and their strength recovery at room temperature as a function of the healing temperature was studied. Furthermore, the microstructural changes related to the strength recovery were also examined.

3.1 Sample Preparation

Yttria-stabilized zirconia, abbreviated as YSZ, powder (TZ-3Y-E, Tosoh Co.), and TiC powder (STD120, H.C. Starck GmbH) were used as starting materials. TZ-3Y-E contains 3 mol.% of Y_2O_3 for stabilizing the cubic phase at room temperature. The average particle sizes of the YSZ and TiC powders were 0.04 and 2 μm, respectively. YSZ powder and TiC powder were mixed at the ratio of 70 vol. %: 30 vol. % in isopropanol with ø 300 μm alumina beads by means of beads milling. LABSTAR mini (DMS, Ashizawa Finetech Ltd.) was used as an apparatus. After 2h mixing, the

mixed powder was dried in the oven for 12h at 80°C. The dried powder was sieved with a ø 200 μm mesh powder sieve. The sieved powder was sintered by hot-pressing at 1450°C for 1h in an Ar atmosphere under 40MPa. The heating and cooling rates were 10°C/min and 5°C/min, respectively. The typical dimensions of the sintered bulk material were 50 x 50 x 6mm. The relative density of the sample as measured by Archimedes' method was 99%. The sintered disc was cut into rectangular samples with a dimension of 3 x 4 x 23mm for three-point bending tests. The surfaces of the samples were mirror finished by using a diamond paste with a particle size of 0.25 μm.

3.2 Strength Recovery Tests

In order to study the strength recovery of YZ30TiC as a function of annealing temperature, the strength values of three types of specimens (smooth, pre-cracked and healed specimens) were determined. Smooth specimen refers to samples without any induced damage prior to testing. Pre-cracked specimens are specimens with a standardized pre-crack introduced by a Vickers' indenter at the centre of the surface. The indentation force was 29.4N and the introduced crack had a surface length of about 110 μm. The two sets of radial indentation cracks were either perpendicular or parallel to the longest dimension of the bend test samples. The healed specimens were pre-cracked and annealed for 1h in air at temperatures ranging from 200°C to 800°C.

The strength of each sample was measured by means of three-point bending test. The span between the supporting 5mm diameter steel rollers was 16mm. The specimen was mounted such that the maximum tensile stress was applied to the pre-crack or healed crack area. All tests were conducted at room temperature and with a cross-head displacement velocity of 0.5 mm/min.

3.3 Surface Characterisation

The external appearance of the healed cracks prior to and after thermal annealing was observed with a laser microscope (KEYENCE, VK-X) and scanning electron microscope (JIB-4501, JEOL Ltd.). The crystal structures of the various phases in the annealed samples were determined by using XRD (ULTIMA Ⅳ Rigaku Co.). Upon XRD analysis, CuKα radiation was the radiation source and a scintillation counter with monochromator was used as a detector.

4 Results and Discussion

4.1 Strength Recovery Behaviour

The results of strength recovery tests for YZ30TiC are shown in Figure 3. The open symbols represent the fracture was initiated from the introduced pre-crack, and the closed symbols represent the fracture origin was the other defects such as internal pore as shown in Figure 4. The strength of the smooth specimens of YZ30TiC at room temperature was 1196MPa, and that of pre-cracked specimens was 300MPa. Figure 3 shows that annealing at 300°C already leads to some strength recovery. Annealing at 400°C led to a complete recovery of the strength for YZ30TiC. Moreover, the fracture initiation was shifted from the introduced pre-crack to other defects. Hence, we conclude that

YZ30TiC can heal cracks completely by annealing at 400°C for 1h.

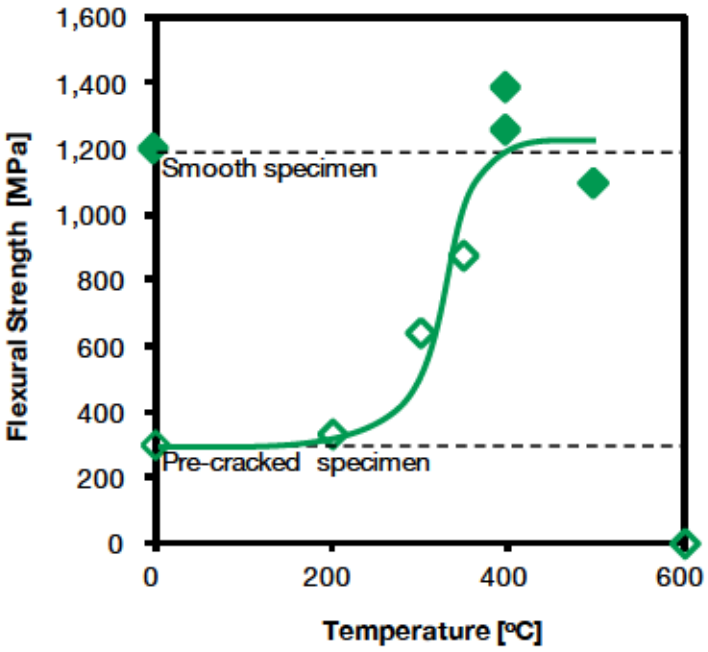

Figure 3 Flexural Strength Values of YZ30TiC Sample After Healing for 1h in Air at Reported Temperatures

However, annealing above 600°C causes catastrophic failure of the specimens and the strength of the sample cannot be measured. Figure 5(a) shows the top view of the specimen annealed at 600°C for 1h. The edge of the specimen is completely collapsed and numerous cracks can be observed. Those cracks are formed as a result of excess internal stress produced during internal oxidation of the TiC particles. As shown in Figure 5(b), oxidized TiC particles can be observed on the surface and all micro-cracks are initiate from the boundary between the TiC particles and the matrix. Considering that ZrO_2 shows high oxygen ion conductivity at high temperatures, it can be predicted that the embedded TiC particles were oxidized and TiO_2 was formed around the particles. Consequently, large internal stresses were produced at the gain boundary due to the formation of TiO_2. In order to avoid this excess internal oxidation, the encapsulation technique for healing agents proposed by Sloof et al. should be utilized[10].

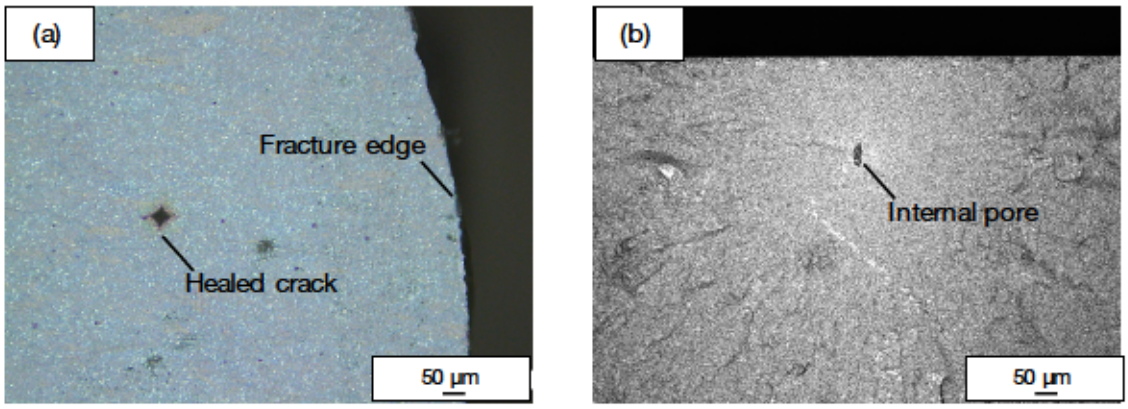

Figure 4 Typical Images of Fracture Initiation

(a) Optical microscope image of surface onYZ30TiC after bending. The fracture is clearly initiated not from the healed crack but from the other spot.

(b) Fractography of YZ30TiC after bending. It is clearly observed that the fracture initiation is the internal pore.

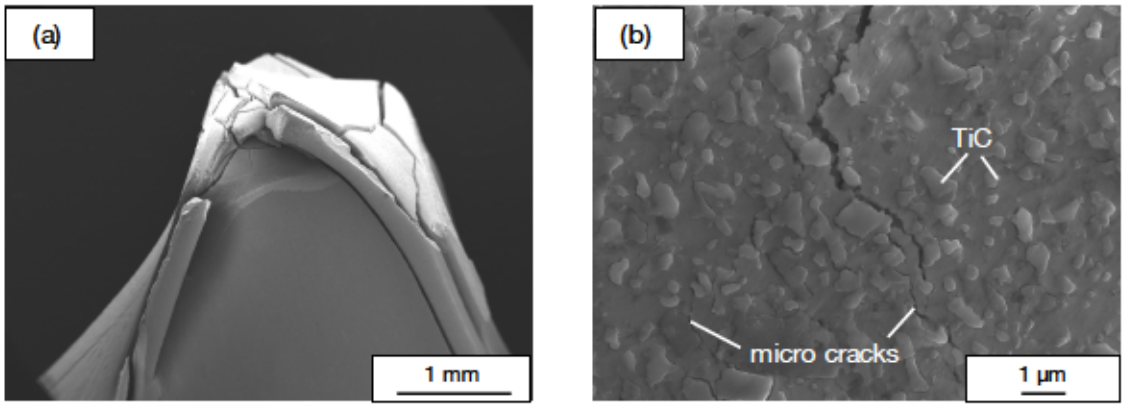

Figure 5 SEM Image of the Surface of YZ30TiC Sample After Annealing at 600°C for 1h in air

(a) low magnification

(b) high magnification

4.2 Microstructural Changes

Laser microscope images of pre-cracked areas before and after annealing are shown in Figures 6 through 8 for annealing temperatures of 200°C, 300°C and 400°C, respectively. The arrows in the figures indicate the location of the pre-crack before and after annealing.

As shown in Figure 6, no clear sign of oxidation can be observed and the introduced pre-crack is still visible in the sample annealed at 200°C for 1h. No clear surface change due to oxidation can be observed at the sample annealed at 300°C, but it can be seen that some parts of the crack have disappeared, as shown in Figure 7. In contrast, Figure 8(a) and 8(b) (samples annealed at 400°C for 1h) shows clear signs of surface oxidation and the crack is no longer visible. The shadowed area around the indentation is swelled as shown in Figure 8(c). This protrusion might be caused by the formation of oxides in the process zone underneath the indentation. Considering that the oxidized surface is

iridescent as shown in Figure 8(d), it can be expected that the formed oxide is the glass phase.

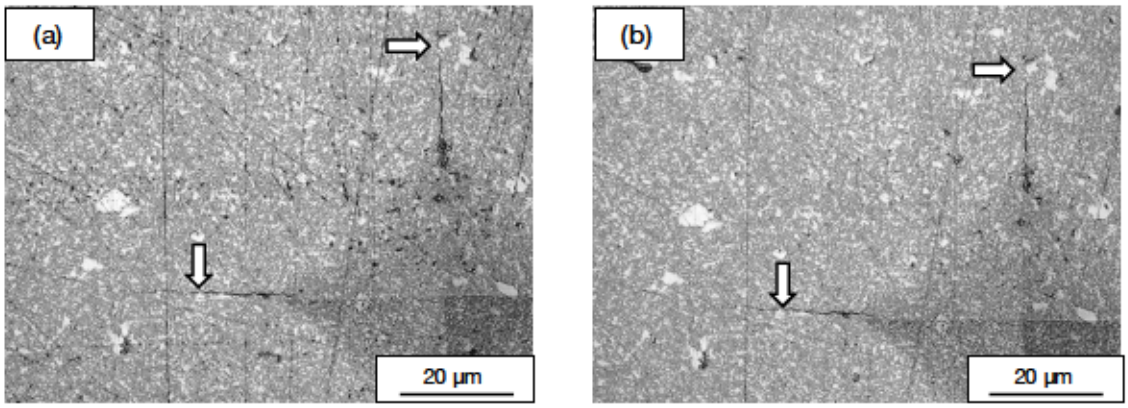

Figure 6 Laser Microscope Image of Pre-Cracked Area of YZ30TiC Before (a) and After (b) Annealing at 200°C for 1h

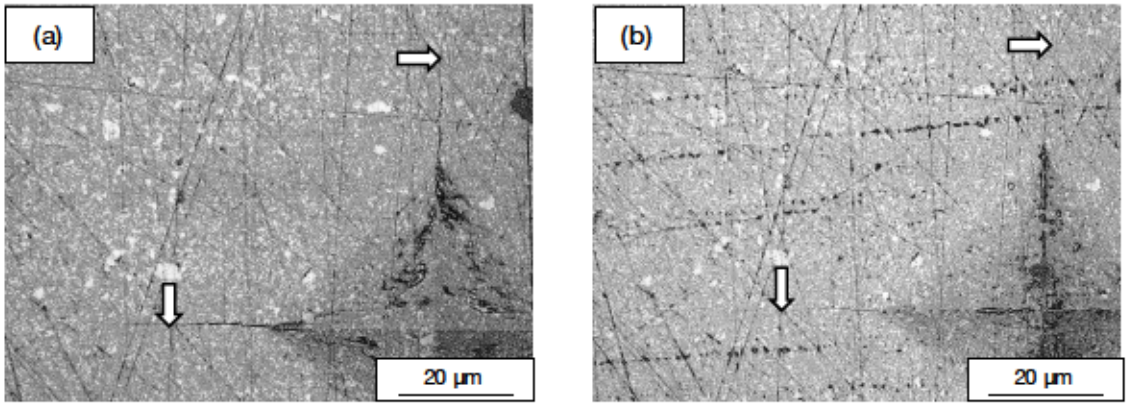

Figure 7 Laser Microscope Image of Pre-Cracked Area of YZ30TiC Before (a) and After (b) Annealing at 300°C for 1h

Arrows indicate the end-points of the radial cracks.

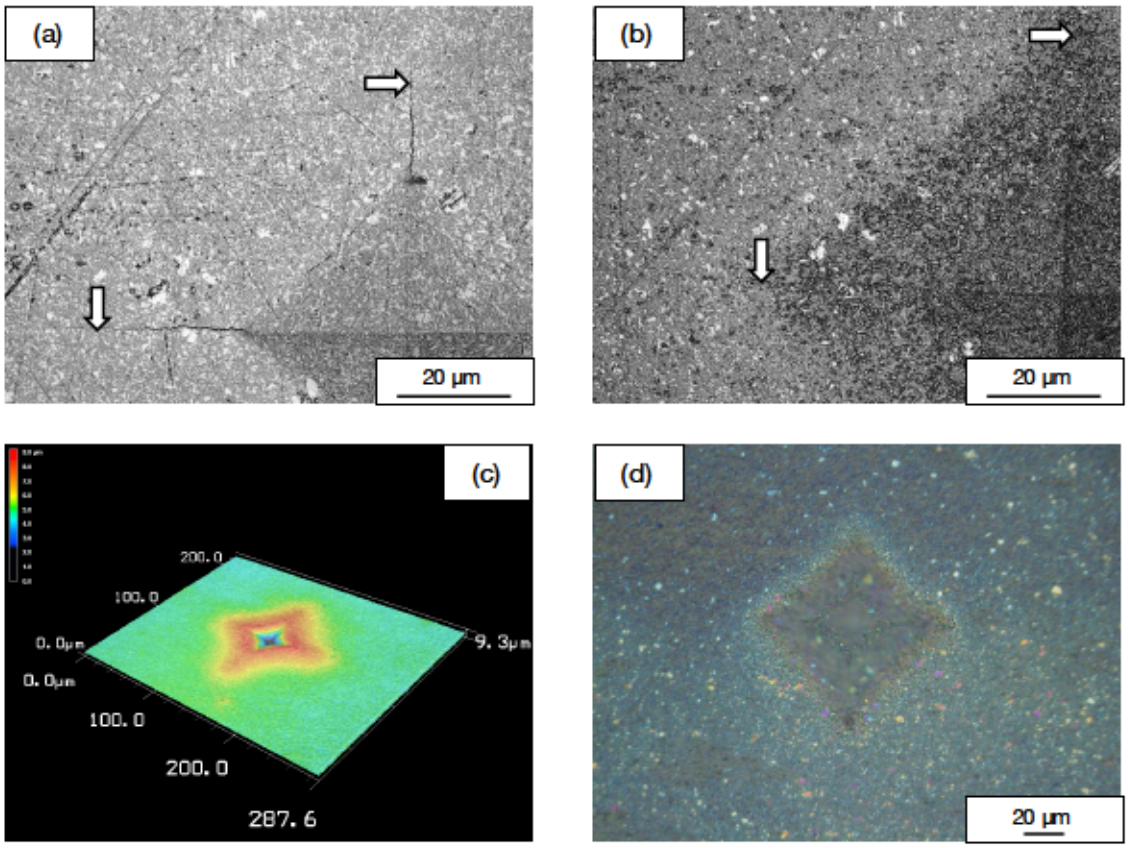

Figure 8 Laser Microscope Image of Pre-Cracked Area of YZ30TiC Before Annealing (a); Laser Microscope Image of Pre-Cracked Area of YZ30TiC After Annealing at 400°C for 1h (b); Height Profile of Pre-Cracked Area After Annealing (c); Optical Microscope Image of Pre-Cracked Area of YZ30TiC After Annealing (d)

Scanning electron microscopy images (SEI) and backscattered electron microscopy images (BEI) of the surface of YZ30TiC after annealing at 400°C for 1h are shown in Figures 9 and 10. Figure 10 is the enlarged image of the squared region in Figure 9. Black particles and white areas shown in the backscattered electron images correspond to the embedded TiC particles and YSZ matrix, respectively. As shown in the scanning electron image of Figure 9, each TiC particle is covered with oxides. Since the surface of the formed oxides is smooth, it can be expected that the phase of those oxides is the glass phase. The backscattered electron image in Figure 10 indicates that the composition of the edge of the TiC particles becomes similar to the matrix, since the colour of the region turned to the same whitish colour as the matrix region. This indicates that Y or Zr ions diffuse or solute into formed oxides or TiC particles.

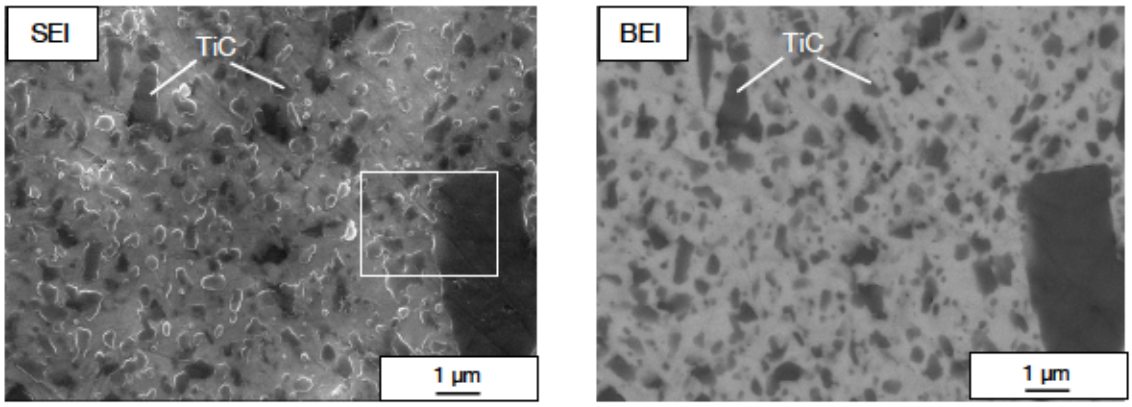

Figure 9 Scanning Electron Microscopy Image (SEI) and Backscattered Electron Microscopy Image (BEI) of the Surface of YZ30TiC After Annealing at 400°C for 1h

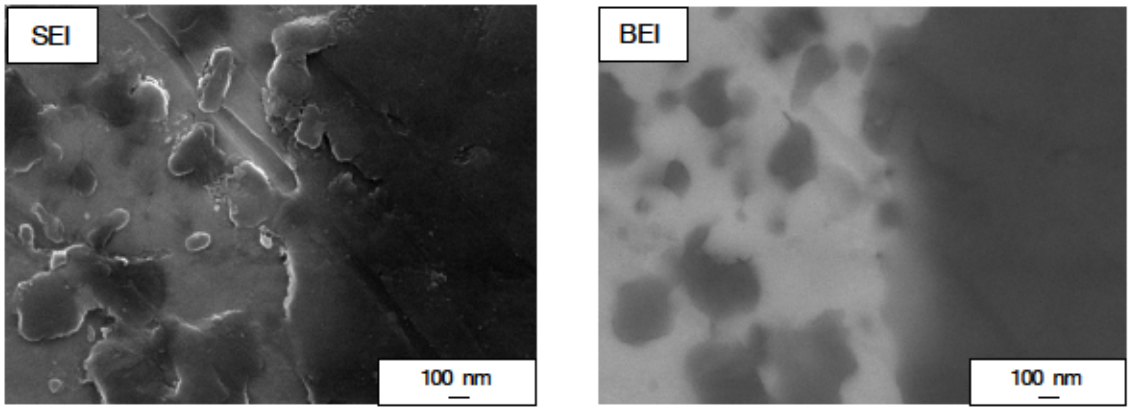

Figure 10 Scanning Electron Microscopy Image (SEI) and Backscattered Electron Microscopy Image (BEI) of the Surface of YZ30TiC After Annealing at 400°C for 1h

4.3 Crystal Structure Changes

Figures 11 and 12 show the results of XRD analysis on the surface of the YZ30TiC samples annealed in various conditions. Figure 12 shows the enlarged view of Figure 11 at the range of 2θ=26.0-32.0°. It should be mentioned here that the peak position has been standardized in order to correct the error that depends on eccentricity. Upon correction for peak shifting, the peak of stabilized zirconia containing 3 mol.% of yttria was used as a standard peak.

Figure 11 shows no clear change in crystal structure between the smooth specimen and the specimens annealed between 200°C and 350°C. Peak broadening in the range of 2θ=20.0-30.0° related to the formation of the amorphous phase is not detected. Those results indicate that the oxidation of TiC has not progressed and that the amount of formed oxide is quite small in that temperature range. In contrast, the formed oxide TiO_2 is detected in the sample annealed above 400°C. Considering that peak broadening is also not detected in those samples, most of the formed TiO_2 should have been crystalized. The expected intermediate compounds between the matrix and TiO_2, such as $ZrTiO_4$, were not detected.

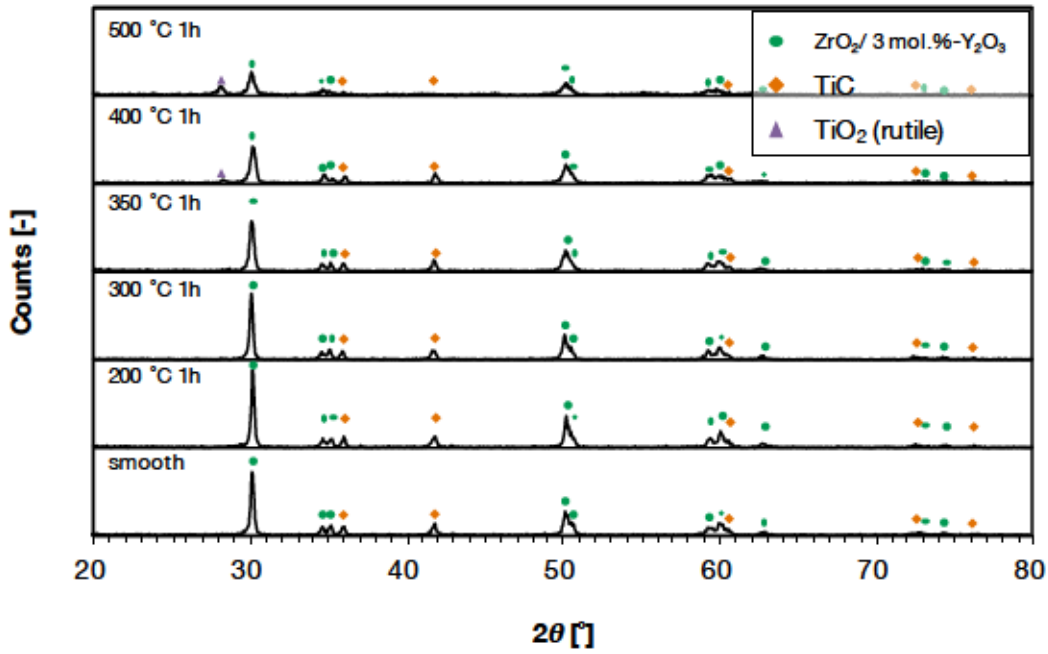

Figure 11 Results of XRD analysis on the surface of the YZ30TiC samples annealed in various conditions

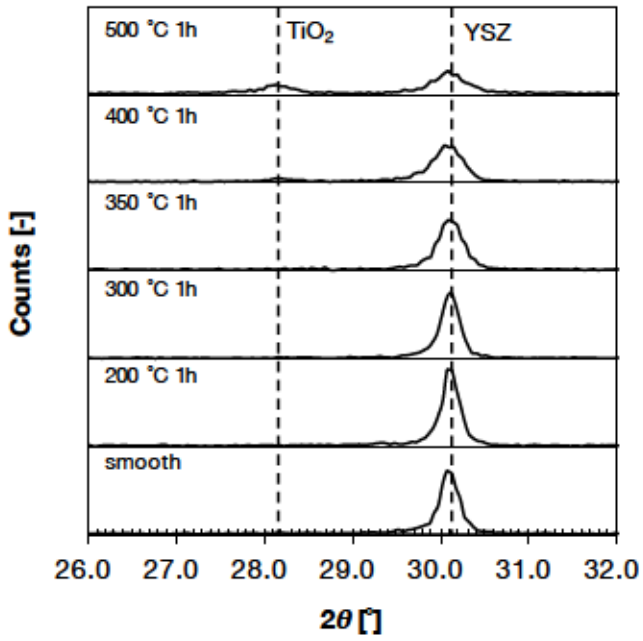

Figure 12 Enlarged view of Figure 11 at the range of 2θ=26.0-32.0°

Figure 12 clearly shows that the peak intensity of YSZ peak decreases and the half width of the peak is broadened in the sample annealed above 350°C, compared to the samples annealed below 300°C. Since the grain growth of YSZ cannot occur at those temperatures, it can be predicted that the peak broadening is due to the solution of the Ti ions into the YSZ.

Based on the obtained results, it was concluded that the strength recovery of YZ30TiC was

achieved by the re-establishment of mechanical integrity resulting from the solid solution of Ti ions into the YSZ.

5 Summary

In this appendix, the strength recovery behaviour of the yttria-stabilized zirconia/30 vol.%-TiC composite was examined. The results are summarized as follows.

I. The strength of the yttria stabilized zirconia/30 vol.%-TiC composite (YZ30TiC) was completely recovered when annealed at 400°C for 1h.

II. From the XRD analysis on the surface of annealed samples, it was indicated that the interfacial bonding in the crack-healed area was attained not by the formation of intermediate compound, but by the solution of Ti ions in the yttria-stabilized zirconia.

III. The new type of self-healing in ceramics, named 'solid-solution induced' self-healing was demonstrated.

Reference

1) Troitzsch, U., & Ellis, D. J. (2005). The ZrO_2-TiO_2 phase diagram. *Journal of materials science*, *40*(17), 4571-4577.
2) Schaedler, T. A., Fabrichnaya, O., & Levi, C. G. (2008). Phase equilibria in the TiO_2–$YO_{1.5}$–ZrO_2 system. *Journal of the European Ceramic Society*, *28*(13), 2509-2520.
3) Bannister, M. J., & Barnes, J. M. (1986). Solubility of TiO_2 in ZrO_2. *Journal of the American Ceramic Society*, *69*(11).
4) Tsukuma, K., Takahata, T. & Tsukidate, T. (1988). Science and Technology of Zirconia III. In Somiya, S., Yamamoto, N. & Yanagida, H. (Eds.), *Advances in Ceramics vol. 24* (pp. 287). Ohaio: Amreican Ceramics Society.
5) Lin, C. L., Gan, D., & Shen, P. (1990). The effects of TiO_2 addition on the microstructure and transformation of ZrO_2 with 3 and 6 mol.% Y_2O_3. *Materials Science and Engineering: A*, *129*(1), 147-155.
6) McHale, A., & Roth, R. S. (1986). Low-Temperature Phase Relationships in the System ZrO_2-TiO_2. *Journal of the American Ceramic Society*, *69*(11), 827-832.
7) Tsukuma, K. (1986). Transparent titania-yttria-zirconia ceramics. *Journal of materials science letters*, *5*(11), 1143-1144.
8) Mizutani, N., Tajima, Y., & Kato, M. (1976). Phase Relations in the System Y_2O_3-TiO_2. *Journal of the American Ceramic Society*, *59*(3-4), 168-168.
9) Konishi, A., kunugi, M. & Outuki, F. (1974). Solid-State Reaction of ZrO_2 and TiO_2. *Journal of The Society of Materials Science*, 23(253), 873-876.
10) Carabat, A. L., Van der Zwaag, S., & Sloof, W. G. (2013). Encapsulation of sacrificial silicon containing particles for SH oxide ceramics via a boehmite precursor route. In *ICSHM 2013: Proceedings of the 4th International Conference on Self-Healing Materials, Ghent, Belgium, June 16-20, 2013*. Ghent University; Delft University of Technology.

Appendix II

High Temperature Strength Recovery Behaviour of Self-Healing Ceramics Containing TiC as a Healing Agent

1 Background

As introduced in Chapter 1, high temperature structural materials like turbine blades of jet engines and automotive components are considered to be primary applications for oxidation-induced self-healing ceramics. Considering the practical operating conditions of those applications, self-healing behaviour of the composites should be discussed based on both the usual conditions, where strength tests are conducted at room temperature and dried air is used as a carrier gas upon annealing, and on conditions simulating actual operating conditions. Within the practical operating conditions, factors such as crack-propagation behaviour due to FOD, oxygen partial pressures in the surrounding atmosphere and in situ strength recovery behaviour at high temperatures should be considered.

In this appendix, special attention is given to the in situ crack-healing behaviour of the alumina/30 vol.%-TiC composite and the yttria stabilized zirconia/30 vol.%-TiC composite based on the results of high temperature bending tests.

2 Experiment

Alumina matrix composites containing 30 vol.% TiC (Al30TiC) were prepared by hot pressing. Yttria stabilized zirconia/ 30 vol.%-TiC composites (YZ30TiC) were prepared using the same procedure detailed in Appendix I. The in situ crack-healing behaviours of these composites at various temperatures were studied by means of high temperature bending tests.

2.1 Sample Preparation

The sample preparation procedure for YZ30TiC is explained in Appendix I. The procedure for Al30TiC is described here.

Alumina powder (AKP-50, Sumitomo Chemical Co., Ltd.), and TiC powder (STD120, H.C. Starck GmbH) were used as starting materials. The average particle sizes of the alumina and TiC powders were 0.2 and 2 μm, respectively. Alumina powder and TiC powder were mixed at the ratio of 70 vol.%: 30 vol.% in isopropanol with ø 300 μm alumina beads by means of bead milling. LABSTAR mini (DMS, Ashizawa Finetech Ltd.) was used as an apparatus. After 2h mixing, the mixed powder was dried in the oven for 12h at 80°C. The dried powder was sieved with a ø 200 μm mesh powder sieve. The sieved powder was sintered by hot-pressing at 1700°C for 1h in an Ar atmosphere under 40MPa. The heating and cooling rates were 10°C/min and 5°C/min, respectively. The typical

dimensions of the sintered bulk material were 50 x 50 x 6mm. The relative density of the sample as measured by Archimedes' method was 99%. The sintered disc was cut into rectangular samples with dimensions of 3 x 4 x 23mm for three-point bending tests. The surface of the samples was mirror finished using a diamond paste with a particle size of 0.25 μm.

2.2 High Temperature Bending Test

To study the in situ strength recovery of Al30TiC and YZ30TiC, the high temperature strength of three types of specimens (smooth, pre-cracked and healed specimens) were examined as shown in Figure 1. Smooth specimens represent the samples without any indentation prior to high temperature bending. Healed specimens are specimens having a standardized pre-crack at the centre of the surface. The introduced pre-cracked has been annealed for 1h in air at either 800°C or 1000°C prior to the high temperature bending test. This indicates that the healed specimen is once cooled down light after the crack-healing at the furnace. The cooling process may cause the crystallization of oxides formed in the crack-healed area. The in situ healed specimens are pre-cracked and directly bent at high temperatures after extra retention time of 1h for crack-healing, meaning that the introduced pre-crack of the in situ healed specimen was healed in situ and was never extracted from the furnace prior to bending.

The high temperature strength of each sample was measured by means of a three-point bending test. The span between the supporting 5mm diameter SiC rollers was 16mm. The specimen was mounted such that the maximum tensile stress was applied to the pre-crack or the healed-crack area. The high temperature bending tests were conducted at either 800°C or 1000°C. The heating and cooling rates were 10°C/min. After reached the target temperature, the furnace temperature was held for 15 min prior to bending in order to stabilize the temperature in the furnace. The cross-head displacement velocity was 0.5mm/min.

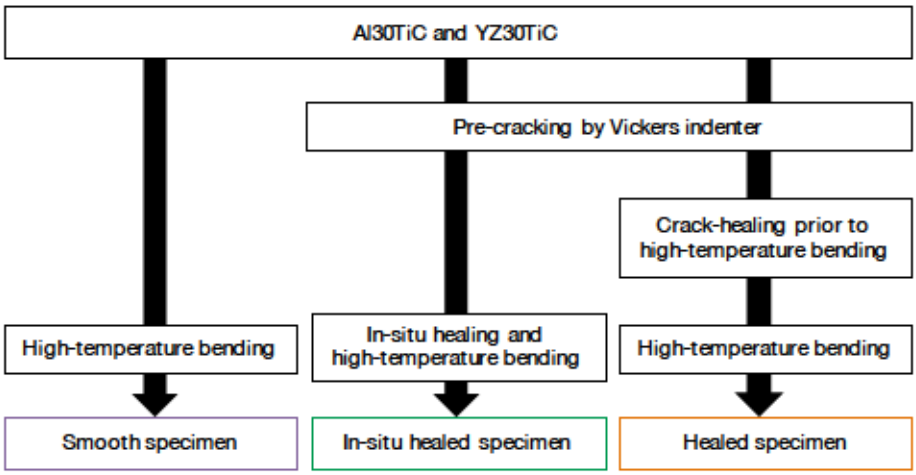

Figure 1 Procedure of High Temperature Bending Tests

3 Results and Discussion

3.1 High Temperature Strength Recovery Behaviour of Al30TiC

The results of the high temperature bending tests for Al30TiC are shown in Figure 2. Purple, green and orange plots correspond to the results of smooth specimen, in situ healed specimen and healed specimen, respectively. The open symbols represent the fracture was initiated from the introduced crack, and the closed symbols represent the fracture origin was the other defects such as inner pore. The bending strength at temperature=0°C corresponds to the result of the room temperature bending test.

The high temperature strength of the smooth specimen at 800°C is comparable to that of the room temperature test, but the value at 1000°C clearly shows degradation. The degradation is caused by the excess diffusion of Ti cation as discussed in Chapter 3. The healed specimen indicated by the orange plot shows no strength recovery at 800°C, but the strength recovery rate becomes 68.0% at 1000°C. Considering that the fracture initiation was shifted from the crack-healed area and that the intermediate compound Al_2TiO_5 was formed at the temperature shown in Chapter 3, it can be concluded that the pre-crack healed at 1000°C has enough a high temperature strength due to the formation of intermediate compounds. The in situ healed specimen also shows no strength recovery at 800°C. The strength recovery rate reaches 45.7% at 1000 °C, but the fracture initiation is still in the crack-healed area. This indicates that the high temperature strength of the crack-healed area has not been recovered. The difference in strength between the healed specimens and the in situ healed specimens may be related to the crystallization of the formed oxides.

3.2 High Temperature Strength Recovery Behaviour of YZ30TiC

Figure 3 shows the results of the high temperature bending test on YZ30TiC. Each symbol has the same meaning as Figure 2. In contrast to the results for Al30TiC, YZ30TiC shows in situ strength recovery at 400°C. Considering that the fracture initiation was shifted from the introduced pre-crack to other defects, it was concludes that the pre-crack was sufficiently diminished.

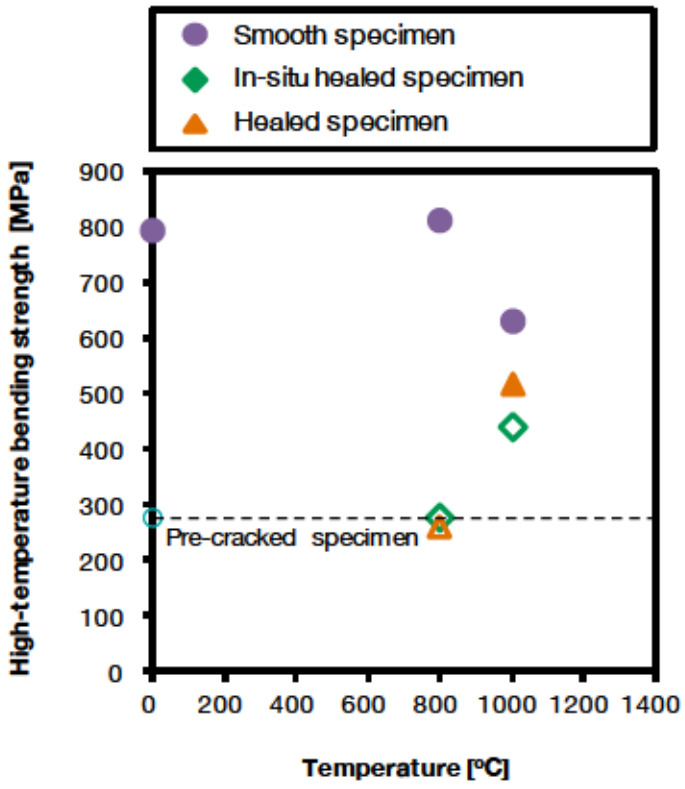

Figure 2 Result of High Temperature Bending Test on Al30TiC

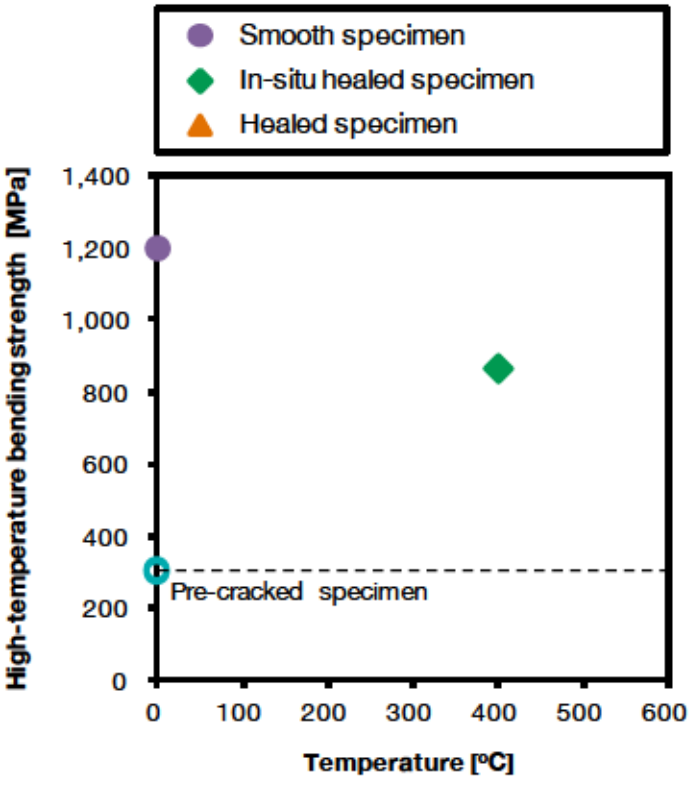

Figure 3 Result of High Temperature Bending Test on YZ30TiC

5 Summary

In this appendix, the high temperature strength recovery behaviour of alumina/30 vol.%-TiC and yttria-stabilized zirconia/30 vol.%-TiC composites were examined. The results are summarized as follows.

1) The high temperature strength of the crack-healed area in Al30TiC was sufficient at 1000°C in air.

2) The in situ high temperature strength recovery in Al30TiC was not achieved at either 800°C or 1000°C for 1h.

3) YZ30TiC shows complete high temperature strength recovery in situ at 400°C within 1h.

Acknowledgement

I would like to express my gratitude to my supervisor Prof. Wataru Nakao, Dr. Wim. G. Sloof, all my colleagues, friends and family for their advices and supports during my Ph.D life in Yokohama and Delft.